UNIVERSITÀ DEGLI STUDI DI TRENTO

Doctoral School in Civil, Environmental and Mechanical Engineering

Topic 1. Civil and Environmental Engineering

Giuseppe Roberto Pisaturo

# Protection infrastructures and methods for reducing the impacts downstream of hydropower plants

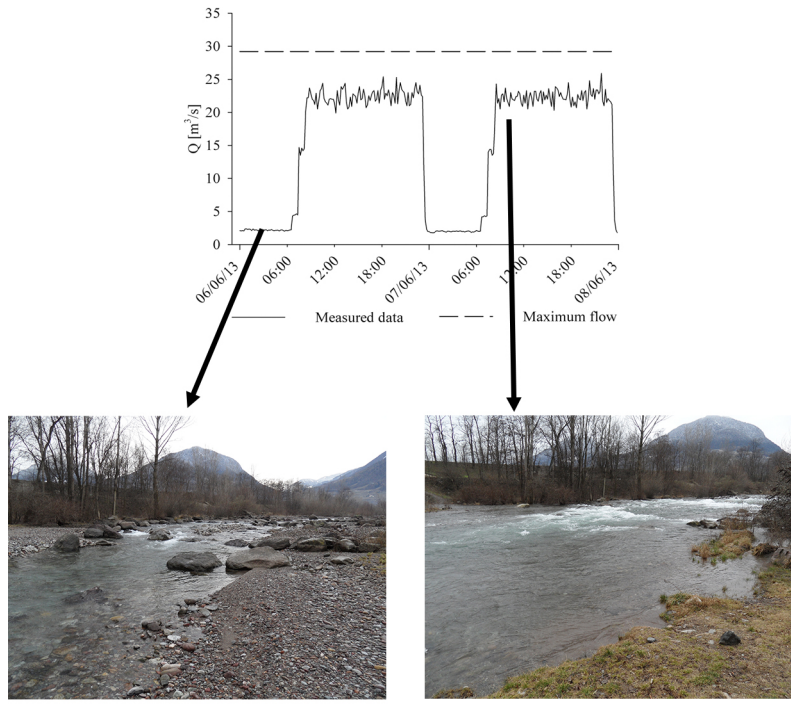


2017 - Doctoral thesis

Hydropower plants, in particular High-head Hydropower Plants (HPPs), are an important source of energy also for their role in covering the daily peaks of energy demand. However, HPPs, especially storage power plants, have several negative effects on the ecosystems of downstream watercourses inducing unnatural changes in flow regime (hydropeaking).

One way to study ecological implications induced by hydropeaking is represented by the coupling of hydrodynamic models (CFD) with habitat suitability models, in which hydrodynamic parameters are typically used to describe the physical habitat of indicator species.

The research activity wanted to investigate possible differences between the use of 2D and 3D CFD approaches to determine the watercourse hydraulic characteristics and their effects on habitat evaluations, performed with CASiMiR software, in complex morphology as usually presents in hydropeaked reaches.

In particular the habitat suitability for the two case studies (Valsura River and Rio Selva dei Molini), is analysed comparing different approaches for the reconstruction of the velocity field (depth-averaged velocities from 2D modelling, bottom velocity field reconstruction with log-law approach from 2D modelling and bottom velocity field from 3D modelling). The results show that the habitat suitability index (HSI) using 2D or 3D hydrodynamic models can be significantly different. Considering the entire flow range of hydropeaking events, the habitat simulations with bottom flow velocities from 3D modelling provide suitable habitats over the entire flow range representing the availability of stable suitable habitats.

The results from the hydraulics and habitat analyses are used to investigate the effects of a hydropeaking mitigation project on the Valsura River (realization of a compensation bypass tunnel to decrease the peak flow rate and to remodel the up and down flow ramping rates) and on Rio Selva dei Molini (morphological measures to reduce the hydropeaking effects).

**Giuseppe Roberto Pisaturo**, PhD student 29th Cycle. Master thesis in Environmental Engineering at University of Trento. The main research topics are hydraulics, habitat evaluations, sediment transport, water supply systems and energy production. The software usually used are Fortran, Matlab, Maple, HecRas, Basement, CASiMiR, Flow3D and Ansys.

UNIVERSITY OF TRENTO - Italy
Department of Civil, Environmental and Mechanical Engineering

Doctoral School in Civil, Environmental and Mechanical Engineering
Topic 1. Civil and Environmental Engineering - XXIX cycle 2015/2017

Doctoral Thesis - June 2017

Giuseppe Roberto Pisaturo

# Protection infrastructures and methods for reducing the impacts downstream of hydropower plants

**Supervisors**
Prof. Maurizio Righetti - University of Bolzano
Prof. Michael Dumbser - University of Trento

Credits of the cover image Pisaturo Giuseppe Roberto



University of Trento
Doctoral School in Civil, Environmental and Mechanical Engineering
*http://web.unitn.it/en/dricam*
Via Mesiano 77, I-38123 Trento
Tel. +39 0461 282670 / 2611 - *dicamphd@unitn.it*

# Contents

**1. Introduction 1**

*1.1 The importance of hydropower production 1*

*1.2 Impacts of hydropower production on ecosystems 2*

*1.3 Objectives of the study 8*

**2. CFD Model description 11**

*2.1 Numerical model approach 11*

*2.2 Test case 14*

*2.3 Discussion 22*

**3. Habitat model description 25**

*3.1 CASiMiR model 25*

*3.2 2D and 3D approach 27*

**4. Case studies 29**

*4.1 Valsura River 29*

4.1.1 Study area 29

4.1.1 Hydraulic characterization 31

4.1.2 Ecological characterization 37

*4.2 Rio Selva dei Molini 41*

4.2.1 Study area 41

4.2.2 Hydraulic characterization 42

4.2.3 Ecological characterization 46

**5. Hydraulic model and Habitat modelling 49**

*5.1 Valsura River hydraulic model 49*

*5.2 Valsura River habitat modelling 53*

5.2.1 Habitat 2D-3D, YOY 53
5.2.2 Habitat 2D-3D, Adult 56

*5.3 Rio Selva dei Molini hydraulic model 60*

*5.4 Rio Selva dei Molini habitat modelling 63*
5.4.1 Habitat 2D-3D, YOY 63
5.4.2 Habitat 2D-3D, Adult 66

*5.5 Discussion 70*

**6. Mitigation projects 75**

*6.1 Valsura River 75*
6.1.1 Operational measures 79
6.1.2 Constructive measures 81

*6.2 Rio Selva dei Molini 86*
6.2.1 Groynes in the right riverbank, habitat 2D-3D, YOY 87
6.2.2 Groynes in the right riverbank, habitat 2D-3D, Adult 90
6.2.3 Alternating groynes, habitat 2D-3D, YOY 94
6.2.4 Alternating groynes, habitat 2D-3D, Adult 97
6.2.5 Comparison and discussion 100

**7. Conclusion 105**

*7.1 Recommendations for future work 108*

**8. APPENDIX 111**

*8.1 Appendix 1 111*

*8.2 Appendix 2 112*

**9. REFERENCES 115**

**Acknowledgements 123**

# List of Figures

*Figure 1. Top view of the laboratory model showing the groynes and the horizontal Plane A and the vertical Plane B for the comparison between measured and simulated velocity fields. ..... 16*

*Figure 2. Comparison between measured velocities (red vectors) and simulated velocities (blue vectors) in the horizontal plane A upstream of the groyne (top) and in the vertical plane B (bottom).. 17*

*Figure 3. Comparison of simulated bottom velocity fields (2 cm above bottom) using 3D hydrodynamic modelling and 2D depth-averaged results (logarithmic velocity profile) with measured bottom velocities..... 18*

*Figure 4. Percentage difference in bottom velocity field between 3D and 2D model. ..... 19*

*Figure 5. 3D vorticity $\omega_z$ representation from 3D CFD model. ..... 20*

*Figure 6. Vorticity $\omega_z$ representation from 3D CFD model. ..... 21*

*Figure 7. Vorticity $\omega_z$ representation from 2D CFD model. ..... 21*

*Figure 8. 3D vorticity $\omega_x$ representation from 3D CFD model. Principals sections of interest. ..... 22*

*Figure 9. Preference curves of flow velocity (A) and water depth (B) for brown trout for both life-stages adult and YOY considering depth-averaged and focal velocities. ..... 26*

*Figure 10. Valsura Hydraulic System and overview of Hydropeaking investigation area. Ecological measuring positions on Passirio and Valsura River are highlighted. The three stretches represented in the figure are morphologically different: Stretch 1 (purple, left photo), upstream, is canalized; Stretch 2 (green middle photo) enlarges and presents several hydraulic structures; Stretch 3 (red, right photo) is in the biotope area with quasi-braided structures. ..... 30*

*Figure 11. Characteristic hydropeaking discharge with single (A) and double (B) peak production mode. ..... 33*

*Figure 12. Characteristic up-ramping and down-ramping. ..... 33*

*Figure 13. Flow rate measured at gauging station. Valsura River 2014. ..... 35*

*Figure 14. Flow duration curve and average flow duration curve. Valsura River 2014. ..... 36*

*Figure 15. Maximum and minimum flow rates. Valsura River 2014. ..... 36*

*Figure 16. Positive and negative ramping rates. Valsura River 2014. ..... 36*

*Figure 17. Ratio between maximum and minimum flow rate. Valsura River 2014. ..... 37*

*Figure 18. A: individual MZB density on Passirio River and on Valsura River. B: number of trout parr/100 m of bank. VAL2 and VAL3b are two measurement points in the Valsura hydropeaked stretch and VAL7 is in the Valsura environmental flow stretch upstream the Lana HPP outlet; PAS3 measuring point is used as comparison. ..... 39*

*Figure 19. Rio Selva dei Molini overview of Hydropeaking investigation area. Ecological measuring positions are highlighted..... 41*

*Figure 20. Typical section of the Rio Selva dei Molini. Right: Molini HPP outlet. Center: Rio Selva dei Molini in the hydropeaked part. Left: confluence between Rio Selva dei Molini and Aurino River. ..... 42*

*Figure 21. Flow rate turbined. Molini HPP 2014. ..... 45*

*Figure 22. Flow duration curve and average flow duration curve. Molini HPP 2014. ..... 45*

*Figure 23. Maximum and minimum flow rates. Molini HPP 2014..... 46*

*Figure 24. Positive and negative ramping rates. Molini HPP 2014. ..... 46*

*Figure 25. MZB population density. Rio Selva dei Molini MTu3 and MTu4. . 48*

*Figure 26. Sample point in Valsura River for water depths measurements. ... 50*

*Figure 27. Spatial distribution of differences at 2 $m^3/s$ and 10 $m^3/s$ between the bottom flow velocities of 3D modelling with 2D depth-averaged flow velocities and bottom flow velocities from 2D modelling using the logarithmic law profile. ..... 52*

*Figure 28. Habitat suitability maps of brown trout (YOY stage) considering different velocity field as input for habitat suitability modelling. The maps represent high flow rates close to the peak flow (Q = 10 $m^3/s$).*

*A: bottom velocities from 3D modelling, B: depth-averaged velocities from 2D modelling, C: bottom velocities from 2D modelling using the logarithmic-law. ..... 54*

*Figure 29. Weighted usable areas (WUA) for the three different velocity inputs in habitat modelling for the entire range of flow rates during hydropeaking events. YOY fish life stage. ..... 55*

*Figure 30. Stranding risk for YOY life stage. ..... 56*

*Figure 31. Habitat suitability maps of brown trout (adult stage) considering different velocity field as input for habitat suitability modelling. The maps represent high flow rates close to the peak flow (Q = 10 $m^3/s$). A: bottom velocities from 3D modelling, B: depth-averaged velocities from 2D modelling, C: bottom velocities from 2D modelling using the logarithmic-law. ..... 58*

*Figure 32. Weighted usable areas (WUA) for the three different velocity inputs in habitat modelling for the entire range of flow rates during hydropeaking events. Adult fish life stage. ..... 59*

*Figure 33. Sample point in Rio Selva dei Molini for water depths and water velocities measurements. ..... 60*

*Figure 34. Comparison between measured and simulated water velocities in Rio Selva dei Molini. Water depth mean velocity (left) and bottom velocities (right). ..... 61*

*Figure 35. Spatial distribution of differences at 3 $m^3/s$ between the bottom flow velocities of 3D modelling with 2D depth-averaged flow velocities and bottom flow velocities from 2D modelling using the logarithmic law profile. ..... 63*

*Figure 36. Habitat suitability maps of brown trout (YOY stage) considering different velocity field as input for habitat suitability modelling. The maps represent high flow rates close to the peak flow (Q = 7 $m^3/s$). A: bottom velocities from 3D modelling, B: depth-averaged velocities from 2D modelling, C: bottom velocities from 2D modelling using the logarithmic-law. ..... 64*

*Figure 37. Weighted usable areas (WUA) for the three different velocity inputs in habitat modelling for the entire range of flow rates during hydropeaking events. YOY fish life stage. ..... 65*

*Figure 38. Habitat suitability maps of brown trout (adult stage) considering different velocity field as input for habitat suitability modelling. The maps represent high flow rates close to the peak flow (Q = 7 $m^3$/s). A: bottom velocities from 3D modelling, B: depth-averaged velocities from 2D modelling, C: bottom velocities from 2D modelling using the logarithmic-law. ..... 68*

*Figure 39. Weighted usable areas (WUA) for the three different velocity inputs in habitat modelling for the entire range of flow rates during hydropeaking events. Adult fish life stage. ..... 69*

*Figure 40. Stranding risk for YOY life stage. Mitigation project. ..... 76*

*Figure 41. Base flow, discharge to add for meeting minimum flow demand and maximum turbine discharge for maintaining maximum flow limit. . 81*

*Figure 42. Constructive mitigation measure for Valsura River. ..... 82*

*Figure 43. Hydraulic scheme of the constructive mitigation measure for Valsura river. ..... 83*

*Figure 44. Comparison between actual and after project state of the flow rates in Valsura River. ..... 85*

*Figure 45. Groynes configuration in the right riverbank. ..... 87*

*Figure 46. Habitat suitability maps of brown trout (YOY stage) considering different velocity field as input for habitat suitability modelling. The maps represent high flow rates close to the peak flow (Q = 7 $m^3$/s). A: bottom velocities from 3D modelling, B: depth-averaged velocities from 2D modelling, C: bottom velocities from 2D modelling using the logarithmic-law. Groynes in the right riverbanks. ..... 89*

*Figure 47. Weighted usable areas (WUA) for the three different velocity inputs in habitat modelling for the entire range of flow rates during hydropeaking events. YOY fish life stage. Groynes in the right*

*riverbanks.* ..... *90*

*Figure 48. Habitat suitability maps of brown trout (adult stage) considering different velocity field as input for habitat suitability modelling. The maps represent high flow rates close to the peak flow (Q = 7 m³/s). A: bottom velocities from 3D modelling, B: depth-averaged velocities from 2D modelling, C: bottom velocities from 2D modelling using the logarithmic-law. Groynes in the right riverbanks.* ..... *92*

*Figure 49. Weighted usable areas (WUA) for the three different velocity inputs in habitat modelling for the entire range of flow rates during hydropeaking events. Adult fish life stage. Groynes in the right riverbanks.* ..... *93*

*Figure 50. Groynes alternating configuration.* ..... *94*

*Figure 51. Habitat suitability maps of brown trout (YOY stage) considering different velocity field as input for habitat suitability modelling. The maps represent high flow rates close to the peak flow (Q = 7 m³/s). A: bottom velocities from 3D modelling, B: depth-averaged velocities from 2D modelling, C: bottom velocities from 2D modelling using the logarithmic-law. Alternating groynes.* ..... *95*

*Figure 52. Weighted usable areas (WUA) for the three different velocity inputs in habitat modelling for the entire range of flow rates during hydropeaking events. YOY fish life stage. Alternating groynes.* ..... *96*

*Figure 53. Habitat suitability maps of brown trout (adult stage) considering different velocity field as input for habitat suitability modelling. The maps represent high flow rates close to the peak flow (Q = 7 m³/s). A: bottom velocities from 3D modelling, B: depth-averaged velocities from 2D modelling, C: bottom velocities from 2D modelling using the logarithmic-law. Alternating groynes.* ..... *99*

*Figure 54. Weighted usable areas (WUA) for the three different velocity inputs in habitat modelling for the entire range of flow rates during hydropeaking events. Adult fish life stage. Alternating groynes.* ... *100*

*Figure 55. Comparison of WUA curves between actual state and the two proposed morphological mitigation measures. WUA curves for YOY life stage (up) and adult life stage (down). ..... 102*

# List of Tables

*Table 1. Mitigation measures proposed in literature against hydropeaking effects.* ..... *4*

*Table 2. Morphological characteristics in the hydropeaked stretch in Valsura River.* ..... *31*

*Table 3. Actual state: typical minimum and maximum flow discharges in Valsura hydropeaked stretch.* ..... *34*

*Table 4. Morphological characteristics in the hydropeaked stretch in Rio Selva dei Molini.* ..... *42*

*Table 5. Upstream monthly flow rate the Molini HPP outlet.* ..... *43*

*Table 6. Minimum and maximum flow rate in the hydropeaked reach.* ..... *44*

*Table 7. Population density and unitary biomass of fish in MTu3 and MTu4.* *47*

*Table 8. Comparison between measured and simulated water depth for the Valsura River (Q = 2.34 $m^3/s$).* ..... *50*

*Table 9. Comparison between measured and simulated water depth for the Rio Selva dei Molini (Q = 2.07 $m^3/s$).* ..... *61*

*Table 10. Comparison of the percentage ratio between good habitat areas and total wet areas. YOY and Adult life stages. Valsura River and Rio Selva dei Molini.* ..... *74*

*Table 11. Ecological and hydrological targets to improve habitat status in Valsura River.* ..... *77*

*Table 12. Annual flow utilization of inflows to Lana HPP. Comparison between actual, operational only and constructive solution at Lana HPP.* ..... *79*

*Table 13. Fundamental characteristics of new Lana di Sotto HPP.* ..... *84*

*Table 14. Comparison between operational and constructive solution against hydropeaking.* ..... *86*

# 1. INTRODUCTION

## 1.1 THE IMPORTANCE OF HYDROPOWER PRODUCTION

Nowadays the demand for nuclear-free and CO2 free energy production is increasing. After the COP21 in 2015 (21th Conference of Parties in Paris) 195 countries have agreed on a plan to hold the "increase in the global average temperature to well below 2° C above pre-industrial levels and to pursue efforts to limit the temperature increase to 1.5 °C". To succeed this goal it is important to limit the energy production from non-renewable resource and therefore increase the use of other resources, among them the hydroelectricity production (Schleiss, 2007).

Hydropower is, in Europe, the first renewable energy resource covering about the 50% of the total energy production from renewable sources. In Europe, the hydroelectric power amounts to about 200 GW with a efficiency between 85% and 95% (Eurelectric, 2015). In Italy, the demand for electricity between January and September 2015 amounted to 237,392 GWh. Of this amount, hydropower has covered 36,257 GWh (15.3%). Moreover, among the renewable resources, hydropower is the most used covering about the 50% of renewable sources, consistent with European values (Terna, 2015).

Since the early 2000, the hydroelectric energy production is being almost unchanged. Instead, a strong production increase from other renewable sources (wind and solar) is present (ISPRA, 2015).

High-head Hydropower Plants (HPPs) (head > 300 m) have an important role in peak energy supply. From an environmental and economic point of view the use of the existing plants for covering peak energy demand seems to be the best feasible choice (Eurelectric, 2015). The ability of hydropower to rapidly follow the demand of the electric

High-Head Hydropower Plants are an important role in peak energy supply.

grid is a very important aspect underlined by (GSEP, 2015). GSEP (2015) supposes that, from a technological point of view, the main challenge is the joint management of hydropower plants and other energy sources in order to optimise water usage and to enhance the electric system's flexibility especially by speeding up the ramping rates of the hydropower plants.

The future of hydropower depends also on geographical context. In Europe hydropower resources are already largely exploited, so future projects will mainly involve renovating and upgrading existing infrastructure (GSEP, 2015).

## 1.2 IMPACTS OF HYDROPOWER PRODUCTION ON ECOSYSTEMS

On the other hand, storage hydropower plants (hydropower plants with a storage basin to support peak energy production) have several negative effects on the ecosystems of the downstream watercourses. The intermittent operation of the storage hydropower plants induces artificial and sudden changes of the downstream hydrological characteristics of the river such as depth, wetted contour, velocity, bottom shear stress (Meile et al., 2011). This phenomenon is called hydropeaking (Charmasson and Zinke, 2011). The hydropeaking phenomena is recently one of the main research topic and the number of publication continuously increase from 2000s (Hauer et al., 2016b).

Hydropeaking substantially differs from natural floods due to the rapidity (the increase or reduction of the flow is almost instantaneous), the magnitude, the time of occurrence (the variations are high and occur during seasons where large natural discharge fluctuations seldom occur) and the frequency of the discharge fluctuations (typically once or twice per day). As a consequence aquatic organisms are not able to accommodate these artificial flow variations (Baumann and Klaus, 2003; Poff et al., 1997). For example, latest investigation has shown that fish

and macrozoobenthos population is less abundant and the population size is reduced in rivers with hydropeaking (Costa et al., 2012; Jungwirth et al., 1990).

Also the morphological characteristics of the downstream course can be affected by the hydropeaking (Hauer et al., 2013; Tuhtan et al., 2012). During peak flow, the sediments are transported and erosion phenomena can occur (Anselmetti et al., 2007). During base flow sediments are redeposited, and this may cause clogging of the river bed (Bruno et al., 2009).

Moreover, the water released from HPP can have a different temperature than the receiving river. This phenomenon can create temperature peaks called thermopeaking (Zolezzi et al., 2011).

There are three main methods to reduce the effects of hydropeaking (Charmasson and Zinke, 2011) (Table 1). The first one is operational measures, which focus on a change and reshaping of energy production, for example by limiting the maximum discharge (Qmax) and increasing the minimum flow (Qmin) (Yin et al., 2012), but with a consequent reduction of the gains by the HPP operator (Gostner et al., 2011). The purpose of these measures is to avoid the direct consequences of hydropeaking as stranding, drift of macro-invertebrates (Baumann and Klaus, 2003), fish habitat availability reduction and diversity (Sabaton et al., 2008). For example, studies of the flow discharge and local condition in a 23km long reach of Alpine Rhin, allowed to define the minimum and the maximum discharge and water level rate variation (Schälchli et al., 2003).

Mitigation measures can be divided in three main categories: operational, constructive and morphological.

A second type of mitigation measures are constructive measures that reduce the hydropeaking discharges in the receiving river and smooth peaking variation. The hydraulics structures present in literature are retention ponds (KWO, 2013; Meile et al., 2005), channels to deliver the water in a specific part of the river or in a different lake (Baumann

and Klaus, 2003; Meile et al., 2005; Premstaller et al., 2017). These type of measures are expensive and can entail building of large structures with the consequent high investment costs. (Tonolla et al., 2017) combines a basin and a cavern, allowing for substantial dampening in the flow falling and ramping rates and, in turn, considerable reduction in stranding risk for juvenile trout and in macroinvertebrates drift.

Finally, morphological measures aim to restore a good level of naturalness of the river with a consequent improvement of the flood evacuation capacity of the system and the restoration of areas suitable for the biotic system. These measures are typically represented by river widening (Meile et al., 2005; Pellaud, 2007), sediment placement (Pretty et al., 2003), installation of restoration structures such as weirs, groynes and boulders (Baumann and Klaus, 2003; Pretty et al., 2003; Rosenfeld et al., 2010). Recent studies show that the best choice of intervention is the proper mix of morphological, operational and constructive measures in order to minimize ratio between investment costs and ecological benefits (Gostner et al., 2011). The work of (Hauer et al., 2016a) underline, moreover, the importance of the sediment quality (substrate sorting) that is essential in these sheltering habitat.

Table 1. Mitigation measures proposed in literature against hydropeaking effects.

| | Mitigation measures | | |
|---|---|---|---|
| | Operational | Constructive | Morphological |
| actions | Limit Qmax; Increase Qmin; Reduce up and down ramping rate | Retention ponds; By-pass. | River widening; Sediment placement; Groynes and boulders |
| cons | Reduction of the HPP operator gains | Expensive and large structure | Can change hydraulic safety |

One way to assess the ecological implications of hydropeaking and understand the efficiency of mitigation measures are physical habitat

suitability evaluations (Schneider and Noack, 2009) and the main indicators for assessing the effects of hydropeaking on the biota are macrozoobenthos and fish. The first are excellent indicators and have been used to understand the long (Jackson et al., 2007) and short (Carolli et al., 2012) term effects of hydropeaking.

Local fish species, for example the brown trout, are good indicators of the ecological state of the ecosystem and therefore are used for studying hydropeaking impacts. Fish population is less abundant and the population size is reduced in rivers subjected to hydropeaking (Costa et al., 2012).

The impact of hydropeaking, for example, on trout habitat is seasonal and magnified in winter (Person, 2013). For the adult stage an increase of stress is observed (Taylor and Cooke, 2012). The deposition of the eggs is strongly influenced by clogging effects of the substrate (Tanno, 2012) and because of the variation of flow rate a catastrophic drift and a subsequent stranding of the eggs themselves can be observed (Riedl and Peter, 2013). Finally, individuals in juvenile life stage prefer shallow habitats near the riverbank, which are highly unstable in hydropeaking regimes with important variations of flow velocity and water depth (Korman and Campana, 2009). However, the severity of the impact of hydropeaking strongly depends on the morphology and on the hydraulics of river and it is therefore closely site specific.

The change of the habitat suitability can be estimated by means of a detailed hydraulic simulation of the flow field in the river reach affected by hydropeaking.

According to (Maddock, 1999) the physical habitat is a key factor in evaluating the ecological status of rivers. The basic principle of physical habitat simulation tools quantifying habitat suitability consists of a comparison between existing and preferred conditions of aquatic organisms. The linkage between biological responses and abiotic factors

can be approached through a number of different techniques. They are mainly classified as univariate methods (e.g. preference functions) or multivariate approaches (e.g. fuzzy-logic), taking into account interactions between habitat variables to determine the target species or life stage response to the abiotic factors.

Moreover, there are two different approaches to study the habitat suitability in dependence of the scale of the problem. The first approach is based on micro-scale study that is useful for small reach or part of a river. With this approach is possible to study the local effect of mitigation measures that affect the hydraulics of the river, such as morphological mitigation measures. A well-known habitat simulation tool among others is CASiMiR (Computer Aided Simulation Model for Instream Flow and Riparia), in which hydromorphological simulations are coupled with habitat preferences of target species by means of a fuzzy logic approach or preference curves (Noack et al., 2013; Schneider, 2001).

The second approach is conducted at basin scale. The upscaling of microhabitat models to larger scales can introduce a high level of uncertainty and can be time consuming and labour intensive (Maddock, 1999). Therefore, a meso-scale approach can be useful if a large part of the river has to be studied. The first developed physical habitat simulation model for meso-scale is PHABSIM (Milhous and Waddle, 2012) that is followed by others models such as MesoHABSIM (Parasiewicz, 2007) and MesoCASiMiR (Noack et al., 2013).

In physical habitat simulation tools usually three variables are used to determine the habitat suitability: water depth, flow velocity and substrate particle size (Heggenes and Wollebæk, 2013).

For the present study, the target species analysed is the brown trout which presents specific and diversified habitat requirements during the life stage. For this reason this species is usually widely used as target species to perform habitat analysis during hydropeaking events (Person,

Necessity to correctly coupling hydraulic simulations with habitat suitability software.

2013). In particular the young fish stage is more sensitive, compared with adult life stage, to flow rates variations (Auer et al., 2017; Boavida et al., 2013).

Experiments on brown trout show that flow velocity may be the dominant factor compared to the other ones (Shirvell and Dungey, 1983). Indeed, flow velocity, especially focal water velocity, is directly related to fish net energy gain (Hill and Grossman, 1993), which means to optimize the positions with respect to maximize access to food while minimizing energy expenditure. The brown trout selection for focal velocities is relatively narrow for all brown trout life stages. However, literature observations focus mainly on small parr (< 7 cm) and larger (> 7 cm). During different life stages, brown trout occupy different positions in water column but they prefer positions close to the river bottom (Greenberg et al., 1996). Heggenes' observations (Heggenes et al., 1991) show that fishes tend to place at a distance from the bottom between 4 cm and 9 cm, with a mean value of 6 cm. This aspect needs to be considered for adequate predictions of physical habitat suitability because the difference between depth-averaged flow velocity and bottom flow velocity (focal velocity) can be substantially (Heggenes, 1996). According to Heggenes (2002) the focal velocity is a better predictor of brown trout positions compared to depth-integrated velocities (Heggenes, 2002). Moreover, given the wide range of substrate preferences (16-256 mm), the distance from the bottom seems not to be directly dependent on substrate size (Heggenes et al., 1999).

For this reason, particular attention has to be paid in the proper reproduction of the flow field along the water column. This aspect can be challenging in reaches with high morphological diversity, which induces high heterogeneities in the flow field, e.g. high velocity regions alternate with zones of flow separation and recirculation together with regions at relative low submergence (Armanini et al., 2010a). Therefore, reliability of habitat suitability modelling is affected by the accuracy of

the numerical simulation, including complex flow fields that may occur (Heggenes, 1996).

## 1.3 OBJECTIVES OF THE STUDY

In the present work, we analyse the influence of 2D versus 3D hydrodynamic numerical simulations on the prediction of habitat suitability for brown trout in two alpine river reaches that are affected by hydropeaking. Due to the higher capability of 3D CFD model to represent complex flow field, we suppose that during hydropeaking events, small niches that are usable over a wide range of flow might be better predicted compared to 2D model (Pisaturo et al., 2017).

We hypothesise that the habitat stability, in terms of a more or less unchanged spatial position of high quality habitats during hydropeaking, might be covered more adequately by 3D hydrodynamic modelling than by 2D depth averaged modelling. This could affect the assessment of hydropeaking impacts based on habitat modelling.

Moreover, in the present work are presented two possible mitigations measures against hydropeaking for the two case studies. The first river studied is Valsura River (SudTirol – Italy) for which a combination of operative and constructive mitigation approach is used. The second river is Rio Selva dei Molini (SudTirol – Italy) for which operative and morphological measures are proposed. For both the case studies, the restore of a good fish reproduction has a primary importance to allow the colonization of the reach by brown trout.

To estimate the impact of hydropeaking on fish habitat, the entire range of flow rates during hydropeaking events need to be investigated. Hence, the hydraulic patterns, in particular the velocity fields of the river reach are simulated for selected flow rates ranging from base flow to peak flow using an original 3D nonhydrostatic k-ε model, developed at University of Trento (Casulli, 1999). The same 3D CFD model can easily be applied as a 2D CFD model, simply adopting only one cell in

the vertical direction. The hydraulic results of the CFD model deliver the required input data for the habitat simulation tool CASiMiR. In detail, we investigate in this study the effect of three different simulated velocity fields on habitat suitability of brown trout for different life-stages: 1. depth-averaged velocity field from 2D modelling; 2. velocity field close to the bottom from 2D modelling supposing a logarithmic law of the wall velocity profile (6 cm above the bottom) and 3. velocity field close to the river bottom from 3D modelling (6 cm above the bottom).

We compare and evaluate differences between obtained habitat suitability values from 2D and 3D hydrodynamic modelling regarding the spatial distribution of habitat suitability for selected discharges and corresponding Weighted Usable Areas (WUA).

# 2. CFD MODEL DESCRIPTION

## 2.1 NUMERICAL MODEL APPROACH

The 3D fluid dynamic model, developed at the University of Trento, is based on the method of Casulli (Casulli and Zanolli, 2002) and allows to simulate water surface motions with nonhydrostatic correction. The CFD model has also the possibility of considering the cells wetting and drying. In the hydrodynamic solver part, Reynolds equations (1) are solved for the continuity and conservation of momentum, coupled with the volume conservation condition (2) and the equation of the free surface (3).

$$\begin{aligned}
&\frac{\partial u}{\partial t}+u\frac{\partial u}{\partial x}+v\frac{\partial u}{\partial y}+w\frac{\partial u}{\partial z}\\
&\qquad=-\frac{\partial P}{\partial x}+\nu\left(\frac{\partial^2 u}{\partial x^2}+\frac{\partial^2 u}{\partial y^2}\right)+\frac{\partial}{\partial z}\left(\nu\frac{\partial u}{\partial z}\right)\\
&\frac{\partial v}{\partial t}+u\frac{\partial v}{\partial x}+v\frac{\partial v}{\partial y}+w\frac{\partial v}{\partial z}\\
&\qquad=-\frac{\partial P}{\partial y}+\nu\left(\frac{\partial^2 v}{\partial x^2}+\frac{\partial^2 v}{\partial y^2}\right)+\frac{\partial}{\partial z}\left(\nu\frac{\partial v}{\partial z}\right)\\
&\frac{\partial w}{\partial t}+u\frac{\partial w}{\partial x}+v\frac{\partial w}{\partial y}+w\frac{\partial w}{\partial z}\\
&\qquad=-\frac{\partial P}{\partial z}+\nu\left(\frac{\partial^2 w}{\partial x^2}+\frac{\partial^2 w}{\partial y^2}\right)+\frac{\partial}{\partial z}\left(\nu\frac{\partial w}{\partial z}\right)
\end{aligned} \tag{1}$$

where $(u, v, w)$ are the velocity components in the horizontal $x$-, $y$-, and vertical $z$-directions respectively; $t$ is the time; $P$ is the normalized pressure (pressure divided by constant reference density) and $\nu$ is the

eddy viscosity.

$$\int_{\Delta V}\left(\frac{\partial u}{\partial x}+\frac{\partial v}{\partial y}+\frac{\partial w}{\partial z}\right)dxdydz=0 \qquad (2)$$

where $\Delta V$ is the numerical element volume.

$$\frac{\partial \eta}{\partial t}+\frac{\partial}{\partial x}\left[\int_{-h}^{\eta} u\,dz\right]+\frac{\partial}{\partial y}\left[\int_{-h}^{\eta} v\,dz\right]=0 \qquad (3)$$

where $\eta$ is the free surface elevation and $h$ is the prescribed bathymetry measured from the undisturbed water surface.

The numerical approach to solve (1) is semi-implicit (Casulli and Zanolli, 2002). For nonlinear convective terms and for the horizontal diffusion is used an explicit approach using Eulerian-Lagrangian scheme (Casulli and Cheng, 1992; Casulli and Walters, 2000). For pressure gradients, vertical diffusion and for the free surface equation is used an implicit approach (Casulli and Zanolli, 2002).

The pressure $P$ in equation (1) is the sum of a hydrostatic and a nonhydrostatic component (4).

$$P=p(x,y)+q(x,y,z)=g\,\eta(x,y)+q(x,y,z) \qquad (4)$$

where $g$ is the gravity acceleration and $q$ is the nonhydrostatic pressure correction. A semi-implicit method is used to take into account the nonhydrostatic pressure gradients (Casulli and Zanolli, 2002; Fambri et al., 2014).

The computational grid used is staggered, Cartesian and unstructured.

For turbulent terms in the RANS equations the $k$-$\varepsilon$ turbulence model is used to determine the eddy viscosity.

$$\frac{\partial k}{\partial t}+\frac{\partial (uk)}{\partial x}+\frac{\partial (vk)}{\partial y}+\frac{\partial (wk)}{\partial z}=G-\varepsilon$$
$$+\frac{\partial}{\partial x}\left((\nu_m+\frac{\nu_t}{\sigma_k})\frac{\partial k}{\partial x}\right)+\frac{\partial}{\partial y}\left((\nu_m+\frac{\nu_t}{\sigma_k})\frac{\partial k}{\partial y}\right) \quad (5)$$
$$+\frac{\partial}{\partial z}\left((\nu_m+\frac{\nu_t}{\sigma_k})\frac{\partial k}{\partial z}\right)$$

$$\frac{\partial \varepsilon}{\partial t}+\frac{\partial (u\varepsilon)}{\partial x}+\frac{\partial (v\varepsilon)}{\partial y}+\frac{\partial (w\varepsilon)}{\partial z}=(c_{\varepsilon 1}G-c_{\varepsilon 2}\varepsilon)\frac{\varepsilon}{k}$$
$$+\frac{\partial}{\partial x}\left((\nu_m+\frac{\nu_t}{\sigma_\varepsilon})\frac{\partial \varepsilon}{\partial x}\right)+\frac{\partial}{\partial y}\left((\nu_m+\frac{\nu_t}{\sigma_\varepsilon})\frac{\partial \varepsilon}{\partial y}\right) \quad (6)$$
$$+\frac{\partial}{\partial z}\left((\nu_m+\frac{\nu_t}{\sigma_\varepsilon})\frac{\partial \varepsilon}{\partial z}\right)$$

$$\nu_t=c_\mu\frac{k^2}{\varepsilon} \quad (7)$$

where $k$ is the turbulent kinetic energy; $\varepsilon$ is the turbulent dissipation; $\sigma_k$ and $\sigma_\varepsilon$ are the Schmidt numbers; $c_\mu$, $c_{\varepsilon 1}$ and $c_{\varepsilon 2}$ are constants; $\nu_m$ is the molecular kinetic viscosity; $\nu_t$ is the eddy viscosity and $G=\nu_t\left(\frac{\partial \nu_i}{\partial x_j}+\frac{\partial \nu_j}{\partial x_i}\right)\frac{\partial u_i}{\partial x_j}$.

The problem of the determination of the eddy viscosity is split in the resolution of two independent transport equations (solved with a semi-implicit approach) and for a pure reaction problem solved locally with an implicit Newton method.

To calculate the shear stress boundary conditions for turbulent fluxes is necessary to solve the law of the wall. It consists in a nonlinear relationship between the dimensionless velocity $u^+=u/u_*$ and the wall dimensionless wall coordinate $z^+=u_*\,z/\nu$, where $u_*=\sqrt{\tau/\rho}$ is

the shear velocity; $\tau$ is the shear stress and $\rho$ is the water density. In particular in the present CFD model is used the law of the wall reported in (Fang and Rodi, 2003; Wu et al., 2000) for hydraulically rough flows. The shear velocity is calculated resolving a weakly nonlinear equation for $u_*$ (Wu et al., 2000) using a locally implicit Newton method.

For the free surface boundary conditions in $k$-$\varepsilon$ model using (Fang and Rodi, 2003) we have

$$\varepsilon = \frac{k^{\frac{3}{2}}}{0.43\ H} \qquad \frac{\partial k}{\partial z} = 0 \tag{8}$$

where $H$ is the water depth. For bottom boundary condition using (Wu et al., 2000) we have

$$k = \frac{u_*^2}{\sqrt{c_\mu}} \qquad \varepsilon = \frac{u_*^3}{\kappa z} \tag{9}$$

where $\kappa$ is the Von Karman constant.

## 2.2 TEST CASE

Before the CFD-model is applied to the case studies, the model is extensively verified in the hydraulic laboratory of the University of Trento. Therefore, we compare measured flow velocities around a groyne in a laboratory channel (Armanini et al., 2010b) with simulated flow velocity fields to ensure a proper reproduction of the three-dimensional flow fields of the CFD-model. The calibration of the 3D CFD model was carried out by adapting the river bottom roughness. For the 2D model approach the roughness as well as the kinematic viscosity were adapted. In this case, the kinematic viscosity is considered as a constant, since the $k$-$\varepsilon$ turbulence model cannot be applied for 2D

modelling.

The laboratory tests are conducted in a flume with a length of 20 m, a width of 2 m and a discharge of $40\times10^{-3}$ $m^3/s$. The flume has a mobile bed and several groynes are implemented to induce complex three-dimensional flow patterns, which are measured with a 3D Micro-ADV (Acoustic Doppler Velocimeter, SonTek). In the CFD-model, the geometry of the laboratory channel is represented by a computational mesh with a resolution of 0.02×0.02 m in the horizontal plane and 0.01 m vertically.

The measured and simulated velocity fields are compared for two different planes close to the first upstream groyne (Figure 1). Plane A is a horizontal plane with 1 m × 1 m located 0.06 m below the free surface and is located just upstream the first groyne with a distance of 3 m from the inlet. Plane B is a vertical plane with an angle of 60° from the model's centreline, while plane C has an angle of 30° and plane D is parallel to the model's centreline.

The test of the CFD-model on laboratory scale, is important to understand the 3D model capabilities to perform simulations with complex bathymetry and small Reynolds numbers. In fact, the $k$-$\varepsilon$ turbulence model adopted is valid for high Reynolds number ($Re$ > 100˙000) (Wilcox, 2006). If the CFD model is able to well represent the velocity field at laboratory scale ($Re \approx 10˙000$), we can suppose that, in the real test case with high Re, the CFD model can predict plausible results.

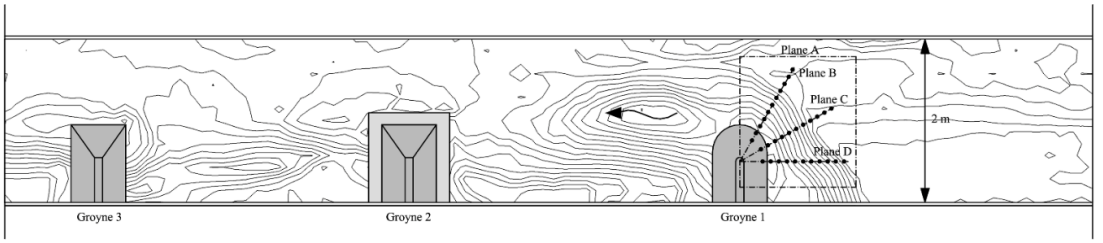


Figure 1. Top view of the laboratory model showing the groynes and the horizontal Plane A and the vertical Plane B for the comparison between measured and simulated velocity fields.

Figure 2A represents the comparison between the measured and the simulated velocity field at the horizontal plane A. Illustrated are the horizontal velocities, which are located 6 cm below the water surface at the planes B, C and D (Figure 1).

The comparison shows that simulated flow velocities of three-dimensional CFD model are in a good agreement with the experimental data, both in magnitude and orientation of velocity vectors. The mean measured velocity (Plane B) is 12.46 cm/s, whereas the mean simulated velocity is 12.66 cm/s yielding a percentage deviation of only 1.6 %. The deviation of the angle between the measured and simulated velocity fields is about 2.5°.

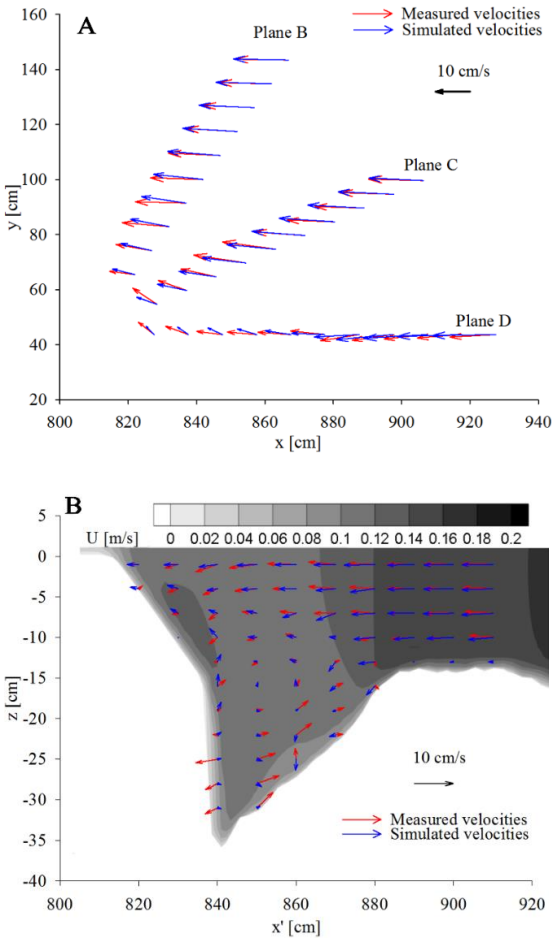


Figure 2. Comparison between measured velocities (red vectors) and simulated velocities (blue vectors) in the horizontal plane A upstream of the groyne (top) and in the vertical plane B (bottom).

In Figure 2B the comparison between the measured and simulated velocity fields at the vertical Plane B is illustrated. Figure 2B indicates that at the upper region of the flow field (0.15 m below the surface) the simulated flow vectors agree well to the measured vectors. In addition, the comparison reveal that the three-dimensional CFD-model seems to properly capture the secondary counter-clockwise circulations that take place in the lower part of the scouring region, although some differences in the vector orientations still occur. It has to be highlighted that Figure

2B represents the velocity vectors projection on plane B, so it does not show the velocity magnitude. From an ecological point of view, is more important to compare the velocity magnitude between measured and simulated values. In this case, we choose to compare bottom velocity values.

To illustrate the differences between 2D and 3D hydrodynamic modelling, the differences of simulated velocity magnitudes to the measured values are represented in Figure 3. This figure includes the measured velocities for all points of Plane B at a distance of 2 cm above the bottom and compares two different simulated velocity fields that are investigated in this study (bottom flow velocities using 3D modelling and bottom flow velocities assuming a logarithmic velocity profile for 2D modelling).

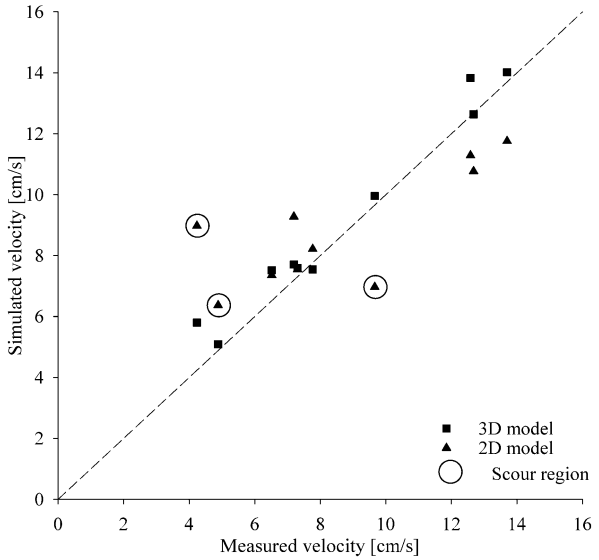


Figure 3. Comparison of simulated bottom velocity fields (2 cm above bottom) using 3D hydrodynamic modelling and 2D depth-averaged results (logarithmic velocity profile) with measured bottom velocities.

The 3D model approach better evaluates the complex velocity field then 2D approach, especially near the bottom.

Figure 3 shows that the velocities magnitudes simulated with the 3D model are in better agreement with the measured values compared

to the depth-averaged velocity magnitudes with a logarithmic velocity profile. The 2D model generally underestimates the velocity values leading to a maximum deviation of 112%. As expected, the largest deviations of the 2D model are concentrated in the area of the recirculation zone of the scour (Figure 1). Consequently, we can argue that the 2D model is not able to properly represent the velocity field in areas of high morphological heterogeneity, where the flow field is characterized by secondary currents.

To further highlight differences between 3D and 2D hydrodynamic modelling (assuming a logarithmic profile), the spatial distribution of the bottom velocity differences is illustrated in Figure 4. This comparison yields a spatial average of 0.02 m/s. This absolute difference seems to be very low, however, the comparison represents laboratory scales. Hence, the mean percentage deviation is a better criterion which is about 25%. Moreover, this difference becomes higher near bathymetric variations, where the formation of secondary circulations strongly alter the hydrodynamic field. If only depth-averaged velocities from 2D modelling are used (as they are commonly used for fish habitat models) the deviations become even higher.

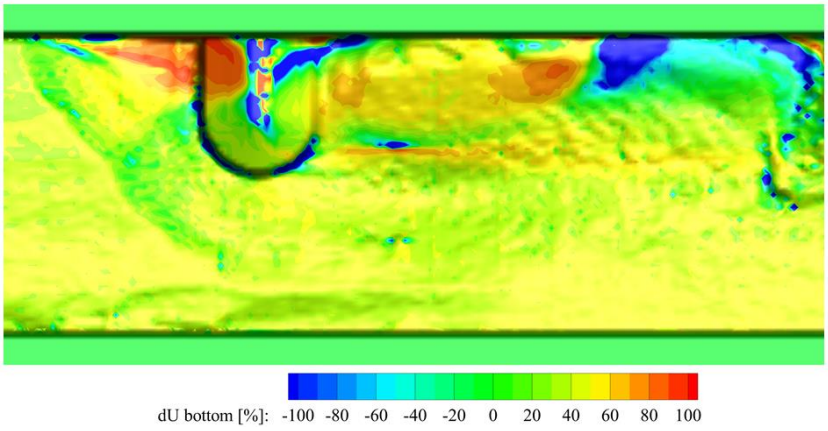


Figure 4. Percentage difference in bottom velocity field between 3D and 2D model.

Moreover, in order to better appreciate the potential of a 3D numerical model and its ability to properly reproduce the fundamental hydrodynamic features in a complex domain, the vorticity fields $\omega_x$ and $\omega_z$ in the proximity of the groyne are reported in Figure 5-Figure 8, both for the 2D and 3D simulations.

Figure 5 shows an isometric view of the vorticity field $\omega_z$ for the 3D model, for values $\omega_z = 0.5\ s^{-1}$ and $\omega_z = -0.5\ s^{-1}$. The figure highlights the formation of a wake zone that starts from the groyne head, and then continues downstream. Figure 6 reports the top view of the depth integrated $\omega_z$ values for 3D simulation. In Figure 6 can be observed the formation of a second recirculation zone in the upstream groyne area. Figure 7 shows the vorticity $\omega_z$ from the 2D CFD model. The comparison between Figure 6 and Figure 7 do not show significant differences in the region downstream the groyne, but significant vorticity discrepancy upstream the groyne can be observed.

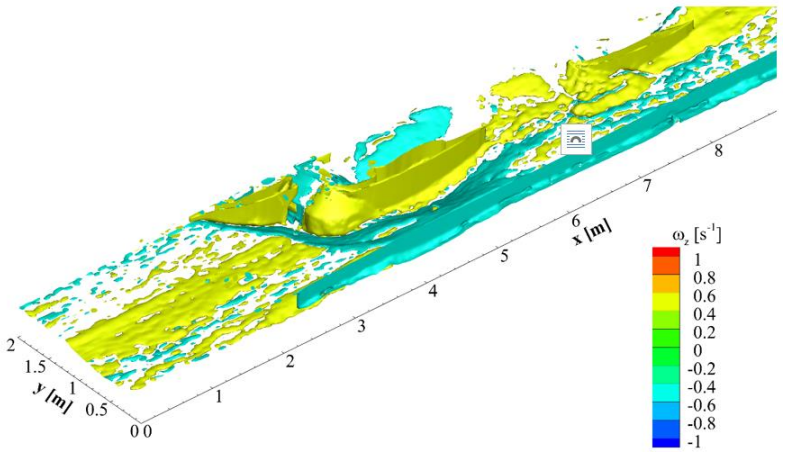


Figure 5. 3D vorticity $\omega_z$ representation from 3D CFD model.

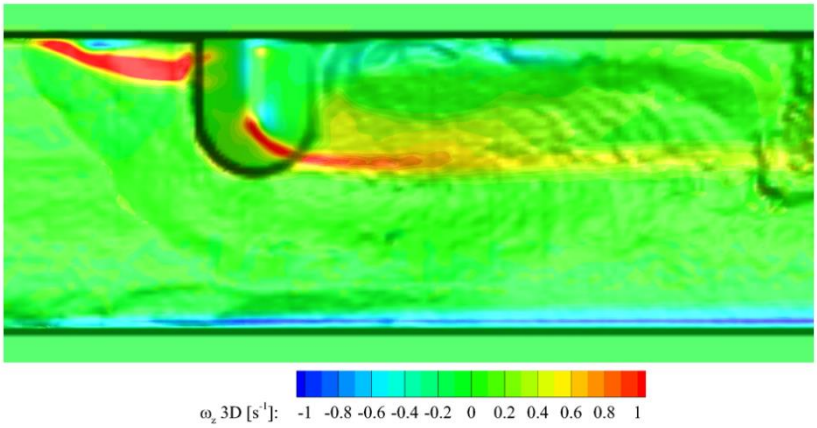


Figure 6. Vorticity $\omega_z$ representation from 3D CFD model.

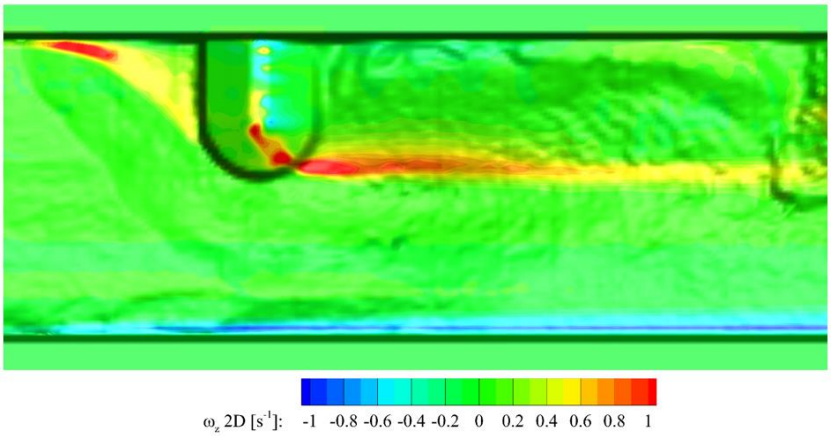


Figure 7. Vorticity $\omega_z$ representation from 2D CFD model.

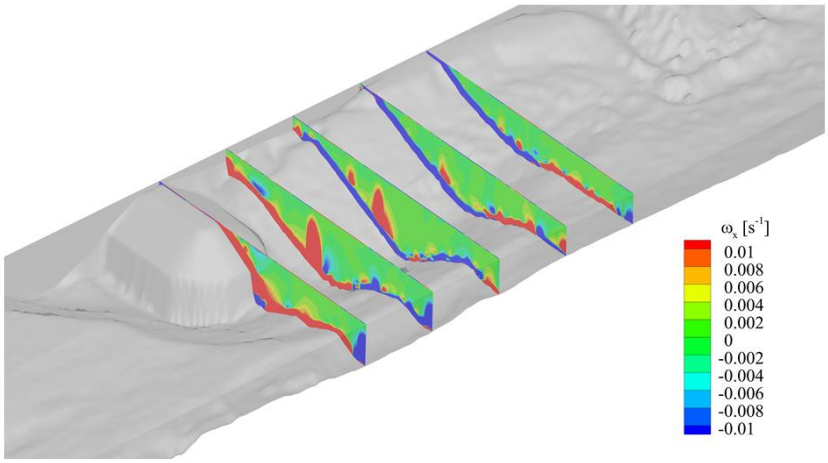


Figure 8. 3D vorticity $\omega_x$ representation from 3D CFD model. Principals sections of interest.

Vorticity $\omega_x$, can not be represented by a 2D model. In Figure 8 the vorticity component $\omega_x$ as obtained by the 3D model is reported at different cross sections. In the figure, the formation of a secondary recirculation is evident, that tends to disappear moving further downstream the groyne head. The evolution of this kind of secondary recirculation is conformal to what observed by (Armanini et al., 2010a), which highlights the importance of the formation of this vortex as a fundamental trigger for the process of sediment deposition and bar formation in intergroynes region.

## 2.3 DISCUSSION

The 3D CFD model was tested through laboratory measurements in a mobile bed laboratory channel with groynes. In this case, the CFD model was able to well represent the flow field near the free surface and the bottom. Although the secondary circulations were not perfectly reproduced in Plane B, the absolute values of the bottom velocities are comparable with the experimental measurements. The average error is 8.6% for the 3D model. The comparison between the experimental measurements and the bottom velocities simulated with a log-law 2D

approach provided an error equal to 26.1%, about 3 times greater than the 3D case. However, it has to be highlighted that these discrepancies between simulated and measured data are unlikely to be due only to the limitations of the numerical simulation, given that at the near bed region, velocity measurements are also affected by a low signal to noise ratio.

Based on the results of the laboratory investigation, the 3D CFD model seems to be capable to well represent the velocity field in very complex bathymetry, especially with regard to the near bottom velocity. This is highly relevant if focal velocities are used as an input in habitat modelling tools, especially because focal flow velocities are more selective from a biological point of view (Heggenes, 2002). Moreover, in context of peak flows during hydropeaking events, the bottom flow velocities are important to adequately represent the availability of shelter habitats.

# 3. HABITAT MODEL DESCRIPTION

## 3.1 CASiMiR MODEL

The habitat simulation tool CASiMiR was developed in the early 1990s at the University of Stuttgart (Germany) and is designed as a habitat tool to facilitate the investigation of riverine habitat suitability for aquatic organisms, with an emphasis on fishes and macrozoobenthos. It enables both modelling habitats via the use of univariate preference curves as well as via a multivariate fuzzy rule – based approach. In this study, the preference curve based approach is applied. In univariate preference functions the suitability of a habitat is a function of a single variable characterizing one of the physical characteristic of the habitat. Each of the univariate preference curves is compared with the physical properties of a location in the river to derive a variable-specific HSI-value (between 0 and 1). Subsequently, the single suitability indices must be combined to define a composite suitability index, which can be done using different mathematical operators (product, minimum, arithmetic mean, geometric mean) (Kopecki, 2008). An overview of the univariate preferences approach using the habitat variables water depth, flow velocity and dominant substrate is present in (Schneider et al., 2010).

The required input data (water depth, flow velocity) are usually provided from hydrodynamic models, while the dominant substrate is a mapped parameter. Hence, the performance of habitat simulations strongly depend on the quality of the simulated and mapped input parameter. CASiMiR conducts the habitat simulation for each grid cell of the computational mesh to provide information about the spatial habitat distribution of HSI-values in form of habitat maps. Another evaluation is based on the integration of HSI values and the hydraulic characteristics of the stream, the Weighted Usable Area (WUA) or the

Hydraulic Habitat Index for a target species or life stage that can be estimated as a function of the flow rate.

In this study, the parameter-specific habitat suitability values are linked using the product method, which represent the most applied approach (Ahmadi-Nedushan et al., 2006). The product method is based on the assumption that fish selects each particular variable independently of other variables (Bovee, 1986). The target species in this study is the brown trout, of which we investigate the life stages of the young-of-the-year (YOY) and the adult life stage.

The applied preference curves are based on a literature study (Heggenes, 1996; Heggenes and Wollebæk, 2013) including a wide range of different river types. The actual habitat state of the Valsura River is strongly influenced by hydropeaking, resulting in a quasi-complete absence of fish. Hence, potential habitat areas in the present case study are defined in close collaboration with local limnology experts during a field campaign. Based on this survey, the preference curves are slightly modified (Figure 9) to better represent the present case study.

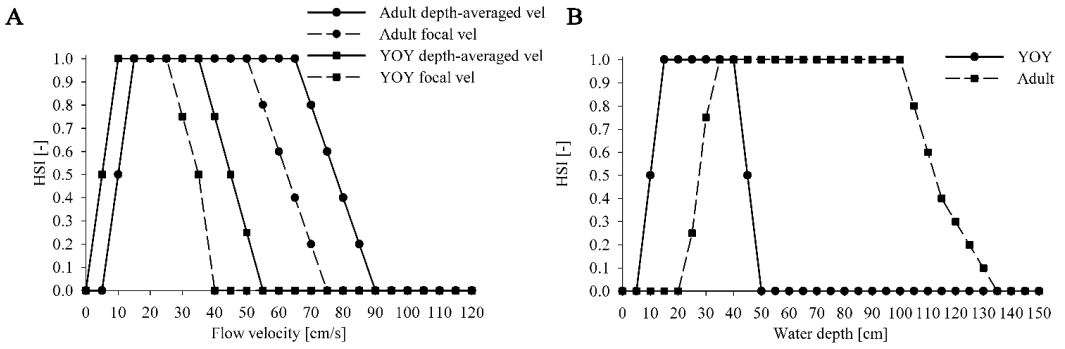


Figure 9. Preference curves of flow velocity (A) and water depth (B) for brown trout for both life-stages adult and YOY considering depth-averaged and focal velocities.

Figure 9 indicates that the preferences of the focal velocities (dashed line) are more restrictive compared to the preferences of the depth-averaged velocities, because the focal velocity is related to net energy gain (Hill and Grossman, 1993).

In this study, we use the preference curves for depth-averaged velocity for habitat simulations with the output from 2D hydrodynamic modelling, while the preference curves for the focal velocity are used for the velocity fields obtained by applying the logarithmic law on the 2D model results as well as for the bottom velocities obtained from fully 3D hydrodynamic modelling. In literature, differences in preference curves depending the n-dimensional hydraulic model have not been found.

Three types of velocity field are investigated.

Therefore, the three investigated methods (depth-averaged velocities from 2D modelling; bottom velocities from 2D modelling using the logarithmic-law; bottom velocities from 3D modelling) to simulate the velocity field are used as input for habitat modelling with CASiMiR.

## 3.2 2D AND 3D APPROACH

The method of Casulli and Zanolli (2002) to solve the RANS equations allows for a straightforward conversion of 3D modelling to 2D modelling, simply by using only one cell in the vertical direction. In this way, the depth-averaged flow velocity field is calculated, which is consistent with the common two-dimensional shallow water approach (Casulli and Zanolli, 2002).

One opportunity to obtain information on bottom flow velocity using 2D hydrodynamic modelling is represented by the application of the modified velocity distribution law of (Bezzola, 2002). Based on his approach the flow velocity 6 cm above the bottom $U_{0.06}$ can be calculated using the depth-averaged velocity ($U_{2D}$), the shear velocity ($u^*$) and the water depth ($h$)). The $U_{2D}$ is considered as the velocity at

0.4 $h_t$ (Kopecki, 2008).

$$U_{0.06} = U_{2D} + \frac{u^*}{c_r\,\kappa}\ln\left(\frac{0.06}{0.4\,h_t}\right) \tag{10}$$

where $\kappa$ is the Von Karman constant, $h_t$ is the total water depth for a log-law velocity profile and $c_r$ (always lower than one) is the damping factor that accounts for the reduction of the relative near-bed velocity with decreasing relative submergence (Kopecki, 2008).

# 4. CASE STUDIES

## 4.1 VALSURA RIVER

### 4.1.1 Study area

Valsura River flows through Val D'Ultimo Valley and springs in the eastern Ortles mountain range on the foot of the 3,439 meters high mount Zufritt (46° 30' 7'' N, 10° 46' 56'' E) in the Italian Alps. It draws water from a catchment area of 282 km$^2$ and is 41.4 km long (Figure in Appendix 1).

The last hydropower plant in the Valsura cascade is Lana HPP. Lana HPP draws the water of Alborelo weekly reservoir on Valsura River and of the auxiliary intakes on Marano Creek and on Monte Chiesa Creek. When the discharge from the auxiliary intakes exceeds the turbined discharge at Lana HPP, the water flows back to the intake of the plant and gets stored in Alborelo reservoir. In average, 11% of the annual total water volume inflowing Alborelo reservoir is released as reserve flow into Valsura River. Over the whole year, Lana HPP has to release water from its tailrace channel in order to meet irrigational demand (Figure 10).

The hydropeaked stretch on Valsura River starts from the outlet of Lana hydropower plant on 314 m a.s.l. and ends, on 265 m a.s.l. at the confluence with Adige River. The hydropeaked stretch is approximately 4.5 km long, with a catchment area of 10 km$^2$ and a moderate average bed slope of about 1.2%.

Different morphological characteristics can be observed (Figure 10, Table 2) in the hydropeaked stretch (Appendix 2). The upstream stretch (Stretch 1), where the riverbed is restricted between retaining walls and riverbanks, is 1.1 km long. Natural bars and islands formed by larger masses and gravel banks are present in the 1.4 km long intermediate stretch (Stretch 2), together with hydraulic elements such as step-pools,

embankments and floodbanks; at the end of this stretch the discharge gauging station is located.

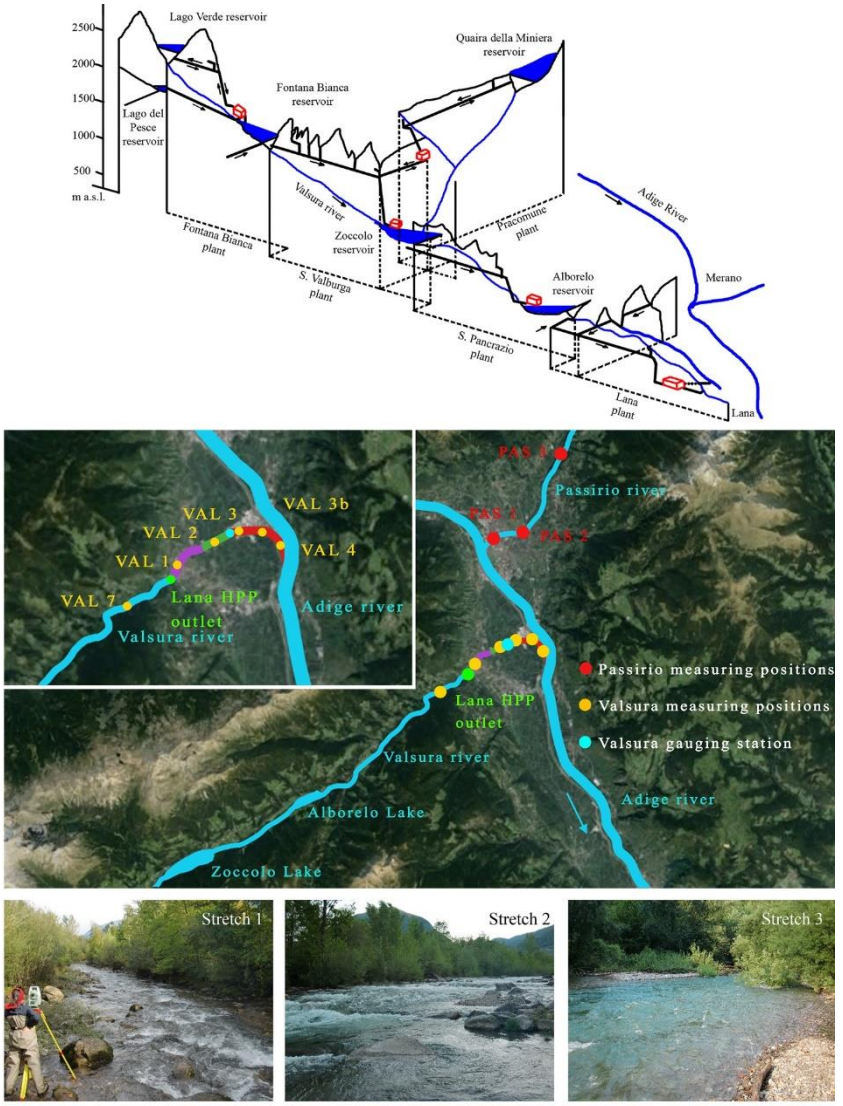


Figure 10. Valsura Hydraulic System and overview of Hydropeaking investigation area. Ecological measuring positions on Passirio and Valsura River are highlighted. The three stretches represented in the figure are morphologically different: Stretch 1 (purple, left photo), upstream, is canalized; Stretch 2 (green middle photo) enlarges and presents several hydraulic structures; Stretch 3 (red, right photo) is in the biotope area with quasi-braided structures.

In the final stretch reaching from the gauging station to the confluence with Adige River, the Valsura has similar characteristics to a natural stream, with large gravel banks and braiding morphology. Here the river flows through a biotope; during peaking operation of the hydropower plant, the river floods a riparian forest; the vegetation, the morphological characteristics, the discharge conditions and the riparian forest create important ecological niches for plants and animals.

Over the last years, river training structures such a sills and bars were removed or modified in order to allow fish migration over the hydropeaked stretch.

Table 2. Morphological characteristics in the hydropeaked stretch in Valsura River.

| | Slope | $d_{50}$ | $d_{90}$ | Width $Q_{min}$ | Width $Q_{hydropeaking}$ | Floodplain width |
|---|---|---|---|---|---|---|
| | [-] | [mm] | [mm] | [m] | [m] | [m] |
| Stretch 1 | 2.9 % | 8.6 | 32.7 | 10 | 15 | 20 |
| Stretch 2 | 1.9 % | 4.4 | 22.7 | 20 | 30 | 55 |
| Stretch 3 | 0.3 % | 6.3 | 31.0 | 13 | 70 | 100 |

### 4.1.1 Hydraulic characterization

In order to gain a comprehensive picture of the hydropeaking impact and to being able to assess the biological and ecological quality and potential of the Valsura River, hydrological analyses of the flow regime and an extensive biological measurement campaign were performed.

The hydrological analysis was based on the data publically available in 10 minutes resolution at the gauging station of the period between 2011 and 2014.

The hydrological parameters investigated in first place were the maximum discharge ($Q_{max}$ [$m^3/s$] = maximum discharge), the minimum discharge ($Q_{min}$ [$m^3/s$] = minimum discharge), the positive ramp rate

($\Delta Q^+$ [$m^3/s/min$] = average positive flow rate variation in one minute (from minimum to maximum), the negative ramp rate ($\Delta Q^-$ [$m^3/s/min$] = average negative flow rate variation in one minute (from maximum to minimum)). The typical minimum and maximum flow in Valsura River downstream of the tailrace channel are listed in Table 3.

Lana HPP produces peak energy throughout the whole year. The maximum turbine discharge of the HPP is 26.25 $m^3/s$. In the investigated period (2011-2014) two typical hydropeaking hydrographs could be observed at Valsura gauging station downstream of Lana HPP:

- single peak production profile (e.g. in the first week of June 2013) (Figure 11A): the plant produces for several hours without interruptions; in this regime the maximum discharge does not necessarily reach the design flow of the HPP;
- double peak production profile (e.g. last week of June 2013) (Figure 11B): during a single day the plant does not produce continuously and the hydrograph shows two or more maximum flow situation during the day.

After the series of accidents in which bathing persons were trapped on gravel banks in the hydropeaked stretch, the operator of Lana HPP decided to adopt a 3-stage step-wise up-ramping hydrograph in order to increase the hydraulic safety as displayed in Figure 12.

Table 3 shows that the ratio between maximum and minimum flow rate can reach values of about 34 during maximum load energy production in January. Furthermore, the positive ramp rate, measured at the gauging station, is on average equal to 2.33 $m^3/s/min$. Consequently, in the gauging station cross section, the complete variation from minimum to maximum flow rate takes place in about 10 minutes.

The negative ramp rate is on average equal to 1.40 $m^3/s/min$. In about 17 minutes, actually, the flow rate returns from maximum to minimum.

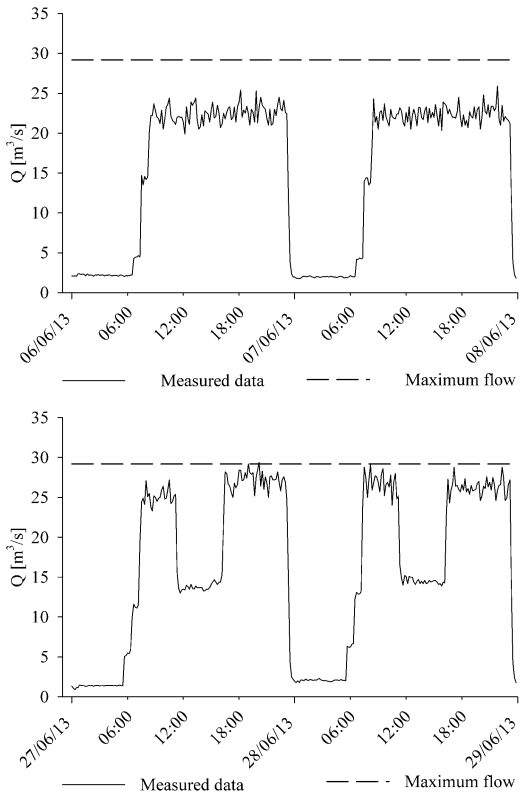


Figure 11. Characteristic hydropeaking discharge with single (A) and double (B) peak production mode.

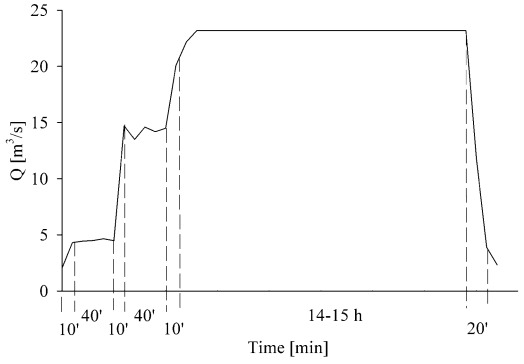


Figure 12. Characteristic up-ramping and down-ramping.

Table 3. Actual state: typical minimum and maximum flow discharges in Valsura hydropeaked stretch.

| Month | | Jan | Feb | Mar | Apr | May | Jun | Jul | Ago | Sep | Oct | Nov | Dec |
|---|---|---|---|---|---|---|---|---|---|---|---|---|---|
| **Minimum flow in the hydropeaked stretch $Q_{max}$** | **[m³/s]** | **0.79** | **0.73** | **0.80** | **1.10** | **2.63** | **2.94** | **1.80** | **1.50** | **1.38** | **1.60** | **1.52** | **1.04** |
| Design Discharge Lana HPP | [m³/s] | | | | | | 26.25 | | | | | | |
| Min. Irrigation withdrawal | [m³/s] | 0.30 | 0.30 | 0.30 | 2.65 | 2.65 | 2.65 | 2.65 | 2.65 | 2.65 | 1.00 | 0.30 | 0.30 |
| **Maximum flow in the hydropeaked stretch $Q_{min}$** | **[m³/s]** | **26.74** | **26.68** | **26.75** | **24.70** | **26.23** | **26.54** | **25.40** | **25.10** | **24.98** | **26.85** | **27.47** | **26.99** |
| **Pos. ramp rate $\Delta Q^+$** | **[m³/s/min]** | **1.99** | **2.12** | **2.32** | **2.47** | **2.89** | **2.41** | **2.74** | **2.37** | **1.90** | **2.54** | **2.09** | **2.07** |
| **Neg. ramp rate $\Delta Q^-$** | **[m³/s/min]** | **1.26** | **1.18** | **1.20** | **1.32** | **1.65** | **1.41** | **1.66** | **1.36** | **1.23** | **2.19** | **2.18** | **1.62** |

The analysis of flow rates measured by the gauging station for the year 2014 are reported below.

Figure 13 show the complete flow rate for year 2014. Is possible to observe that the Valsura River is strongly influenced by Lana HPP energy production with daily and sub daily flow peaks. Moreover, the natural flow is modified by the Zoccolo and Alborelo reservoirs.

In Figure 14 the flow duration curve (solid line) and the duration curve considering daily average flow rate (dashed line) are reported. The curves are significantly different, meaning that the daily intermittency induced by production is strong. Hydropeaking implies an increase of frequency of high and low flow rates in the studied reach. The average flow duration curve, in fact, can be considered as the "natural" flow rate in the reach as the Lana HPP is not operating.

Figure 15 shows the comparison between maximum, minimum and average flow rate for each month. It is possible to note that in October the mean flow rate is very low. It is due to a long period of no production by Lana HPP. Moreover, the maximum flow rate between May and August present values higher than 26.25 m³/s due to a higher base flow. In the same figure are also reported the 95 and the 60 percentile both for maximum ($Q_{max,95\%}$; $Q_{max,60\%}$) and minimum flow rate ($Q_{max,95\%}$; $Q_{max,60\%}$). Theses values are used to remove possible errors during measurements. Figure 16 represent the up (max) and down (min)

The Valsura River is strongly influenced by Lana hydropower plant

ramping rate in [$m^3$/s/min]. Is possible to observe that the up ramping rate is always higher, in absolute value, respect the down ramping rate. This aspect is due to a different celerity propagation between the front and the tail a water wave (Toffolon et al., 2010).

Finally, in Figure 17 the ratio between maximum and minimum flow rate ($R_Q$) are reported. The maximum ratio ($R_{Q,max}$) in July, September and October is influenced by the presence of high flow rate and a very low minimum flow rates. For this reason, are also reported the 95 percentile ($R_{Q,95\%}$). The $R_{Q,95\%}$ presents more uniform values than $R_{Q,max}$.

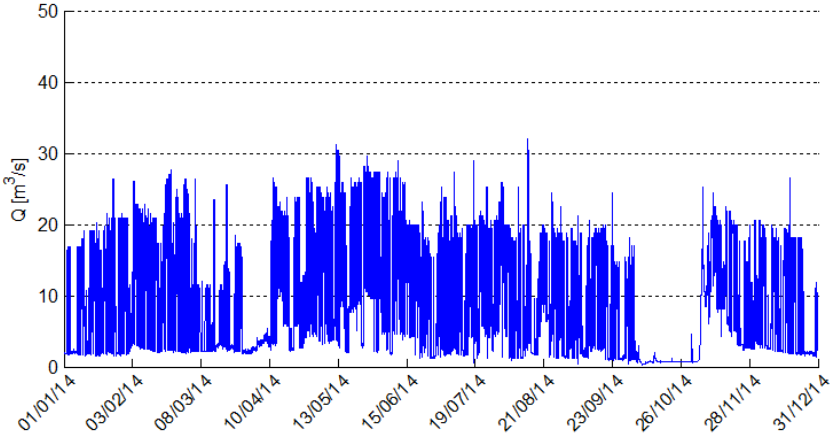


Figure 13. Flow rate measured at gauging station. Valsura River 2014.

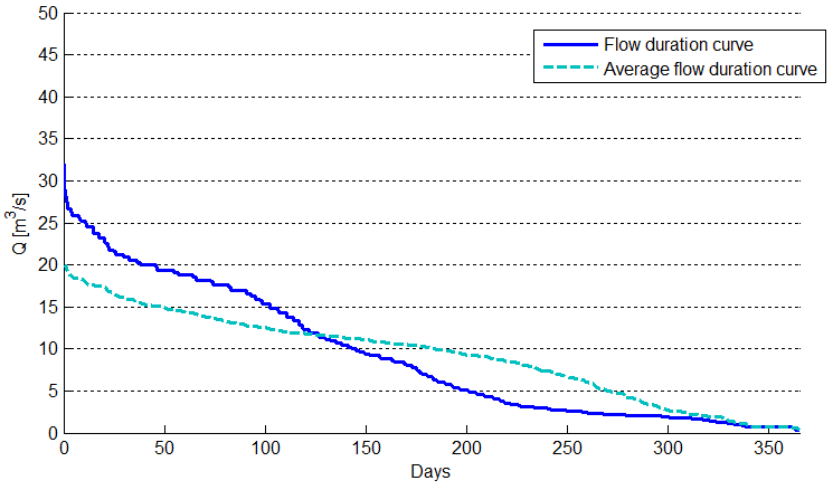


Figure 14. Flow duration curve and average flow duration curve. Valsura River 2014.

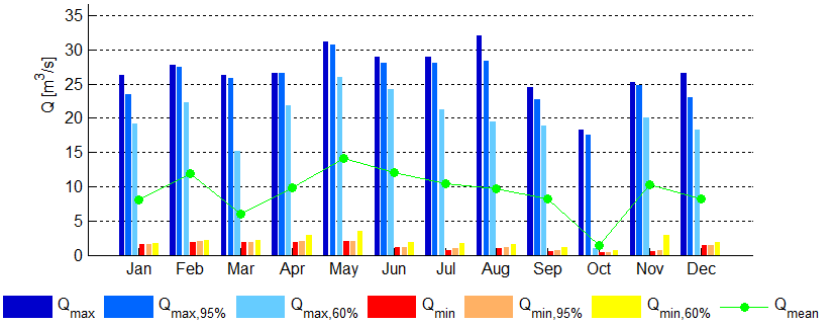


Figure 15. Maximum and minimum flow rates. Valsura River 2014.

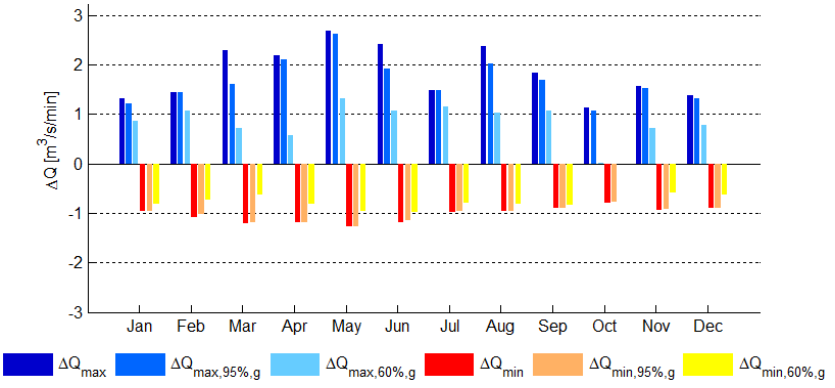


Figure 16. Positive and negative ramping rates. Valsura River 2014.

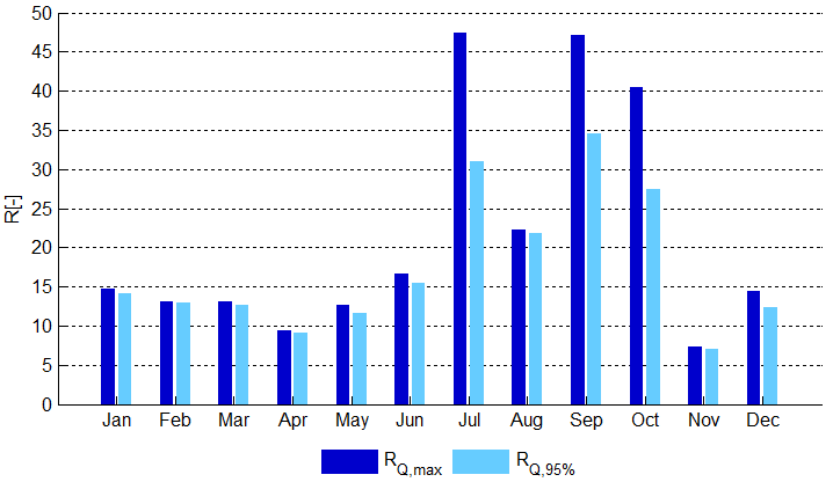


Figure 17. Ratio between maximum and minimum flow rate. Valsura River 2014.

### 4.1.2 Ecological characterization

Hydropeaking can affect the aquatic organisms in different ways (Schweizer et al., 2015). Since the hydropower plants on Valsura Cascade had been already constructed in the fifties, there is no ecological evidence available on the original natural ecological state of the Valsura River before the hydropower development. Therefore, an ecological and hydrological similar alpine river has to be investigated as a natural reference river for a water body not influenced by hydropeaking (Schweizer et al., 2013). The Passirio River is the river chosen for the ecological comparison, whose confluence with Adige River is located approximately 10 km upstream of Valsura River's confluence. With a catchment area of 427 km$^2$, it presents similar morphological and hydraulic characteristics to Valsura River. The biological and ecological samplings in Passirio River were performed at three sites located in the lower reach, and are called PAS1, PAS2 and PAS3, VAL3b (Figure 10).

Due to the strong influence of Lana HPP on Valsura River, the ecological status is compared with unaffected Passirio River.

In order to assess the ecological situation in the hydropeaked Valsura River biological and ecological samplings in Valsura River were

performed at 6 sites located. The positions located downstream of the Lana HPP are called VAL1, VAL2, VAL3, VAL3b,VAL4, and the only site not located in the hydropeaked stretch is located upstream of Lana HPP, at position VAL7.

Figure 10 shows the measuring points used for ecological comparison between the two streams.

The species used for biological comparisons are the macrozoobenthos (MZB) (Plecoptera, Trichoptera, Coleoptera and Ephemeroptera) and parr life stage for the brown trout. Even if the brown trout is not a target species, the brown trout, compared with Salmo trutta marmoratus, presents similar habitat preference especially for young life stages. In fact, in literature, the two species are usually confused and both used as a reference for habitat analysis (Armstrong et al., 2003).

The choice of the above MZB is due by the fact that they are usually present in similar Alpine rivers. The MZB samplings are performed to quantify the number of individuals per $m^2$. Nine small areas (33 × 33 cm) are used to quantify the MZB for each measuring point. The areas present uniform gravel size (2-8 cm of diameter). For the parr life stage for brown trout, instead, the sampling regards the count of individuals per 100 m of bank where the water depth is between 1 cm and 20 cm. The parr life stage, which is a young fish phase, tends to locate in areas with low water depths and low flow velocities, hydraulic conditions that are typically present along banks (Heggenes, 1996).

Figure 18A represents the MZB individual density on three measuring positions on Passirio River (PAS1, PAS2 and PAS 3) and on Valsura River (VAL1, VAL2, VAL 3, VAL 3b, VAL4) (Figure 10).

It can be noted that in Valsura River the MZB density is much lower than in Passirio River, thus indicating that the MZB conditions in Valsura River are widely compromised, despite the substrate characteristics in Valsura reach (Table 2) appears generally favourable

The Valsura River is strongly impacted by hydropower production with a consequent low habitat quality

(Tanno, 2012).

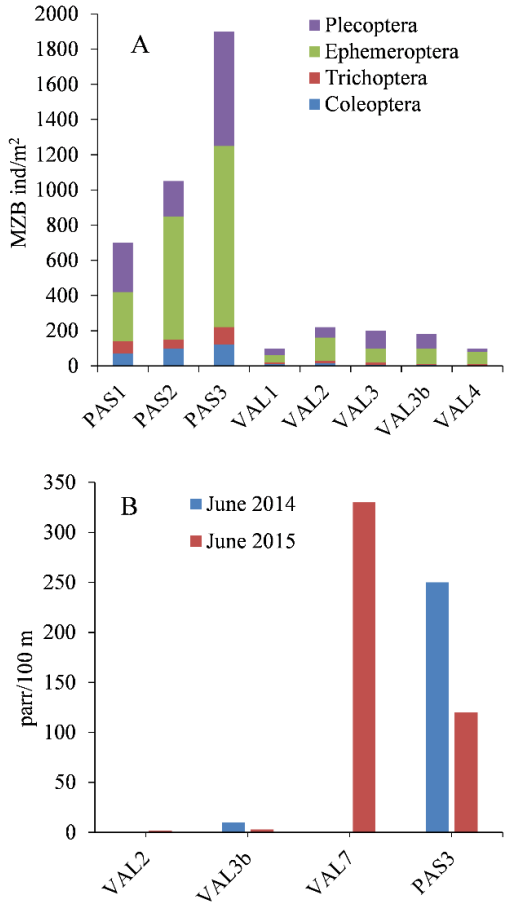


Figure 18. A: individual MZB density on Passirio River and on Valsura River. B: number of trout parr/100 m of bank. VAL2 and VAL3b are two measurement points in the Valsura hydropeaked stretch and VAL7 is in the Valsura environmental flow stretch upstream the Lana HPP outlet; PAS3 measuring point is used as comparison.

Finally, the fish population is analysed (Figure 18B). It is evident that upstream the Lana HPP (VAL7), the number of trout parr/100 m are similar or higher to the number measured at Passirio River (PAS3). Downstream Lana HPP (VAL2 and VAL3b) there is a dramatic reduction of fish population density, thus indicating the strong effect of

hydropeaking.

The results show that the food supply for fish (MZB) is limited and much lower than in other reaches not subject to hydropeaking. This is underlined by a macrozoobenthos measuring campaign performed at the unaffected Passirio River.

## 4.2 RIO SELVA DEI MOLINI

### 4.2.1 Study area

Rio Selva dei Molini flows through the same name valley and springs after the confluence between the Rio Evis and the Rio Cesa. The higher point of the catchment area is Mesule mount with 3,749 m a.s.l. (46° 59' 34'' N, 11° 47' 03'' E). It draws water from a catchment area of 110 km$^2$ and is 14.7 km long.

The last hydropower plant in the Rio Selva dei Molini is Molini di Tures HPP (Molini HPP). Molini HPP draws the water of the small Selva dei Molini Lake and of the auxiliary intakes on Luppoleto Creek, on Canopi Creek and on Ponte Creek.

The hydropeaked stretch on Rio Selva dei Molini starts from the outlet of Molini HPP on 876 m a.s.l. and ends, on 850 m a.s.l. at the confluence with Aurino River. The hydropeaked stretch is approximately 940 m long, with an average bed slope of about 2.1%.

The hydropeaked reach presents uniform morphological characteristics (Figure 20 center, Table 4). The stretch, in fact, is restricted between retaining walls and riverbanks with vegetation. The only instream structure is present near the confluence with Aurino River and it is made of boulders (Figure 20, right).


Figure 19. Rio Selva dei Molini overview of Hydropeaking investigation area. Ecological measuring positions are highlighted.

Table 4. Morphological characteristics in the hydropeaked stretch in Rio Selva dei Molini.

| Slope | $d_{50}$ | $d_{90}$ | Width $Q_{min}$ | Width $Q_{hydropeaking}$ | Floodplain width |
|---|---|---|---|---|---|
| [-] | [mm] | [mm] | [m] | [m] | [m] |
| 2.1 % | 9.3 | 45.0 | 6 | 7 | 7 |

Figure 20. Typical section of the Rio Selva dei Molini. Right: Molini HPP outlet. Center: Rio Selva dei Molini in the hydropeaked part. Left: confluence between Rio Selva dei Molini and Aurino River.

### 4.2.2 Hydraulic characterization

In order to gain a comprehensive picture of the hydropeaking impact and to being able to assess the biological and ecological quality and potential of the Rio Selva dei Molini, hydrological analyses of the flow regime and an extensive biological measurement campaign were performed.

Unfortunately, in the hydropeaked reach a gauging station for the flow measurements is not present.

The flow that characterizes the hydropeaked reach is calculated by the sum of different components as described below:

1. Rio Luppoleto and Rio dei Canopi;
2. minimum release flow from Selva dei Molini lake;
3. natural flow from catchment area.

The flow from Rio Luppoleto and Rio dei Canopi is know only for its annual mean value and defined by the Province of Bolzano. To obtain a monthly value, the annual mean value is scaled by the average monthly

flow rate and by the relative catchment areas.

The natural flow from the catchment area is obtained by the monthly unitary flow rates [$m^3/km^2/s$]. These coefficients are proposed by the Province of Bolzano.

Table 5. Upstream monthly flow rate the Molini HPP outlet.

| Month | Jan | Feb | Mar | Apr | May | Jun | Jul | Aug | Sep | Oct | Nov | Dec |
|---|---|---|---|---|---|---|---|---|---|---|---|---|
| **Rio Luppoleto e Rio dei Canopi [$m^3/s$]** | 0.026 | 0.020 | 0.025 | 0.040 | 0.163 | 0.248 | 0.202 | 0.121 | 0.092 | 0.093 | 0.065 | 0.039 |
| **Minimum release flow [$m^3/s$]** | 0.230 | 0.230 | 0.230 | 0.230 | 0.230 | 0.230 | 0.230 | 0.230 | 0.230 | 0.230 | 0.230 | 0.230 |
| **Natural flow [$m^3/s$]** | 0.202 | 0.153 | 0.191 | 0.315 | 1.268 | 1.934 | 1.572 | 0.947 | 0.717 | 0.726 | 0.508 | 0.304 |
| **Total flow rate upstream the outlet [$m^3/s$]** | **0.458** | **0.403** | **0.446** | **0.585** | **1.661** | **2.411** | **2.002** | **1.296** | **1.039** | **1.050** | **0.804** | **0.573** |

In the hydropeaked reach, the total flow rate reported in Table 5 is increased by the Molini HPP release. The maximum turbined flow rate is 7 $m^3/s$, but a part of this flow rate is derived to feed the artificial channel "Mühlener Wiere" where seven small hydropower plants are present. The minimum flow rate in Mühlener Wiere is 0.59 $m^3/s$, whereas the maximum flow rate is 1.5 $m^3/s$. The total flow rate in hydropeaked reach is reported in Table 6.

Moreover, an analysis of the turbined flow rates are performed in order to study the hydrological parameters: the maximum discharge ($Q_{max}$ [$m^3/s$] = maximum discharge), the minimum discharge ($Q_{min}$ [$m^3/s$] = minimum discharge), the positive ramp rate ($\Delta Q^+$ [$m^3/s/min$] = average positive flow rate variation in one minute (from minimum to maximum), the negative ramp rate ($\Delta Q^-$ [$m^3/s/min$] = average negative flow rate variation in one minute (from maximum to minimum)).

Table 6. Minimum and maximum flow rate in the hydropeaked reach.

| **Month** | **Jan** | **Feb** | **Mar** | **Apr** | **May** | **Jun** | **Jul** | **Aug** | **Sep** | **Oct** | **Nov** | **Dec** |
|---|---|---|---|---|---|---|---|---|---|---|---|---|
| **Total flow rate upstream the outlet [$m^3/s$]** | 0.46 | 0.40 | 0.45 | 0.59 | 1.66 | 2.41 | 2.00 | 1.30 | 1.04 | 1.05 | 0.80 | 0.57 |
| **Maximum flow rate from Molini HPP [$m^3/s$]** | | | | | | | 7.0 | | | | | |
| **Mühlener Wiere [$m^3/s$]** | | | | | | | -0,59 / -1.5 | | | | | |
| **Maximum flow rate in hydropeak reach [$m^3/s$]** | **5.96** | **5.90** | **5.95** | **6.09** | **7.16** | **7.91** | **7.50** | **6.80** | **6.54** | **6.55** | **6.30** | **6.07** |
| **$Q_{max}/Q_{min}$ [-]** | **12.95** | **14.75** | **13.22** | **10.32** | **4.31** | **3.28** | **3.75** | **5.23** | **6.29** | **6.24** | **7.88** | **10.65** |

The turbined flow rates are not directly measured by the Alperia company, but derived by the energy production measured every 10 minutes.

The analysis of turbined flow rates for the year 2014 are reported below.

Figure 21 show the complete turbined flow rate for year 2014. Is possible to observe that the Molini HPP strongly influences Rio Selva dei Molini during energy production with daily and subdaily flow peaks.

In Figure 22 the flow duration curve (solid line) and the duration curve considering daily average flow rate (dashed line) are reported. The flow rate alteration induced by energy production is clears visible. Hydropeaking implicate an increase of frequency of high and low flow rates in the studied reach.

Figure 23 shows the comparison between maximum, minimum and average flow rate for each month. The maximum flow rate is always lower than 7 $m^3/s$. In the same figure are also reported the 95 and the 60 percentile both for maximum ($Q_{max,95\%}$; $Q_{max,60\%}$) and minimum flow rate ($Q_{max,95\%}$; $Q_{max,60\%}$). Theses values are used to remove possible errors during measurements.

Figure 24 represent the up (max) and down (min) ramping rate in [$m^3/s/min$]. Is possible to observe that the up ramping rate is, in absolute value, very similar to the down ramping rate. Therefore, the duration of

HPP's startup and shutdown is very similar.

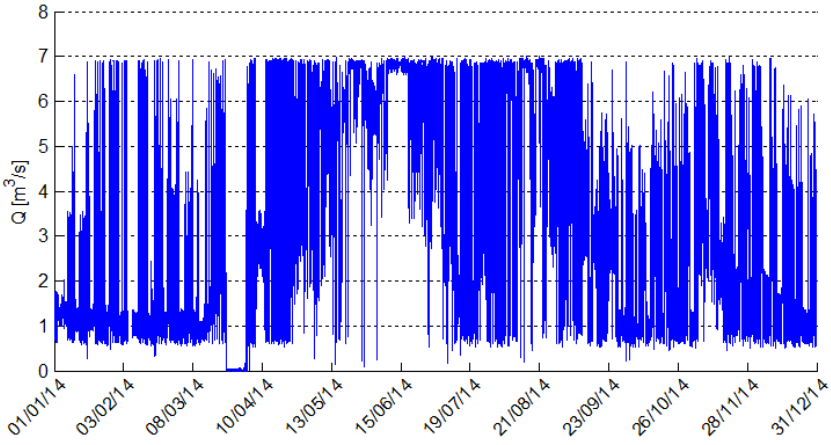


Figure 21. Flow rate turbined. Molini HPP 2014.

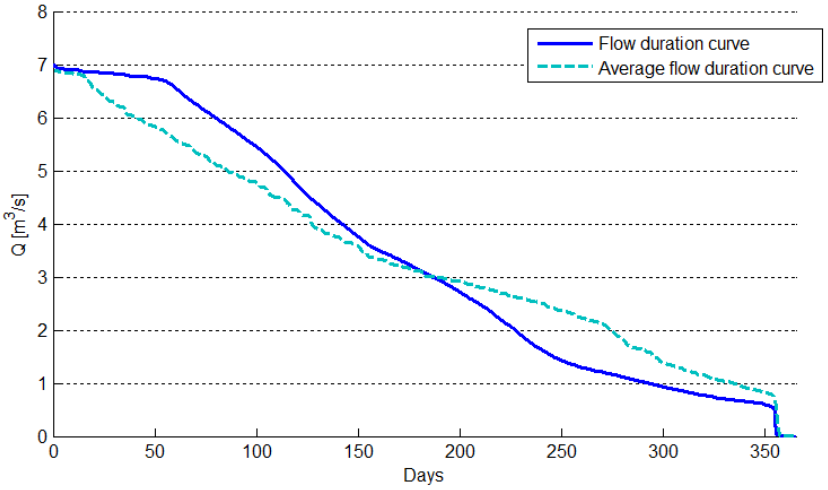


Figure 22. Flow duration curve and average flow duration curve. Molini HPP 2014.

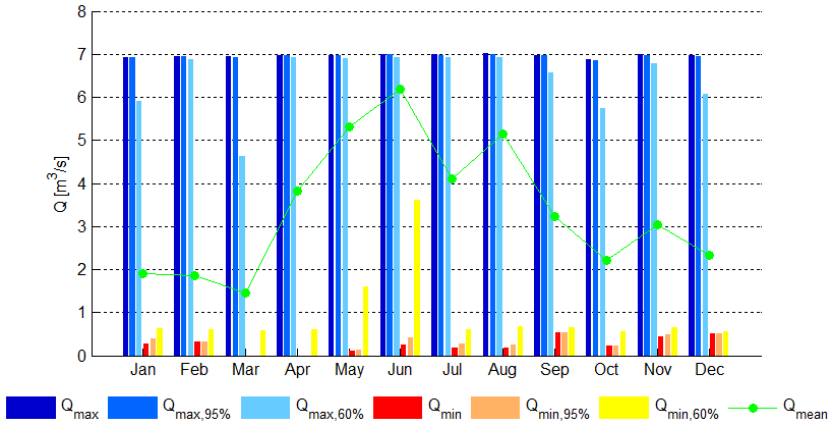


Figure 23. Maximum and minimum flow rates. Molini HPP 2014.

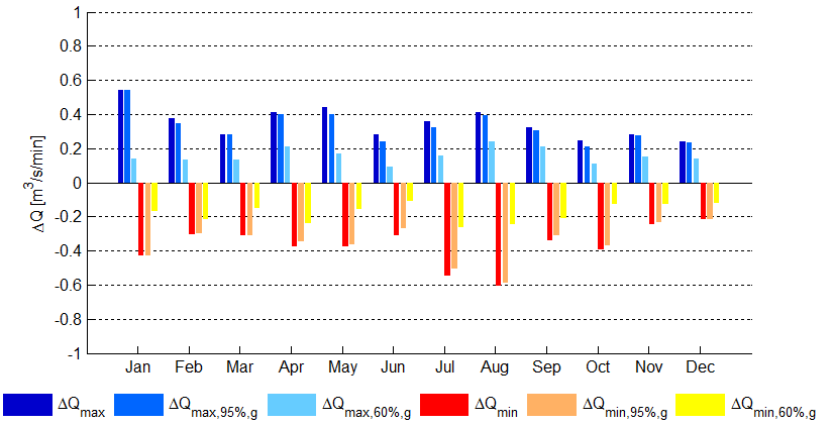


Figure 24. Positive and negative ramping rates. Molini HPP 2014.

### 4.2.3 Ecological characterization

In order to assess the ecological situation in the hydropeaked Rio Selva dei Molini, biological and ecological samplings in two sites were performed. The position located downstream of the Molini HPP is called MTu4 (140 m upstream the confluence with Aurino River), and the site not located in the hydropeaked stretch is located upstream of Molini HPP outlet, at position MTu3 (Figure 19). It must be highlighted that MTu3 could not be used as a reference site for a not disturbed reach by hydropeaking, because the flow rate present is the minimum environmental flow. However, the comparison between MTu3 and

MTu4 can show the influence of flow oscillation on biota.

The species used for biological comparisons are the macrozoobenthos (MZB) (Diptera, Plecoptera, Trichoptera, Coleoptera and Ephemeroptera) and the brown trout. Even if the brown trout is not a target species, the brown trout, compared with Salmo trutta marmoratus, presents similar habitat preference especially for young life stages. In fact, in literature, the two species are usually confused and both used as a reference for habitat analysis (Armstrong et al., 2003).

As for Valsura River, the choice of the above MZB is due by the fact that they are usually present in similar Alpine rivers. The MZB samplings are performed to quantify the number of individuals per $m^2$. Nine small areas (33 × 33 cm) are used to quantify the MZB for each measuring point. The areas present uniform gravel size.

For the brown trout the indices used are the population density [ind/ha] and the unitary biomass [kg/ha]. The samples are taken using electrofishing.

Table 7. Population density and unitary biomass of fish in MTu3 and MTu4.

| Sample point | Date | Length [m] | Width [m] | Population density [ind/ha] | Unitary biomass [kg/ha] |
|---|---|---|---|---|---|
| **MTu3** | 24/07/2013 | 82 | 7 | 2364 | 192 |
| **MTu4** | 12/09/2013 | 87 | 6 | 1760 | 158 |
| **MTu3** | 24/07/2014 | 82 | 7 | 3151 | 270 |
| **MTu4** | 03/09/2014 | 128 | 6 | 1117 | 98 |
| **MTu3** | 07/07/2015 | 82 | 7 | 2577 | 211 |
| **MTu4** | 13/07/2015 | 79 | 6 | 1519 | 138 |

Rio Selva dei Molini is ecologically lower impacted than Valsura River, but shows anyway the effects of hydropeaking on MZB.

Figure 25 represents the MZB individual density on the two measuring positions.

It can be noted that in the hydropeaked reach of Rio Selva dei Molini, the MZB density is much lower than in MTu3, thus indicating that hydropeaking influence the MZB conditions.

Finally, the fish population is analysed (Table 7). It is evident that upstream the Molini HPP outlet, the number of trout ind/ha are higher then in the hydropeaked reach.

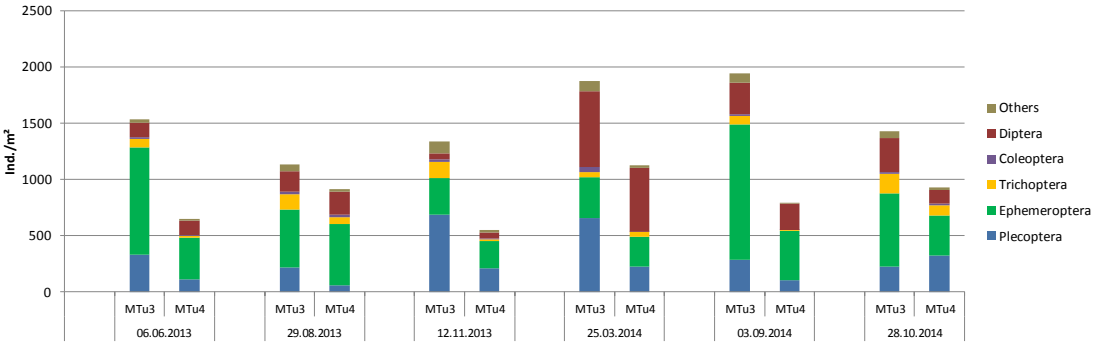


Figure 25. MZB population density. Rio Selva dei Molini MTu3 and MTu4.

# 5. HYDRAULIC MODEL AND HABITAT MODELLING

## 5.1 VALSURA RIVER HYDRAULIC MODEL

The hydraulic model is tested and calibrated for the case study Valsura River (Italy) to assess a correct representation of the hydraulic variables in the study site. For the hydraulics simulations, the mesh has a resolution of 1×1 m in the horizontal plane, also for the 2D model approach, and 5 cm in vertical direction. The calibration is done by comparing simulated and measured water depths at a discharge of 2.34 $m^3/s$. Calibration of the model for higher flow rates was not possible for two reasons. The time between minimum flow rate and maximum flow rate is very limited (< 10 minutes) and it is not possible to measure water depths safely. Unfortunately, no further measurements of velocity fields are available for model calibration. In total eight selected discharges from 1.0 $m^3/s$ to 10.0 $m^3/s$ (Q = 1-2-3-4-5-6-7 and 10 $m^3/s$) are simulated with the CFD-model to investigate the different hydraulic patterns during hydropeaking events in the case study (Pisaturo et al., 2017). The choice of a flow rate of 10 $m^3/s$ is also related to the possible future hydropower management proposed by (Premstaller et al., 2017) to mitigate the hydropeaking impacts according the suggestions proposed by local limnology experts.

The comparison yields a very high similarity with a percentage error of 5% between measured and simulated water depth (Figure 26 and Table 8).

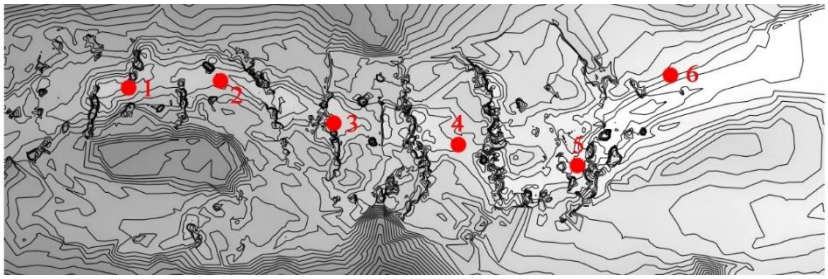


Figure 26. Sample point in Valsura River for water depths measurements.

Table 8. Comparison between measured and simulated water depth for the Valsura River (Q = 2.34 $m^3/s$).

| | Water depth [m] | | | | | |
|---|---|---|---|---|---|---|
| Control point | 1 | 2 | 3 | 4 | 5 | 6 |
| Measured | 0.62 | 0.50 | 0.04 | 0.45 | 0.55 | 0.31 |
| Simulated | 0.61 | 0.51 | 0.03 | 0.45 | 0.53 | 0.31 |

While for low discharges (2 $m^3/s$) the mean flow velocities in the main channel are about 0.63 m/s, the flow velocities can increase up to 1.25 m/s during the simulated peak discharge of 10 $m^3/s$. For each discharge, the three different modelling approaches to obtain the velocity fields, as described in §3.1, are applied.

In Figure 27 the differences between bottom velocities from 3D modelling and 2D modelling (with and without log-law assumption) are presented for two discharges, the base flow of 2 $m^3/s$ and a high flow rate of 10 $m^3/s$.

If depth-averaged velocity from 2D model is considered, it is possible to observe that the differences are very marked for both the considered flow rates. In particular, as expected, considering the depth averaged velocity, the 2D model overestimates the flow velocity. For a flow rate of 2 $m^3/s$ the average deviation is about 0.18 m/s, corresponding to a percentage difference of 33.2%. The average in absolute velocities increase if 10 $m^3/s$ is considered; in this case the difference is 0.33 m/s with a percentage difference of 31.1%. Comparing bottom velocity field from 3D model and 2D model (with log-law

Large discrepancies between the different methods to obtain a flow velocity field, especially for high flow rates.

reconstruction), it is possible to observe that the difference in bottom velocity field is limited if a low flow rate (2 $m^3/s$) is considered (average difference 0.002 m/s, percentage difference 0.35%), whereas the difference is very distinct for the high flow rate (10 $m^3/s$) with an average difference of about 0.12 m/s and a percentage difference of 11.6%.

Given these large discrepancies between the different methods to obtain a flow velocity field, especially for high flow rates, a significant impact on simulated habitat qualities can be expected.

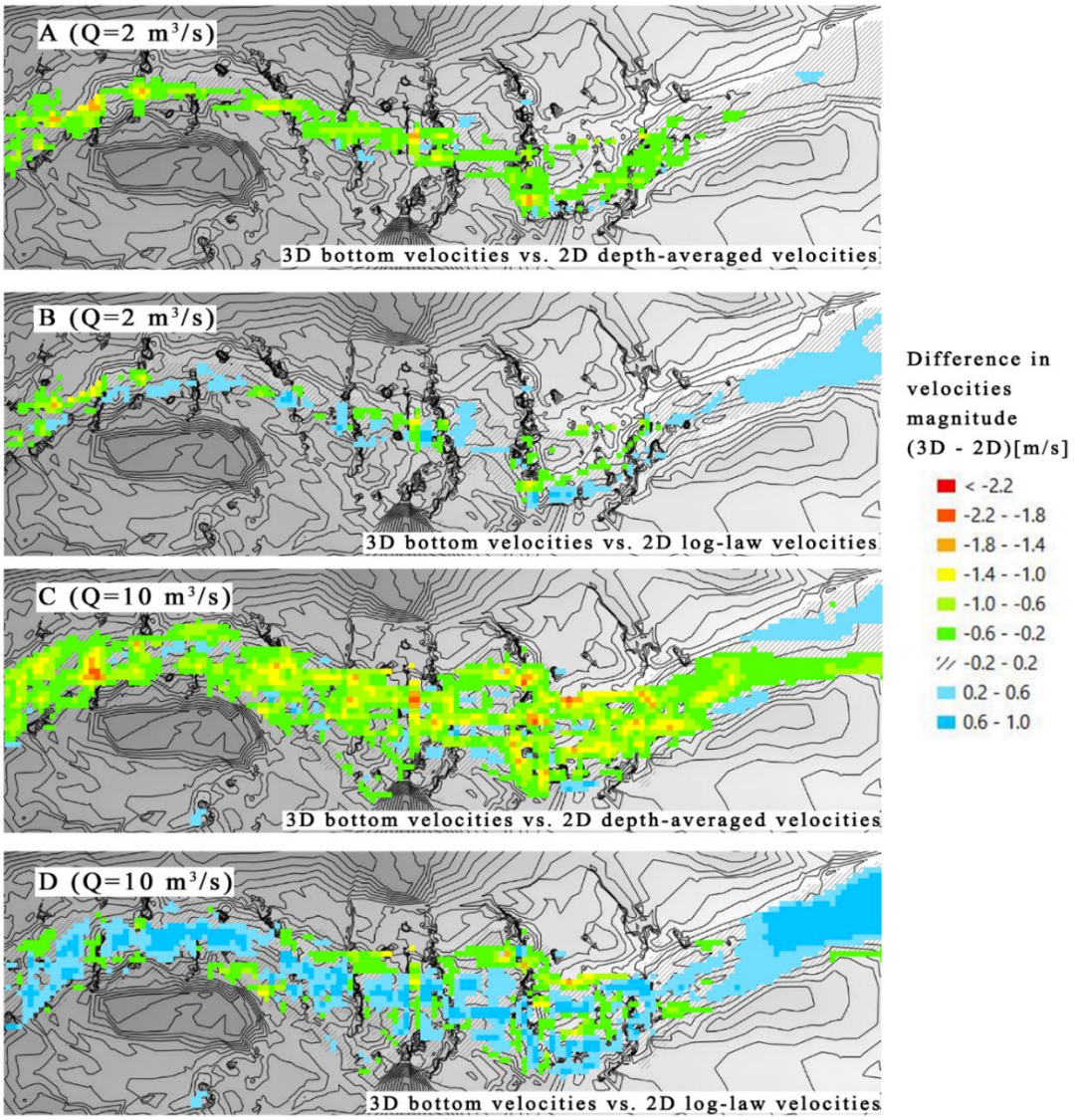


Figure 27. Spatial distribution of differences at 2 $m^3/s$ and 10 $m^3/s$ between the bottom flow velocities of 3D modelling with 2D depth-averaged flow velocities and bottom flow velocities from 2D modelling using the logarithmic law profile.

## 5.2 VALSURA RIVER HABITAT MODELLING

The results of habitat modelling are presented for a high flow rate of 10 $m^3/s$. On the one hand, the HSI-values are shown in form of habitat suitability maps to account for the spatial differences of the input data (Figure 28, left). On the other hand, the results are shown in form of WUA functions (Figure 28, right) that integrate the habitat availability over the entire ranges of flow rates during hydropeaking events.

The habitat simulations are performed as a sequence of different steady state analyses. The current knowledge about unsteady effects of hydropeaking on fish habitats are not clear yet (Shen and Diplas, 2010). To allow for comparisons to other current habitat studies, which are usually done for steady-state conditions, these simulations are conducted for steady-state conditions as well.

### 5.2.1 Habitat 2D-3D, YOY

The first analysis aims on the comparison of HSI-values for the YOY life stage of brown trout, by considering the different velocity fields described in §1.

Therefore, the focus is set on HSI-values > 0.6 to emphasize the relevance of highly suitable habitats (Figure 28, right).

In Figure 28A the results of habitat modelling applying the bottom velocity field from 3D modelling are shown. The habitat suitability map indicates that suitable habitats are only located close to shoreline without suitable habitats in the main channel. Next to the HSI-limitation due to high flow velocities in the main channel, the high selectivity for rather small water depths (Figure 9B) entails no suitable habitats in the main channel. The area of HSI-classes for HSI >0.6 shows up to 3 $m^3/s$ a decrease of habitat quantity given the increase of flow velocities. With further increasing flow YOY habitats increase slightly, assumable because the wetted area is increasing and new shallow areas with moderate flow velocity develop.

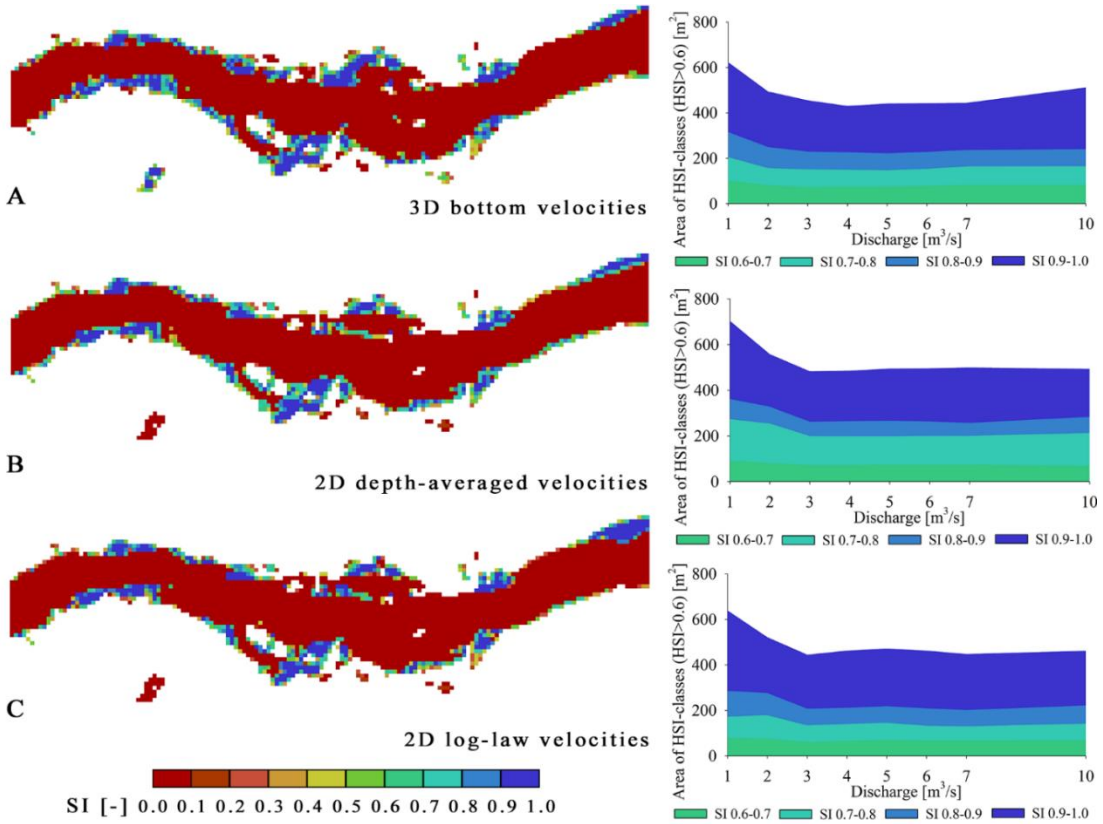


Figure 28. Habitat suitability maps of brown trout (YOY stage) considering different velocity field as input for habitat suitability modelling. The maps represent high flow rates close to the peak flow (Q = 10 $m^3/s$). A: bottom velocities from 3D modelling, B: depth-averaged velocities from 2D modelling, C: bottom velocities from 2D modelling using the logarithmic-law.

Figure 28B illustrates the simulated HSI-values using depth-averaged flow velocities as input for habitat modelling. The habitat suitability map shows less suitable habitat along the upstream shoreline. Although this difference is visible in the habitat map, it reflects in similar results between bottom 3D and depth-averaged 2D approach if integrated assessments, such as WUA functions, are used.

The last comparison includes the habitat results from bottom flow velocities obtained by 3D modelling and 2D modelling using the

logarithmic-law. Similarly to the others velocity field approaches, no suitable habitats are simulated in the main channel. However, the habitats along the shoreline show a slightly higher quantity and quality compared to the habitat results obtained from depth-averaged velocities.

Figure 29 summarizes the results of habitat simulations with different velocity inputs in form of weighted usable areas (WUA) for HSI > 0.6.

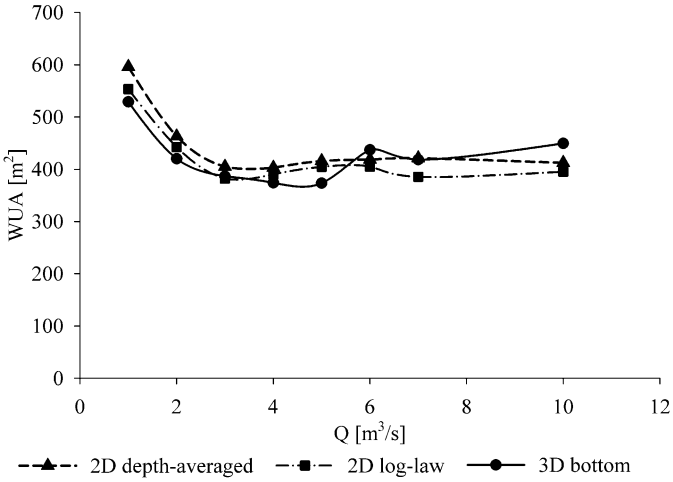


Figure 29. Weighted usable areas (WUA) for the three different velocity inputs in habitat modelling for the entire range of flow rates during hydropeaking events. YOY fish life stage.

We can observe that for all considered velocity fields, an initial decrease of habitat availability occurs (up to 3 $m^3/s$). The velocity is, particularly for the younger stages, the most restrictive parameter for the determination of the habitat suitability. Especially for flow rates up to 3 $m^3/s$ no change in the wetted area occurs but a significant change in the velocities. Therefore, the suitable habitat area decreases in this flow range for the younger life stages.

Comparing the WUA curves from 2D and 3D bottom velocity approach, we can observe that the discrepancy between the two curves increases with increasing flow rate. The differences are, for all

investigated flow velocity fields, not as high as for the adult stage. This aspect is due to a very narrow preference curve for the velocity quantity. Moreover, the YOY stage, presents a high preference for small to moderate water depth that implicate the presence of good habitat areas only near the banks.

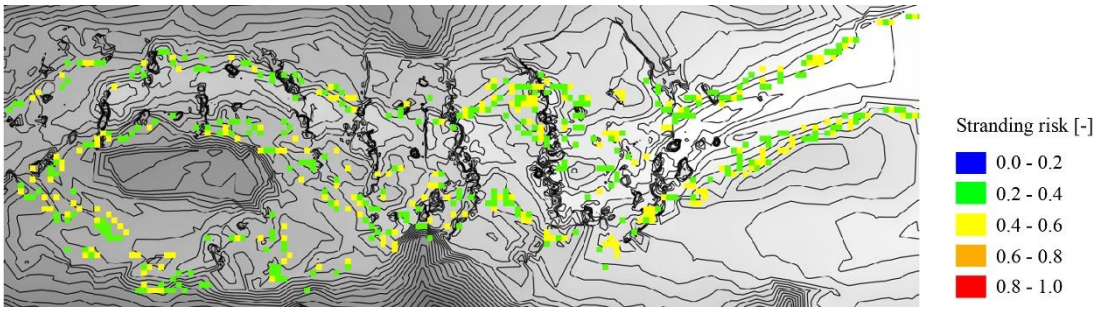


Figure 30. Stranding risk for YOY life stage.

The last analysis examine the stranding risk for the YOY life stage (Figure 30). High stranding risk is associated to value close to 1. It is possible to observe that the stranding risk is medium-high near the riverbank where the higher difference in water depth occurs during Lana HPP turning off. We have to highlight that where stranding risk is not present in Figure 30, does not means that the suitable area is good, but that the initial condition of the habitat was not sufficient for YOY life stage. In fact, the CASiMiR approach consider that is not present stranding risk if the initial habitat is poor.

### 5.2.2 Habitat 2D-3D, Adult

The second comparison aims to compare simulated HSI-values for the adult life stages of brown trout. Similar to the analysis of HSI-values for the YOY stage, the results of habitat modelling (Figure 31) are evaluated based on their spatial distribution in form of habitat maps and on WUA functions.

In Figure 31A the results of habitat modelling applying the bottom

velocity field from 3D modelling are shown. This habitat suitability map indicates that most suitable habitats are located close to shoreline and behind boulders and groynes. This is reasonable because the flow velocities in the main channel exceed the preferred values of adult brown trout during the high flow rates of hydropeaking. The area of HSI-classes for HSI >0.6 shows an increase of habitat quantity up to 3 $m^3/s$, given the increase of the wetted area, followed by a rather constant trend up to 10 $m^3/s$.

The habitat results obtained with the 3D velocity field close to the river bed are used as a reference to determine the difference to the habitat results obtained with the velocity fields from 2D-modelling.

Figure 31B illustrates the simulated HSI-values using depth-averaged flow velocities as input for habitat modelling. Obviously, a remarkable loss of suitable habitats is observed for this investigation. The habitat suitability map shows less suitable habitat along the shoreline and no suitable habitats in the main channel. The habitat loss is also clearly demonstrated for the areas of HSI-classes >0.6. While up to 2 $m^3/s$ no visible differences occur, the suitable areas are reduced continuously from 2 $m^3/s$ to 10 $m^3/s$. In comparison to the WUA of the bottom flow velocity simulated with a 3D model, the habitat loss is 42%. This loss of habitats becomes even more relevant considering the different habitat preferences applied for focal velocities (3D-modelling) and depth-averaged velocities (2D-modelling) because the habitat preferences for focal velocities are more restrictive compared to those for depth-averaged velocities. The reason for this habitat loss is due to the fact that the depth-averaged velocity is a systematic overestimation of the (near bed) focal velocity. Moreover, the 2D model, as already described in §2.2, is not able to properly depict the large scale secondary currents induced by the strong bed heterogeneity, with boulders and groynes.

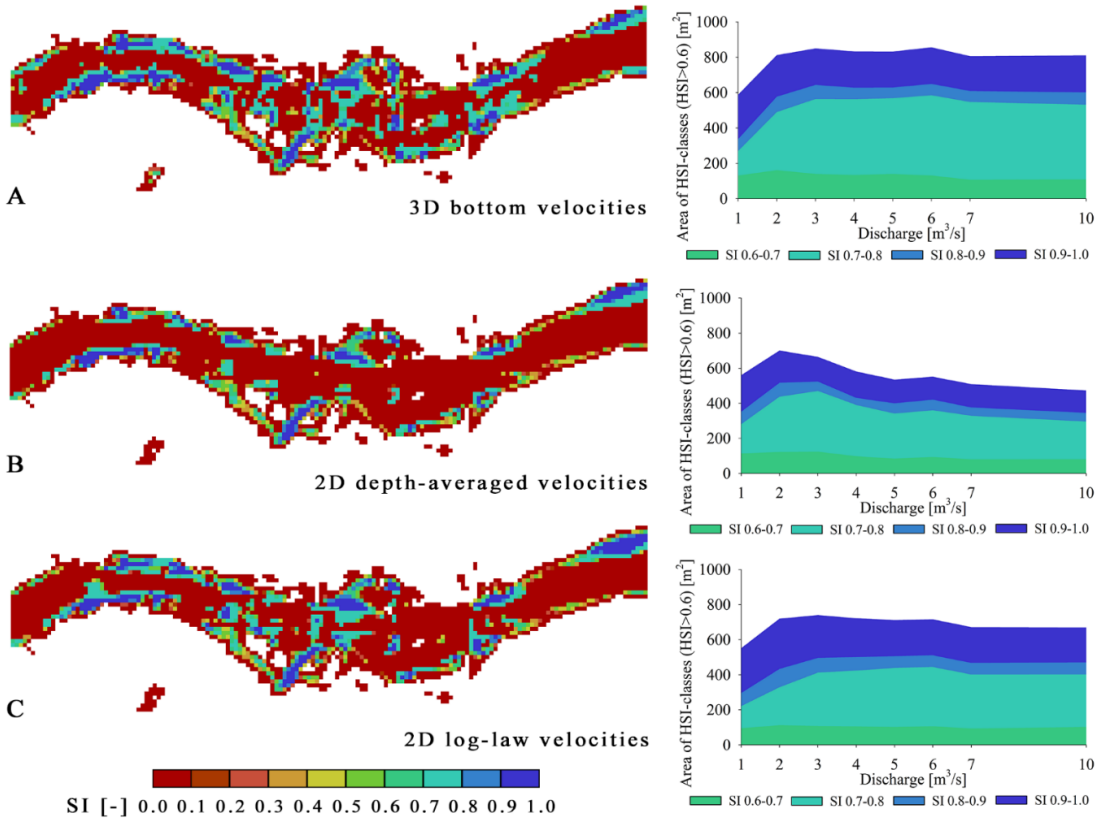


Figure 31. Habitat suitability maps of brown trout (adult stage) considering different velocity field as input for habitat suitability modelling. The maps represent high flow rates close to the peak flow (Q = 10 $m^3/s$). A: bottom velocities from 3D modelling, B: depth-averaged velocities from 2D modelling, C: bottom velocities from 2D modelling using the logarithmic-law.

The last comparison includes the habitat results from bottom flow velocities obtained by 3D modelling and 2D modelling using the logarithmic-law. As both velocity fields represent the velocities close to the river bed the identical habitat preferences (focal velocities) are used. Similarly, to the depth-averaged approach small suitable habitats are simulated in the main channel. However, the habitats along the shoreline show a higher quantity and quality compared to the habitat results obtained from depth-averaged velocities. The areas of HSI-classes for the entire range of flow rates during hydropeaking shows also a

continuous decrease of suitable habitat for flow rates > 2 $m^3/s$. However, the reduction is not as large as for the scenario with depth-averaged velocities. The habitat loss at a discharge of 10 $m^3/s$ is 17% compared to the habitat availability obtained with the bottom velocities of 3D modelling.

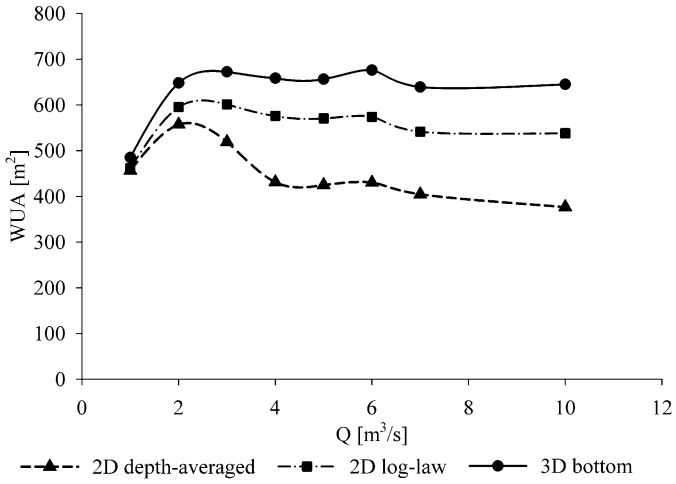


Figure 32. Weighted usable areas (WUA) for the three different velocity inputs in habitat modelling for the entire range of flow rates during hydropeaking events. Adult fish life stage.

Figure 32 summarizes the results of habitat simulations with different velocity inputs in form of weighted usable areas (WUA) for HSI > 0.6.

Figure 32 indicates for all the considered flow velocity fields an initial increase (up to 2 $m^3/s$) of habitat availability because of the increase of the wetted area with velocities in the preferred range of adult brown trouts. For flow rates up to 10 $m^3/s$ a decrease of the WUA-values is observed for all scenarios. However, while for the bottom velocities obtained from 3D modelling the decrease is very low, the decrease for both velocity fields from 2D modelling (depth-averaged and logarithmic-law) is substantially higher.

In addition, Figure 32 reveals an increasing difference between the WUA-values obtained from 3D modelling and 2D modelling with increasing flow rates.

## 5.3 RIO SELVA DEI MOLINI HYDRAULIC MODEL

The hydraulic model is tested and calibrated for the case study Rio Selva dei Molini in Italy to assess a correct representation of the hydraulic variables in the study site. For the hydraulics simulations, the mesh has a resolution of 0.5×0.5 m in the horizontal plane, also for the 2D model approach, and 5 cm in vertical direction. The calibration is done by comparing simulated and measured water depths and water velocities at a discharge of 2.07 $m^3/s$. Calibration of the model for higher flow rates was not possible for two reasons. The time between minimum flow rate and maximum flow rate is very limited (< 10 minutes) and it is not possible to measure water quantities safely.

Figure 33 shows the sample point in Rio Selva dei Molini for the comparison between measured and simulated water depths and velocities. In these sample point the depth averaged velocity and the bottom velocity at 6 cm above the bed were measured.

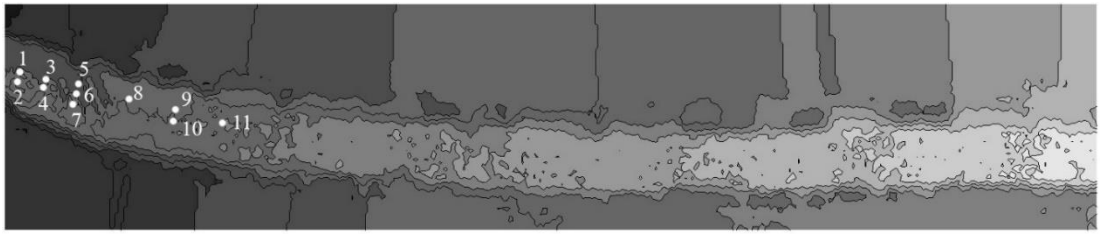


Figure 33. Sample point in Rio Selva dei Molini for water depths and water velocities measurements.

Table 9. Comparison between measured and simulated water depth for the Rio Selva dei Molini (Q = 2.07 $m^3/s$).

| | Water depth [m] | | | | | | | | | | |
|---|---|---|---|---|---|---|---|---|---|---|---|
| Control point | 1 | 2 | 3 | 4 | 5 | 6 | 7 | 8 | 9 | 10 | 11 |
| Measured | 0.31 | 0.4 | 0.2 | 0.49 | 0.2 | 0.17 | 0.28 | 0.19 | 0.28 | 0.45 | 0.33 |
| Simulated | 0.29 | 0.42 | 0.21 | 0.49 | 0.18 | 0.18 | 0.26 | 0.18 | 0.27 | 0.48 | 0.35 |

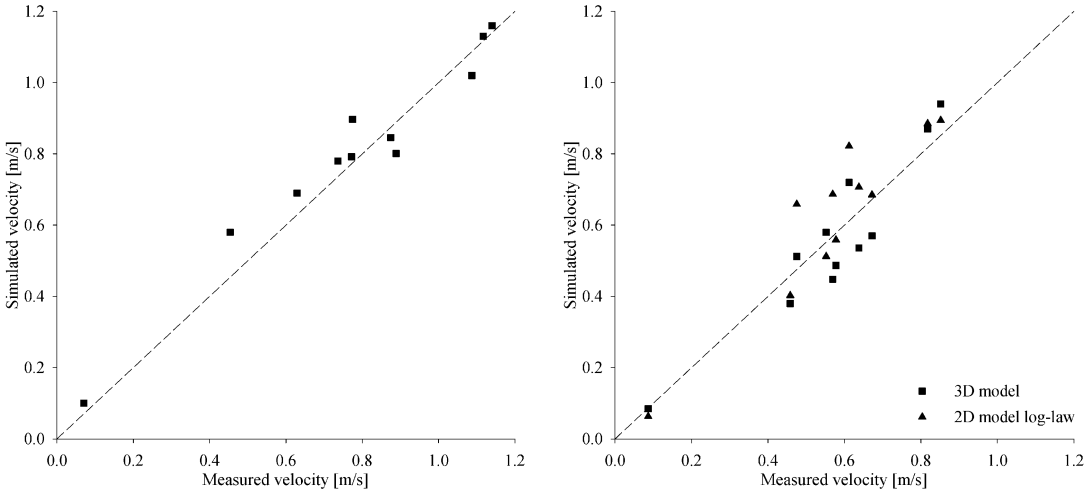


Figure 34. Comparison between measured and simulated water velocities in Rio Selva dei Molini. Water depth mean velocity (left) and bottom velocities (right).

The comparison yields a very high similarity with a percentage error of 5.5% between measured and simulated water depth (Table 9).

In Figure 34 are reported the comparison between measured and simulated velocities. On the left, the depth averaged velocity is considered. In this case, the simulated velocities are in good agreement with measured ones. The average error is about 10%. On the right, the bottom velocities are compared. In this case two approach for simulate the flow velocity are used. The first one with the 3D approach (square points) and the second one with the reconstruction of the bottom velocities with log-law assumption (§3.2). Using the 3D approach, the near bottom simulated velocities well represent the measured values with a percentage error of about 11%. Considering the 2D approach with

log-law reconstruction, the simulated velocities tend to overestimate the measured ones with an average error of 16%.

In total five selected discharges from 1.0 $m^3/s$ to 7.0 $m^3/s$ (Q = 1-2-3-5 and 7 $m^3/s$) are simulated with the CFD-model to investigate the different hydraulic patterns during hydropeaking events in the case study.

In Figure 35 the differences between bottom velocities from 3D modelling and 2D modelling (with and without log-law assumption) are presented for 3 $m^3/s$.

If depth-averaged velocity from 2D model is considered, it is possible to observe that the differences are very marked. In particular, as expected, considering the depth averaged velocity, the 2D model overestimates the flow velocity. For a flow rate of 3 $m^3/s$ the average deviation is about 0.18 m/s, corresponding to a percentage difference of 33.2%. The average in absolute velocities increase if 10 $m^3/s$ is considered; in this case, the difference is 0.33 m/s with a percentage difference of 13%. Comparing bottom velocity field from 3D model and 2D model (with log-law reconstruction), it is possible to observe that the difference in bottom velocity field is reduced with an average difference of about 0.05 m/s and a percentage difference of 3.6%.

The discrepancies between the different methods to obtain a flow velocity field are less evident than in Valsura River case study, however an impact on simulated habitat qualities can be expected.

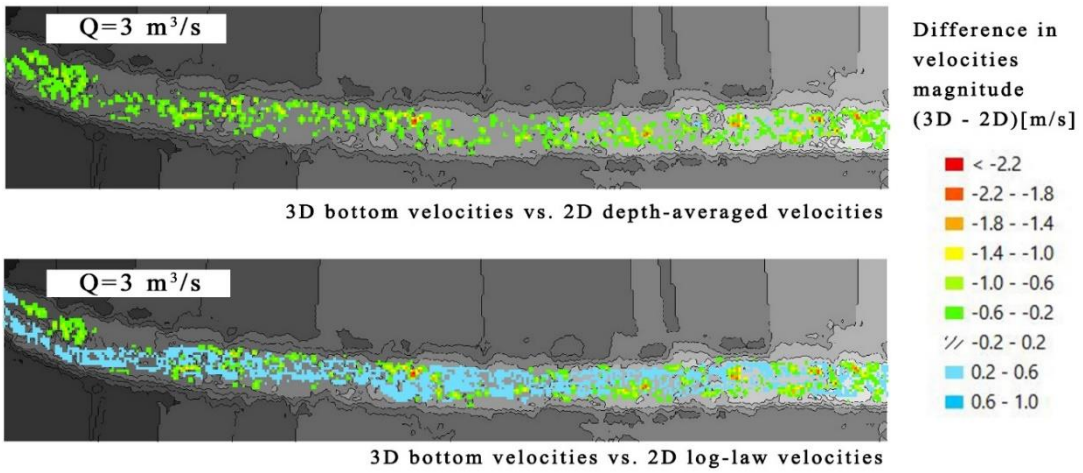


Figure 35. Spatial distribution of differences at 3 $m^3/s$ between the bottom flow velocities of 3D modelling with 2D depth-averaged flow velocities and bottom flow velocities from 2D modelling using the logarithmic law profile.

## 5.4 RIO SELVA DEI MOLINI HABITAT MODELLING

The results of habitat modelling are presented for a high flow rate of 7 $m^3/s$. On the one hand, the HSI-values are shown in form of habitat suitability maps to account for the spatial differences of the input data (Figure 36, left). On the other hand, the results are shown in form of WUA functions (Figure 36, right) that integrate the habitat availability over the entire ranges of flow rates during hydropeaking events.

As for Valsura River, the habitat simulations are performed as a sequence of different steady state analyses. The current knowledge about unsteady effects of hydropeaking on fish habitats are not clear yet (Shen and Diplas, 2010). To allow for comparisons to other current habitat studies, which are usually done for steady-state conditions, these simulations are conducted for steady-state conditions as well.

### 5.4.1 Habitat 2D-3D, YOY

The first analysis aims on the comparison of HSI-values for the YOY life stage of brown trout, by considering the different velocity fields described in §3.2.

Therefore, the focus is set on HSI-values > 0.6 to emphasize the relevance of highly suitable habitats (Figure 36, right).

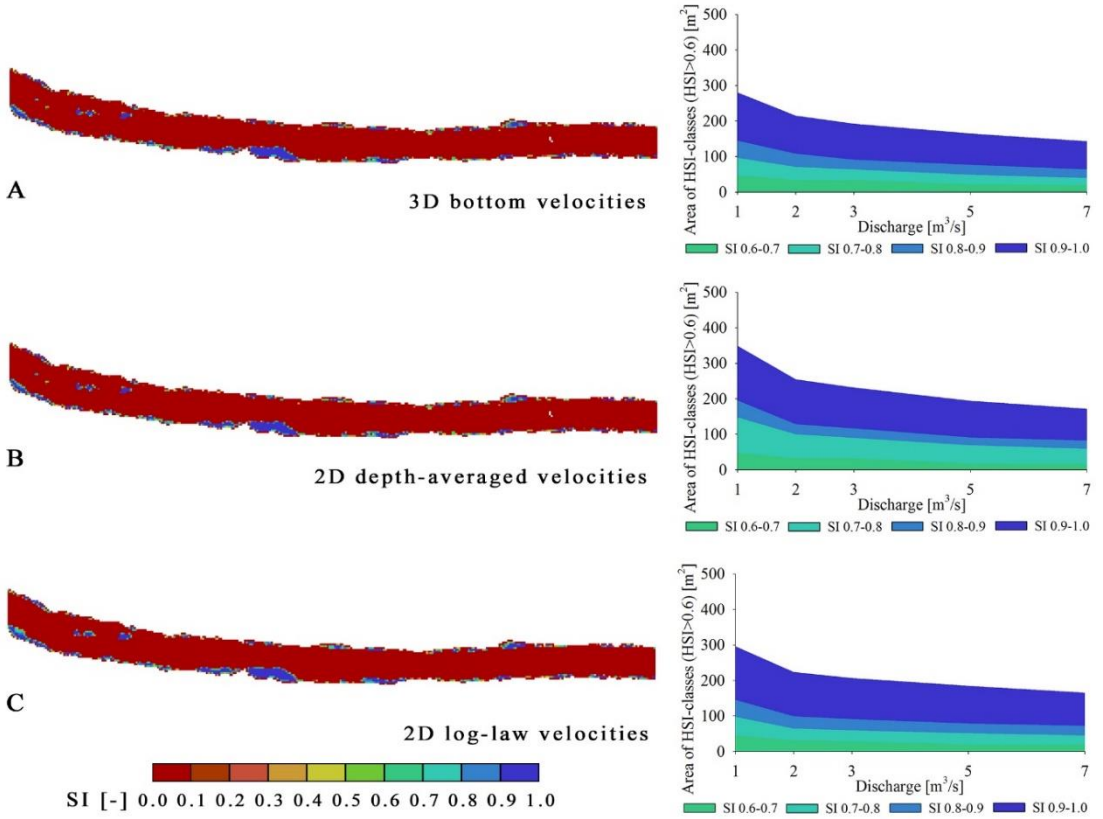


Figure 36. Habitat suitability maps of brown trout (YOY stage) considering different velocity field as input for habitat suitability modelling. The maps represent high flow rates close to the peak flow (Q = 7 $m^3/s$). A: bottom velocities from 3D modelling, B: depth-averaged velocities from 2D modelling, C: bottom velocities from 2D modelling using the logarithmic-law.

In Figure 36A the results of habitat modelling applying the bottom velocity field from 3D modelling are shown. The habitat suitability map indicates that suitable habitats are located only close to the shoreline, without suitable habitats in the main channel. Next to the HSI-limitation due to high flow velocities in the main channel, the high selectivity for rather small water depths (Figure 9B) entails no suitable habitats in the

main channel. The area of HSI-classes for HSI > 0.6 shows a continuous decrease of habitat quantity given the increase of flow velocities.

Figure 36B illustrates the simulated HSI-values using depth-averaged flow velocities as input for habitat modelling. The habitat suitability map shows very similar results with Figure 36A. Similar results between bottom 3D and depth-averaged 2D approach are visible if integrated assessments, such as WUA functions, are used.

The last comparison includes the habitat results from bottom flow velocities obtained by 3D modelling and 2D modelling using the logarithmic-law. Similarly, to the others velocity field approaches no suitable habitats are simulated in the main channel.

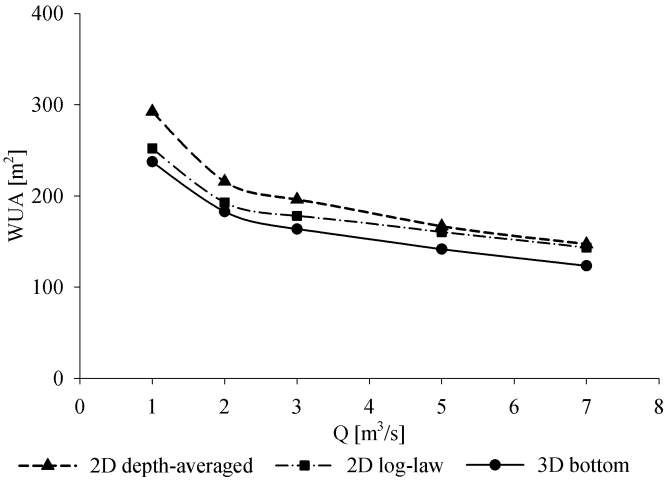


Figure 37. Weighted usable areas (WUA) for the three different velocity inputs in habitat modelling for the entire range of flow rates during hydropeaking events. YOY fish life stage.

Figure 37 summarizes the results of habitat simulations with different velocity inputs in form of weighted usable areas (WUA) for HSI > 0.6.

We can observe that for all considered velocity fields, a decrease of habitat availability occurs. The velocity is, particularly for the younger stages, the most restrictive parameter for the determination of the habitat

suitability. Due to the morphological characteristics of the Rio Selva dei Molini, no change in the wetted area occurs but a significant change in the velocities. Therefore, the suitable habitat area decreases in this flow range for the younger life stages.

Comparing the WUA curves from 2D and 3D bottom velocity approach, we can observe that the results are very similar. The differences are, for all investigated flow velocity fields, not as high as for the adult stage. This aspect is due to a very narrow preference curve for the velocity quantity. Moreover, the YOY stage, presents a high preference for small to moderate water depth that implicate the presence of good habitat areas only near the banks.

### 5.4.2 Habitat 2D-3D, Adult

The second comparison aims to compare simulated HSI-values for the adult life stages of brown trout. Similar to the analysis of HSI-values for the YOY stage, the results of habitat modelling (Figure 38) are evaluated based on their spatial distribution in form of habitat maps and on WUA functions.

In Figure 38A the results of habitat modelling applying the bottom velocity field from 3D modelling are shown. This habitat suitability map indicates that most suitable habitats are located close to the shoreline and behind boulders. This is reasonable because the flow velocities in the main channel exceed the preferred values of adult brown trout during the high flow rates of hydropeaking. The area of HSI-classes for HSI >0.6 shows up to 2 $m^3/s$ an increase of habitat quantity given the increase of the wetted area followed by a rather constant trend up to 7 $m^3/s$.

The habitat results obtained with the 3D velocity field close to the river bed are used as a reference to determine the difference to the habitat results obtained with the velocity fields from 2D-modelling.

Figure 38B illustrates the simulated HSI-values using depth-averaged flow velocities as input for habitat modelling. A small loss of

suitable habitats is observed for this investigation. The habitat suitability map shows less suitable habitat along the shoreline and no suitable habitats in the main channel. The habitat loss is also clearly evident for the areas of HSI-classes >0.6. While up to 2 $m^3/s$ no visible differences occur, the suitable areas assume lower value from 2 $m^3/s$ to 7 $m^3/s$. In comparison to the WUA of the bottom flow velocity simulated with a 3D model, the habitat loss is 17%. This loss of habitats becomes even more relevant considering the different habitat preferences applied for focal velocities (3D-modelling) and depth-averaged velocities (2D-modelling) because the habitat preferences for focal velocities are more restrictive compared to those for depth-averaged velocities. The reason for this habitat loss is, once more, a systematic overestimation of depth-averaged velocities, which neglect the strong bed heterogeneity and secondary currents induced by boulders leading to a reduction of the velocity magnitudes.

The last comparison includes the habitat results from bottom flow velocities obtained by 3D modelling and 2D modelling using the logarithmic-law. As both velocity fields represent the velocities close to the river bed the identical habitat preferences (focal velocities) are used. Similarly, to the depth-averaged approach small suitable habitats are simulated in the main channel. However, the habitats along the shoreline show a higher quantity and quality compared to the habitat results obtained from depth-averaged velocities. The areas of HSI-classes for the entire range of flow rates during hydropeaking shows also a constant trend flow rates > 3 $m^3/s$. However, the reduction is not as large as for the scenario with depth-averaged velocities. The habitat loss at a discharge of 7 $m^3/s$ is 10% compared to the habitat availability obtained with the bottom velocities of 3D modelling.

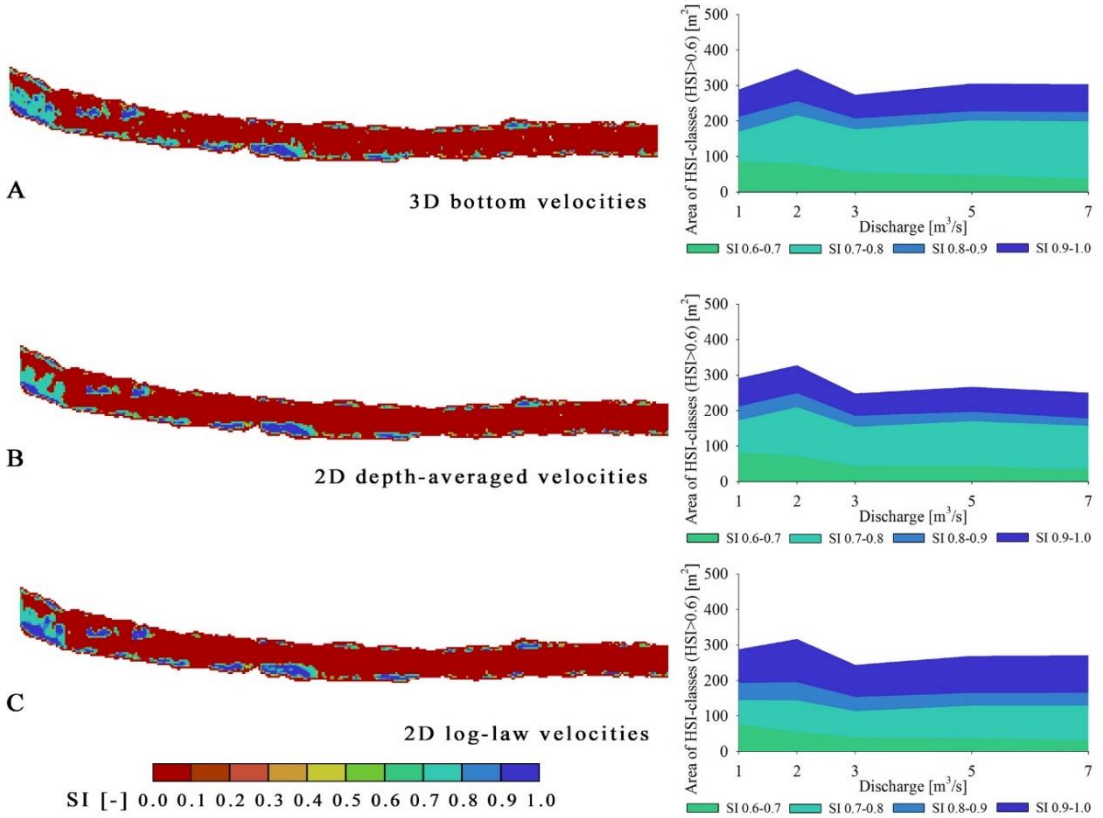


Figure 38. Habitat suitability maps of brown trout (adult stage) considering different velocity field as input for habitat suitability modelling. The maps represent high flow rates close to the peak flow (Q = 7 $m^3/s$). A: bottom velocities from 3D modelling, B: depth-averaged velocities from 2D modelling, C: bottom velocities from 2D modelling using the logarithmic-law.

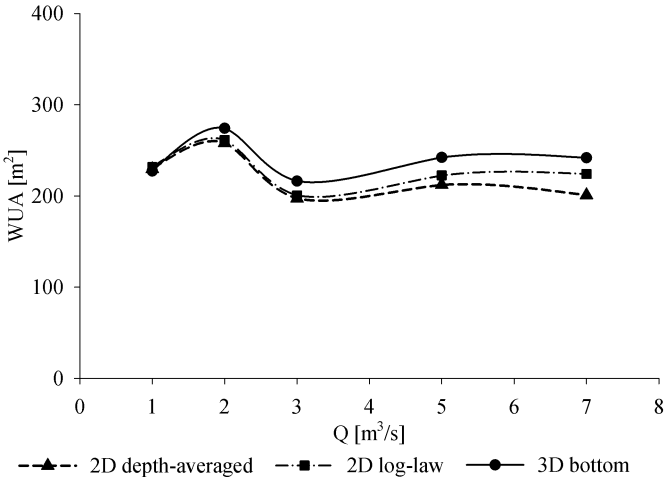


Figure 39. Weighted usable areas (WUA) for the three different velocity inputs in habitat modelling for the entire range of flow rates during hydropeaking events. Adult fish life stage.

Figure 39 summarizes the results of habitat simulations with different velocity inputs in form of weighted usable areas (WUA) for HSI > 0.6.

Figure 39 indicates for all considered flow velocity fields an initial increase (up to 2 $m^3/s$) of habitat availability because of the increase of the wetted area with velocities in the preferred range of adult brown trouts. For flow rates up to 7 $m^3/s$ a decrease of the WUA-values is observed for all scenarios. However, while for the bottom velocities obtained from 3D modelling the decrease is very low, the decrease for both velocity fields from 2D modelling (depth-averaged and logarithmic-law) is higher.

In addition, Figure 39 reveals an increasing difference between the WUA-values obtained from 3D modelling and 2D modelling with increasing flow rates.

## 5.5 DISCUSSION

The present part of the study has compared the availability of suitable habitat areas for brown trout in a reach of the Valsura River and Rio Selva dei Molini (Bolzano, Italy) using three different approaches to reconstruct the velocity field. In particular, although a comparison between theoretical approaches to simulate bottom velocities and different suitable habitat is present in the scientific literature (Martínez-Capel et al., 2004; Milhous, 1999), the use of a fully 3D CFD model has never been thoroughly analysed.

The 3D CFD model was used for both the case studies.

For Valsura River the measured and simulated water depths were compared for a calibration flow rate equal to 2.34 $m^3/s$. Unfortunately, it was not possible to obtain field velocity measurements for higher discharges because we did not obtain the authorisation from the province and for safety reasons. Despite the absence of field velocity measures, the results from laboratory measures with low Reynolds numbers ($\approx 10^{\cdot}000$) were in good agreement with simulated results (§2.2). Moreover, the main aim of this work is to emphasize the different capability of a 3D model against a 2D model to determine good habitat areas in the proximity of the morphological measures that determine a strong riverbed heterogeneity. We can assume that the effects of increasing morphological diversity on the flow field are more properly represented by a 3D model compared with a 2D approach (depth-averaged velocity and log-law reconstruction).

For Rio Selva dei Molini the measured and simulated water depths and velocities were compared for a calibration flow rate equal to 2.07 $m^3/s$. The CFD model well represents water depths and the velocity field. If 2D approach is used, the simulated bottom velocity tends to slightly overestimate the measured one.

The first analysis consisted in comparing the velocity field between different approaches (3D, 2D and log-law 2D models). The largest

Larger differences of velocity field are located downstream of groynes and boulders.

differences were located downstream of groynes and boulders. These areas are very important for fish because they can be used as shelter and an accurate estimation of these areas is essential to have a more realistic habitat suitability map (Person, 2013). This complex bathymetry can strongly affect the hydrodynamic field (Armanini et al., 2010a). In these cases, a 2D model is not able to adequately reproduce the water velocity field (§2.2). In particular, the depth-averaged 2D approach clearly overestimates flow velocities in the entire reach if compared with 3D bottom velocities (Figure 27 and Figure 35). Also considering bottom velocity reconstruction with a log-law profile, the 2D model cannot reproduce, for very complex bathymetry, the velocity field very well. The log-law assumption, in fact, is correct only for uniform flow and simple bottom geometry, which are rarely present in a natural reach (Stansby and Zhou, 1998).

The use of the depth-averaged velocity and the related preference curves is the standard method that is currently used for habitat estimations. The method to calculate the HSI is the product approach. It is currently the most common method to calculate composite suitability using univariate preference functions (Ahmadi-Nedushan et al., 2006). It is the most conservative approach since each single parameter has the same strong influence on the composite suitability (Ahmadi-Nedushan et al., 2006). Moreover, using the product approach is possible to highlight the influence of different velocity field reconstruction, since the second hydraulic parameter used for habitat simulations is the water depth that is slightly influenced by CFD approach.

The proposed approach with bottom velocity (bottom 3D and log-law 2D model) represents a new approach to determining the habitat suitability (Pisaturo et al., 2017). The comparison between 2D-modelling and 3D-modelling results shows that the two methods can lead to substantial differences. This not only provides the possibility to simulate more accurate flow velocity fields but also the possibility to

use focal velocities for habitat preferences.

The calibration of the numerical model, for both the case studies, showed that the 3D model is able to properly depict the main features of the flow field (such as recirculation zones) that the 2D model cannot reproduce. Despite the fact that the model was not calibrated for higher discharges we have extended the simulations also to these cases bearing in mind that:

- for higher discharges it is expected that the limits of application of a k-ε model are less stringent (Wilcox, 2006) and the differences in the results between them persist;
- the main aim of the study is to highlight the differences between 2D and 3D hydraulic modelling in the context of habitat suitability assessments rather than to assess the absolute performance of a CFD.

The use of different approaches for the reconstruction of the hydrodynamic field entails different possible scenarios on the simulation of suitable areas for brown trout.

Moreover, the use of different velocity field approaches (§3.1) and different preference curves for depth-averaged and bottom velocities (§3.1) entails cross-effects in habitat evaluation. In particular, the preference curves for depth-averaged velocities cover a wider velocity range (Figure 9). Using only this velocity preference curve entails suitable areas overestimation, if it is used also for bottom velocity. To use bottom velocity reconstruction, it is more correct to modify preference curves to decrease the range of suitable flow velocities (Heggenes and Wollebæk, 2013). The final result is that, using bottom velocities with respective preference curves, we can obtain a decrease in suitable areas estimation, but a more realistic representation of the real state.

The habitat analysis was performed for YOY and adult stage. For the YOY life stage, the similarity in habitat areas, can be explained

The habitat for YOY life stage is less sensitive to different velocity field reconstruction approaches.

considering the different habitat preferences applied for focal velocities (3D-modelling) and depth-averaged velocities (2D-modelling) because the habitat preferences for focal velocities are more restrictive compared to those for depth-averaged velocities (Figure 9). Hence, the effect of differences in the velocity fields were partly compensated by the habitat preferences. For the present case study, the use of different velocity profile approaches, does not seem to have a noticeable consequence in habitat simulation for the YOY life stage. This can be ascribed to three possible reasons:

1. the use of different preferences curves for focal velocities and depth-averaged velocities can provide different habitat results for each CFD model used;
2. the YOY life stage present more narrow preference curves for flow velocity (that is described more accurately close to the river bottom by the 3D approach) compared to the adult stage (Heggenes and Wollebæk, 2013). This aspect leads to no suitable habitats for flow velocities higher than 0.5 m/s for both focal velocities and depth-averaged velocities;
3. YOY prefers shallow areas, which are present only near the banks (Ayllón et al., 2010). In these areas the differences between the 3D approach and the other approaches are not as distinct as in deeper areas.

The habitat for adult life stage is very sensitive to different velocity field reconstruction approaches.

For the adult life stage, in contrast to the habitat results simulated with 2D modelling, the three-dimensional approach allowed for an adequate representation of the flow field near the bed considering the three-dimensional effects of river bed heterogeneity on local flow velocities (e.g. flow separation zones, secondary currents, recirculated areas). Considering the entire flow range of hydropeaking events, the habitat simulations with bottom flow velocities from 3D modelling provided suitable habitats over the entire flow range representing the availability of stable suitable habitats (close to groynes and boulders),

while the habitat availability of 2D modelled flow velocity was continuously decreasing with increasing flow rates.

An additional comment can be done comparing habitat suitability in Valsura River and in Rio Selva dei Molini. Table 10 report the percentage ratio between good habitat areas and total wet areas. Is possible to observe that in the Valsura River the percentage of good habitat areas are always higher than in Rio Selva dei Molini. This behaviour can be easily ascribed to the strong difference in the morphology between the two reaches.

The different morphology between Valsura River and Rio Selva dei Molini entails different habitat suitability.

Table 10. Comparison of the percentage ratio between good habitat areas and total wet areas. YOY and Adult life stages. Valsura River and Rio Selva dei Molini.

| Q [$m^3/s$] | 1 | 2 | 3 | 5 | 7 |
|---|---|---|---|---|---|
| WUA/Wet [%] YOY Valsura | 24.6 | 18.0 | 15.6 | 13.7 | 14.0 |
| WUA/Wet [%] YOY Molini | 16.7 | 11.7 | 10.2 | 8.3 | 7.0 |
| WUA/Wet [%] Adult Valsura | 22.5 | 27.7 | 25.0 | 24.1 | 21.4 |
| WUA/Wet [%] Adult Molini | 16.0 | 17.6 | 13.4 | 14.2 | 13.7 |

The Valsura River in fact presents, as described in §4.1.1, a complex morphology that influence the potential habitat quality. The presence of large boulder and groynes and the wider wetted area, allow to increase the habitat quality but with a consequent higher risk of stranding during the HPP turning off.

# 6. MITIGATION PROJECTS

In the present chapter two possible mitigations measures against hydropeaking for the two case studies are presented. For the first river (Valsura River, SudTirol – Italy) a combination of operative and constructive mitigation approach is studied. For the Rio Selva dei Molini (SudTirol – Italy) a morphological and an operative measure is proposed.

## 6.1 VALSURA RIVER

As described in §1.2, in literature three types of mitigations measures are present. For the Valsura River a constructive mitigation measure is proposed in collaboration with Alperia company (Premstaller et al., 2017).

From the results of the hydraulic simulations (Figure 27), the habitat simulations (Figure 28 and Figure 29) and of the ecological field survey described in the previous chapters, is possible to propose hydrological discharge targets to achieve a sustainable future ecological condition.

For a successful fish reproduction of brown trout, the different requirements of all life stages have to be fulfilled. The requirements regard mainly certain water depth and flow velocity conditions (Heggenes and Wollebæk, 2013).

The deficit analysis showed that the early life stages are the most critically affected by the hydropeaking in Valsura reach.

Expert limnologist suggested flow rate range and limits on down-ramping rate to minimize the hydropeaking effects (Table 11).

Additional care has to be taken during grayling spawning (March), where lower discharge variations are acceptable $Q_{min}$ is 3 $m^3/s$ while $Q_{max}$ is 5 $m^3/s$. In this case, the $Q_{max}$ is the lowest flow rate in the year. Additionally, at the same time the water depth down-ramping rate shall be limited to 0.2 cm/min to avoid stranding risk at the shorelines of the wetted branches.

In the same manner, also the juvenile and adult fish stages are taken into account. In this case the $Q_{max}$ can increase to 10 $m^3/s$, because fish in this life stage are less sensitive to high water velocity (Heggenes and Wollebæk, 2013).

Even if the macrozoobenthos (MZB) is not directly taken into account, macroinvertebrates can in any case take advantage from these flow limitations (lower stranding risk for invertebrates, lower risk of drift of invertebrates).

Following the limnological targets, habitat simulations are performed considering the suggested flow rate range and the down ramping rate.

The habitat simulations (Figure 28, Figure 30, Figure 31) highlights that the respect of hydrological targets, can involve an increase of habitat stable areas for the flow rate range 3-10 $m^3/s$ for YOY and Adult life stages. In particular, since there is no longer a stranding risk (Figure 40), the brown trout reproduction can be guaranteed.

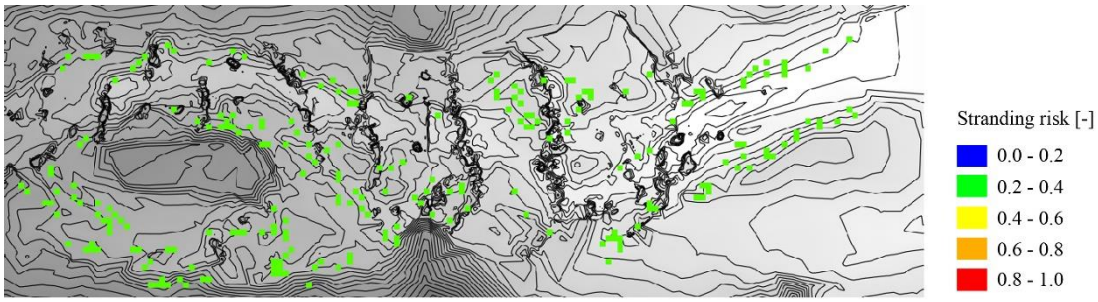


Figure 40. Stranding risk for YOY life stage. Mitigation project.

Table 11. Ecological and hydrological targets to improve habitat status in Valsura River.

| | $Q_{min}$ | $Q_{max}$ | Water depth max down ramping rate 7 $m^3/s \rightarrow Q_{min}$ | Operational mitigation measures | Fish ecology |
|---|---|---|---|---|---|
| Month | [$m^3/s$] | [$m^3/s$] | [cm/min] | | Important factors |
| Jan | 2 | 10 | 0.4 | | Water depth for juvenile and adult; redd stability; |
| Feb | 2 | 10 | 0.2 | | Water depth for juvenile and adult; redd stability; brown trout alevin emergency |
| Mar | 3 | 5 | 0.2 | Few days with 5 $m^3/s<Q<8$ $m^3/s$ | Water depth for juvenile and adult; redd stability; brown trout alevin emergency; grayling spawning |
| Apr | 3 | 10 | 0.2 | | Water depth for juvenile and adult; redd stability; grayling spawning; grayling alevin emergency |
| May | 3 | 10 | 0.2 | Flood of riparian forest $Q>25$ $m^3/s$ | Water depth for juvenile and adult; grayling alevin emergency |
| Jun | 3 | 10 | 0.4 | Flood of riparian forest $Q>25$ $m^3/s$ | Water depth for juvenile and adult; juvenile brown trout |
| Jul | 3 | 10 | 0.4 | | Water depth for juvenile and adult; juvenile brown trout |
| Aug | 3 | 10 | 0.4 | | Water depth for juvenile and adult; juvenile brown trout |
| Sep | 3 | 10 | 0.4 | | Water depth for juvenile and adult; juvenile brown trout |
| Oct | 3 | 10 | 0.4 | Declogging $Q \approx 15$ $m^3/s$ | Water depth for juvenile and adult; juvenile brown trout |
| Nov | 2 | 10 | 0.4 | Few days with 5 $m^3/s<Q<8$ $m^3/s$ | Water depth for juvenile and adult; brown trout spawning; redd stability |
| Dec | 2 | 10 | 0.4 | | Water depth for juvenile and adult; brown trout spawning; redd stability |

Even though habitat simulations suggested that a water depth down ramping rate of 0.4 cm/min might be acceptable, for the month of the most delicate fish life stage case a slower rate of 0.2 cm/min is retained necessary.

Based on the results above, the following ecological improvements are expected:

an increase of population density and average MZB mass density per unit area due to a decrease of the risk of drifting or stranding; in this way the food supply for fish will increase;

- a significant reduction of the risk for drifting or stranding;
- a significant improvement of the living conditions for young fish, adults and sub-adults thanks to the increase of the minimum flow and to the permanently wetted areas;
- fish habitat recovery due to a better ecological connection with the Adige River.

Obviously, the above minimum and maximum flow targets will also improve the aspects on human safety on Valsura River.

The minimum flow values indicated in Table 11 represent the discharge values to obtain immediately upstream of the restitution of Lana HPP. Since the water discharge upstream of the outlet of the hydropower plant is actually lower than the values indicated in Table 11, in future additional discharge will have to be released by Lana HPP in a continuous way.

Comparing Table 11 and Table 3, the minimum additional discharges reach from approximately 0.1 $m^3/s$ during the period of snowmelt (June) to 2.2 $m^3/s$ during late winter (March). The maximum discharge $Q_{max}$ immediately downstream of the Lana HPP outlet in Valsura River will have to be drastically reduced to 5.0 $m^3/s$ during the month of March and to 10 $m^3/s$ during the remaining months.

Another critical value is the down-ramping rate. In order to define the vertical down-ramping velocity, which during the month from

February to May should not exceed 0.2 cm/min and from June to January should not exceed 0.4 cm/min. To pass from 10 $m^3/s$ to 3 $m^3/s$ using a down-ramping rate of 0.2 cm/min approximately 70 min are necessary.

### 6.1.1 Operational measures

The first hypothesis to respect values in Table 11 is to adopting operational measures. We have to remind that Lana HPP is a multi-purpose hydropower plant. Besides hydropower production releases irrigational discharge to the local farming cooperatives from two different point in the hydraulic system. Approximately, 1% of the total annual water inflow is released at the surge tank of the plant, while 28% of the annual total water inflow is released at the tailrace channel of Lana HPP. These irrigational discharges have to be released continuously without interruptions, leading to a continuous service of at least one production unit and reducing the availability of the plant for peak energy production.

Since the tailrace channel doesn't have a regulating storage volume, only 60% of the annual water inflow to Lana HPP can be stored in Alborelo reservoir for peak energy production (Table 12). This share of water can be used to produce energy in hours of biggest demand and be sold on the day-ahead-market with favourable peak energy prices. In Table 12 is also reported the annual flow utilization of inflows for the constructive measure, described in §6.1.2.

Table 12. Annual flow utilization of inflows to Lana HPP. Comparison between actual, operational only and constructive solution at Lana HPP.

| Purpose | Actual state | Operational measures | Constructive solution |
|---|---|---|---|
| Peak energy flow | 60% | 40% | 88% |
| Off-peak energy flow | 28% | 48% | |
| Reverse flow | 11% | 11% | 11% |
| Irrigational flow surge tank | 1% | 1% | 1% |

The environmental target values represented in Table 11 leads to

several restrictions to energy production on the Valsura cascade. To reach the above conditions by operational measures only, the operation of Lana HPP would have to consider the following additional restrictions:

1. in order to reach the minimum flow requirements downstream of the restitution of Lana HPP as described in Figure 41, additional 20% of the gross annual inflow at the intakes of Lana HPP would have to continuously turbined for increasing the base flow downstream of its restitution. In terms of energy, this share cannot be used for peak energy production but in future will be used for off-peak energy production. Water availability for peak energy production would fall from 60% to 40% of the annual average inflow;
2. furthermore, in order to maintain maximum flow limits at Lana HPP, the maximum turbined discharge would have to be reduced from 26.25 $m^3/s$ to, for example, 9.3 $m^3/s$ in February and 4.2 $m^3/s$ in March. Hence, 40% of the total water inflow, water that can be used for peak energy production with 9.3 $m^3/s$, would have to be discharged during longer period of time, which leads to a lower average annual energy selling price.

Summarizing the above, the application of the environmental targets by mere operational measures leads to severe energetic and economic restrictions for energy and especially for peak energy production on Lana HPP on Valsura River.

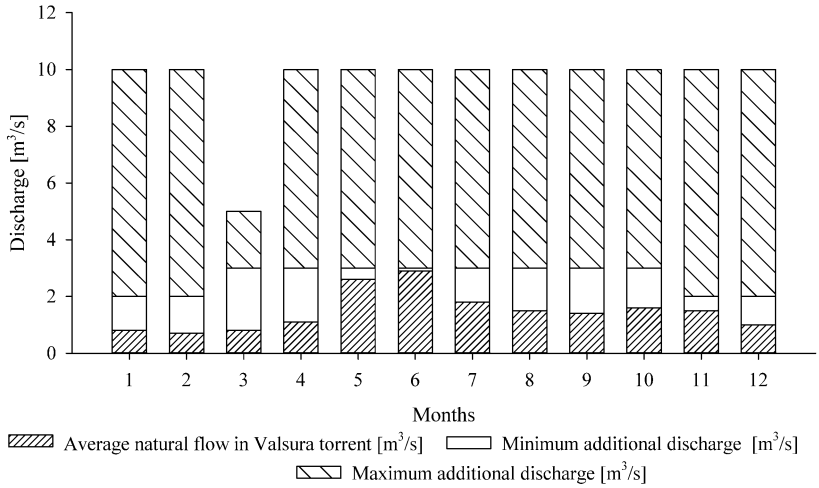


Figure 41. Base flow, discharge to add for meeting minimum flow demand and maximum turbine discharge for maintaining maximum flow limit.

From a social point of view, the reduction peak energy production is in contrast with the development of large reservoirs during the 60's and 70's of the last century, which lead to a resettling of large parts of the population from the best grass-lands of the valley to the stepper mountain shores in order to being able to construct large reservoirs for peak energy production.

Considering the above, alternatives to the extremely expensive operational limitations are desirable.

### 6.1.2 Constructive measures

Additionally to the already performed morphological improvement measures already present in the Valsura River (groynes, boulders, etc.) and in alternative to the previously described operational mitigation measures, constructive measures, even though extremely expensive in terms of investment costs, were investigated. As a constructive solution a mitigation concept was proposed that consists in the construction of a new tailrace hydropower plant (Lana di Sotto), combined with a large free-surface demodulation storage gallery (Premstaller et al., 2017).

The intake, the demodulation gallery and the penstock of the new hydropower plant will derive waters from the tailrace channel of Lana hydropower plant and redirect them directly to the Adige River, approximately 1 km downstream of the confluence of Valsura Torrent.

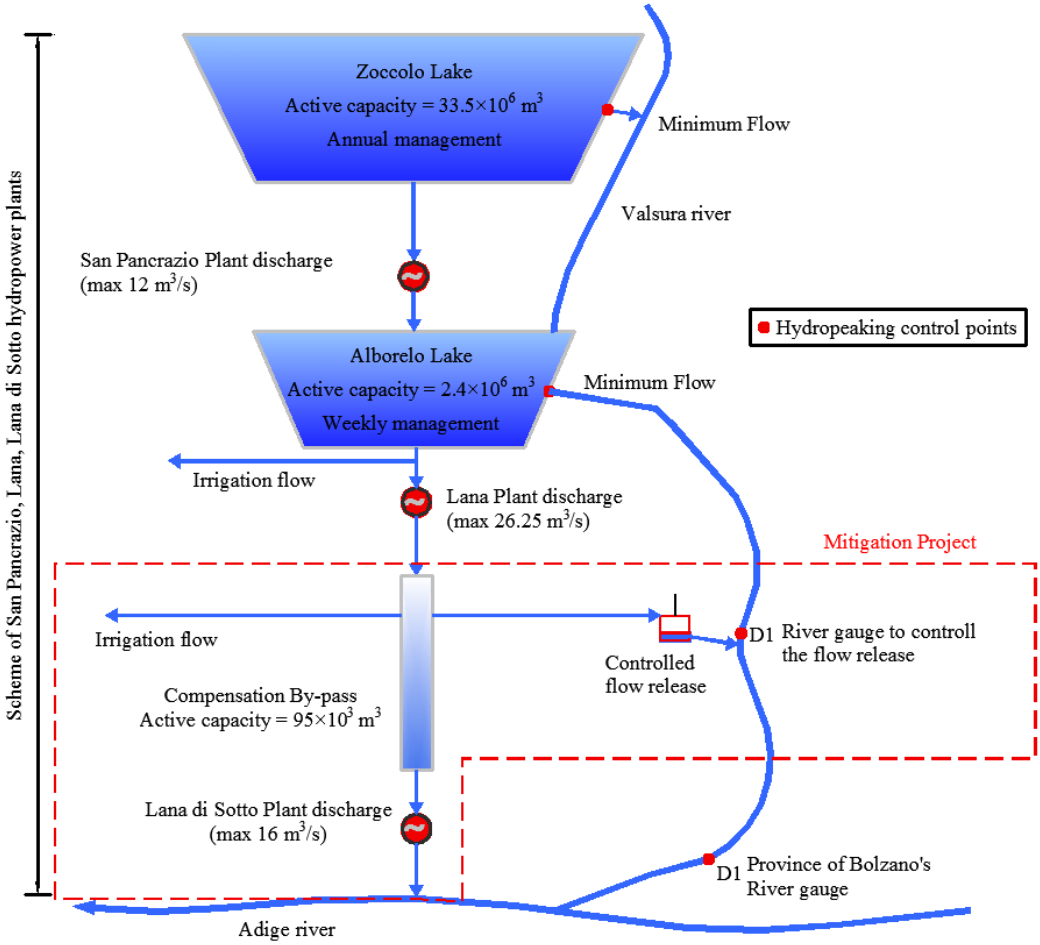


Figure 42. Constructive mitigation measure for Valsura River.

The project consists of the following elements (Figure 42 and Figure 43):

1. a combined, approximately 3.5 km long, compensation by-pass, which consists in a free surface hydropeaking demodulation and an irrigation gallery. The active water storage volume is 95000 $m^3$. Jointly, these function contribute to the reduction of

hydropeaking and to the increase of minimum flow in Valsura Torrent;

2. a new penstock, which transports the release discharge from the demodulation basin to the tailwater plant, where the water will be further used for production of electric energy;
3. a new hydropower plant (Lana di Sotto) with a restitution on the Adige River;
4. a new restitution of Lana hydropower plant on the Valsura Torrent, which will be operated to release eventual residual water to Valsura River in a controlled manner and will guarantee the irrigation water releases to the agricultural cooperative societies;
5. the installation of a new gauging station upstream of the restitution of Lana hydropower plant, which will serve to operate the integrative water releases sluice gate from the compensation basin to the Valsura Torrent.

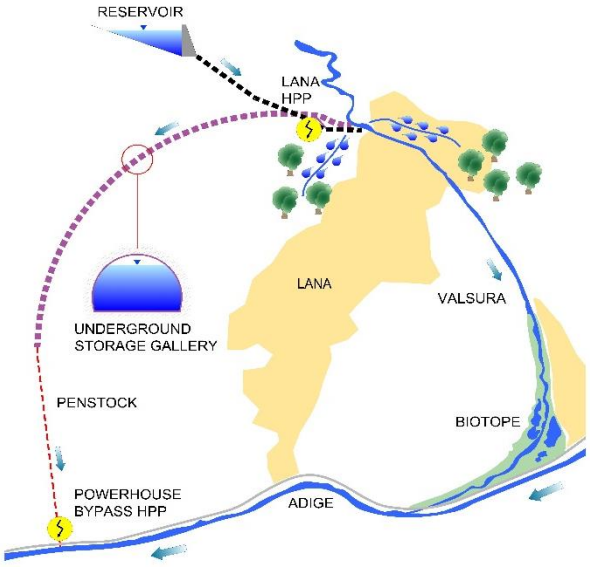


Figure 43. Hydraulic scheme of the constructive mitigation measure for Valsura river.

Operationally, the new hydropower scheme requires a joint

operation of the upstream hydropower plant (Lana HPP), of the downstream hydropower plant (Lana di Sotto HPP) and of the new restitution of Lana HPP in the Valsura. Furthermore, for the sake of civil protection, the hydropower operator and the local community of Lana started an information campaign on the risks of hydropeaking for river stakeholders.

The choice of adopting a demodulation gallery to limit the flow rate oscillations that affects the Valsura River has the advantages to use the accumulated water volume also as a storage for irrigation purposes and to permit Lana HPP to reduce continuous production of off-peak energy for irrigation water release and increase of more valuable peak energy. Moreover, this flow rate can be used enhancing system flexibility in order to improve starting and shut-down times. Finally, the accumulation volume is used for releasing the flow according to the required down-ramping rates (Table 11).

The functionality of the demodulation gallery leads to a greater flexibility of the existing Lana HPP leading to additional economic benefits from energy production. Additionally, approximately 38% of the water volume inflowing Lana HPP can be reused for energy production in new “Lana di Sotto” HPP. The benefits of the selling of the electric energy there can further contribute to the economical feasibility of the solution. Table 13 reports the main characteristics of the new Lana di Sotto HPP plant.

Table 13. Fundamental characteristics of new Lana di Sotto HPP.

| Hydropower plant | | Lana di Sotto |
|---|---|---|
| Max flow rate | [$m^3/s$] | 16.0 |
| Net hydraulic head | [m] | 56.0 |
| Max Power | [MW] | 8.0 |
| Annual generation | [GWh] | 9.2 |

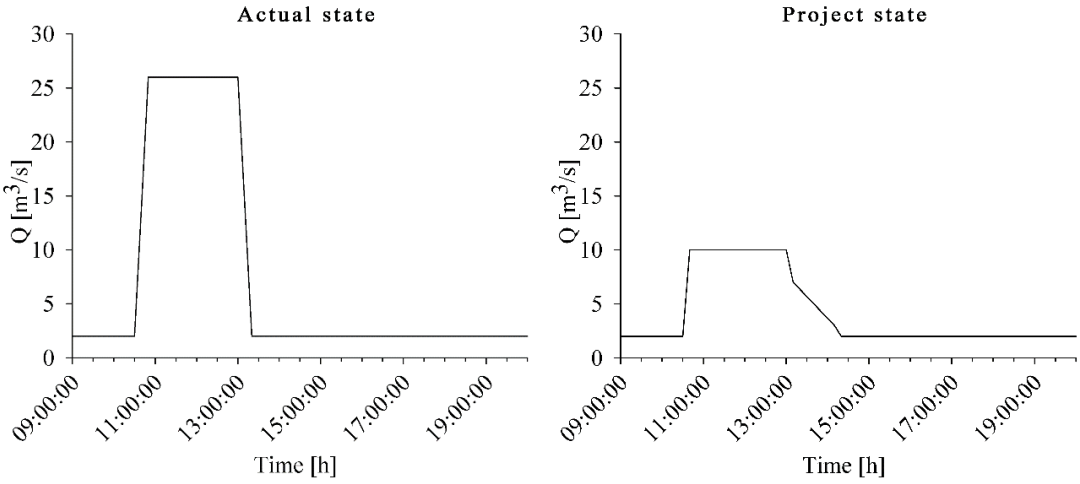


Figure 44. Comparison between actual and after project state of the flow rates in Valsura River.

Figure 44 shows the comparison between the typical actual hydropeaking wave in the Valsura Torrent and the future typical hydropeaking wave with operational and constructive mitigation measures. As for operational solutions, also in present constructive solution, the flow parameters reported in Table 11 are respected. It has to be highlighted that the project state flow rates in Figure 44 are the same both for operational and constructive projects.

However, the operational measures require more frequent and longer peak periods in order to produce energy with the residual hydropeaking volume in Valsura River of 40% (Table 12 and Table 14).

The constructive project is able to drastically reduce the frequency of hydropeaking in the Valsura Torrent, with a residual hydropeaking volume of approximately 2% of the annual average inflow to Lana HPP (Table 12 and Table 14). The residual hydropeaking discharge in the Valsura River occurs only in the case when the demodulation gallery is full, and at the same time, Lana di Sotto HPP and Lana HPP, produce at full discharge.

As shown in Table 14, the operational and the constructive

measures differ in the frequency of residual hydropeaking events.

Table 14. Comparison between operational and constructive solution against hydropeaking.

| | | Actual state | Operational measures | Constructive measures |
|---|---|---|---|---|
| Max. peaking discharge $Q_{max}$ | [m3/s] | 28 | 10 | 10 |
| Min. peaking discharge $Q_{min}$ | [m3/s] | 1 | 2 | 2 |
| Residual hydropeaking volume | [%] | 88 | 40 | 2 |
| Residual hydropeaking frequency | [-] | Daily | Daily | Sporadic |

## 6.2 RIO SELVA DEI MOLINI

From hydraulic and habitat simulation for the actual state reported in §5.4, is evident that the ecological condition of the Rio Selva dei Molini is strongly influenced by the morphology. Rio Selva dei Molini is in fact, from the outlet of Molini HPP to the confluence with Aurino River, restricted between retaining walls and riverbanks (§4.2.1), so turning out to be a channelized water course. This type of morphology can determine two effects in the habitat. The first one is related to a strong effect of flow rate to the presence of suitable area for fish. In fact, a channelized morphology implies a generalized increase of water velocity in all the reach for increasing flow rates. This aspect is evident if YOY life stage is considered (§5.4.1) where the WUA functions present a decreasing trend increasing the flow rate. This is due to the strong YOY sensitivity to flow velocity.

On the other side, a channelized morphology tends to minimize the stranding risk due to the absence of secondary channels and flood plain that tend to be wetted during peak flow and to be dried during the base flow.

For the Rio Selva dei Molini, the proposed mitigation measure is

based on a morphological approach and is a pure academic study without considering the economical implication. The study, therefore, is focalized to maximize the habitat for brown trout for YOY and adult life stages.

The proposed morphological mitigation measures consists in the insertion of small groynes organized in two configurations. The first one consist to insert groynes in proximity of the right riverbank. The second configuration presents alternating groynes from right to left riverbank.

As for the actual state analysis, mitigations measures are studied performing hydraulic simulations and habitat simulations with CASiMiR. The selected discharges are the same already analysed (Q = 1-2-3-5 and 7 $m^3/s$). For the hydraulics simulations, the mesh has a resolution of 0.5×0.5 m in the horizontal plane, also for the 2D model approach, and 5 cm in vertical direction.

### 6.2.1 Groynes in the right riverbank, habitat 2D-3D, YOY

The present proposed mitigation measure consist in the installation of five groynes along the right riverbank (Figure 45).

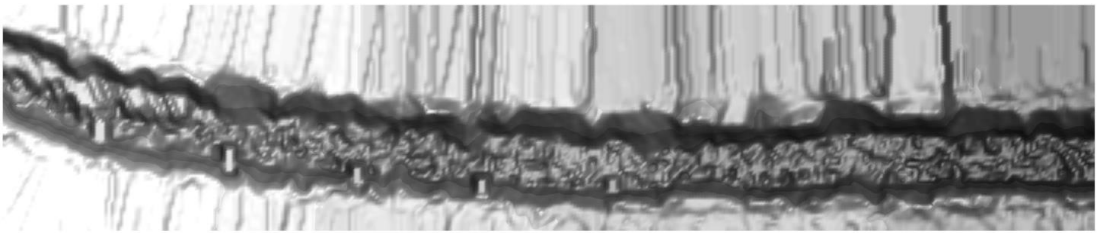

Figure 45. Groynes configuration in the right riverbank.

The focus is set on HSI-values > 0.6 to emphasize the relevance of highly suitable habitats (Figure 46, right).

In Figure 46A the results of habitat modelling applying the bottom velocity field from 3D modelling are shown. The habitat suitability map indicates that suitable habitats for YOY life stage are mainly located

close to shoreline without suitable habitats in the main channel.

Comparing Figure 46 with Figure 36 is possible to observe an increase of suitable areas along the shoreline especially on the right riverbank where are present the suggested groynes.

The area of HSI-classes for HSI > 0.6 shows a decrease of habitat quantity given the increase of flow velocities with an asymptote.

Figure 46B illustrates the simulated HSI-values using depth-averaged flow velocities as input for habitat modelling. The habitat suitability map shows very similar results with Figure 46A. Similar results between bottom 3D and depth-averaged 2D approach are visible if integrated assessments, such as WUA functions, are used.

The last comparison includes the habitat results from bottom flow velocities obtained by 3D modelling and 2D modelling using the logarithmic-law. Similarly to the other velocity field approaches, no suitable habitats are simulated in the main channel.

Figure 47 summarizes the results of habitat simulations with different velocity inputs in form of weighted usable areas (WUA) for HSI > 0.6.

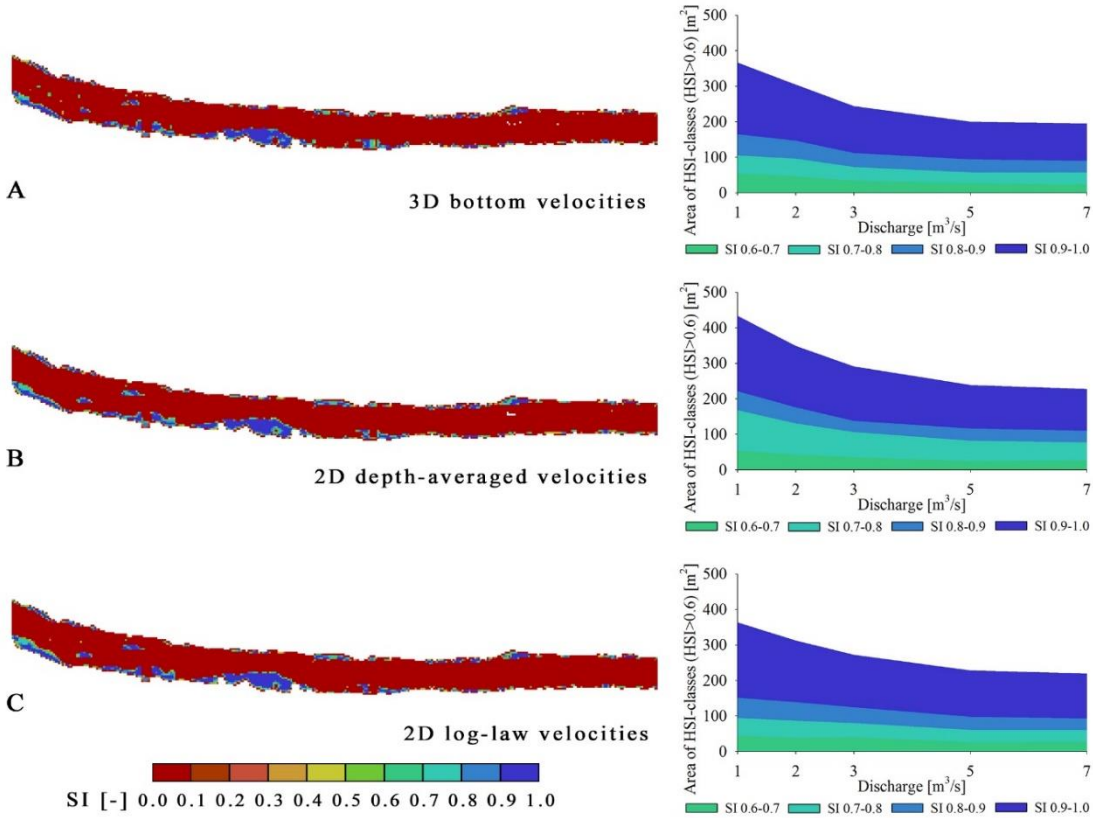


Figure 46. Habitat suitability maps of brown trout (YOY stage) considering different velocity field as input for habitat suitability modelling. The maps represent high flow rates close to the peak flow (Q = 7 $m^3/s$). A: bottom velocities from 3D modelling, B: depth-averaged velocities from 2D modelling, C: bottom velocities from 2D modelling using the logarithmic-law. Groynes in the right riverbanks.

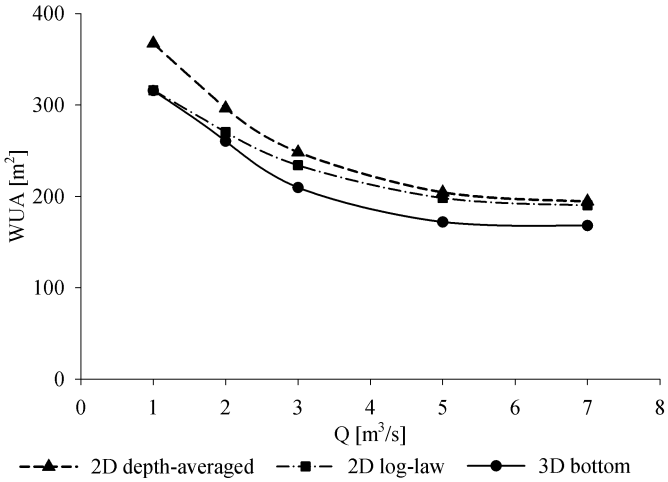


Figure 47. Weighted usable areas (WUA) for the three different velocity inputs in habitat modelling for the entire range of flow rates during hydropeaking events. YOY fish life stage. Groynes in the right riverbanks.

Comparing Figure 47 with Figure 37 is possible to observe two aspects. The first one is the increase of WUA values for all the discharges considered, with a consequent habitat increasing. The second aspect regards the shape of WUA curves. Adopting this type of mitigation measures, the WUA trend still shows a continuous decrease trend but tends to an asymptotic value higher than the actual state. At Q = 7 $m^3/s$ the difference between actual state and mitigated is about 36%.

### 6.2.2 Groynes in the right riverbank, habitat 2D-3D, Adult

The second comparison aims to compare simulated HSI-values for the adult life stages of brown trout. Similar to the analysis of HSI-values for the YOY stage, the results of habitat modelling (Figure 48) are evaluated based on their spatial distribution in form of habitat maps and on WUA functions.

In Figure 48A the results of habitat modelling applying the bottom velocity field from 3D modelling are shown. This habitat suitability map indicates that most suitable habitats are located close to the right

shoreline and behind boulders. The area of HSI-classes for HSI >0.6 shows, for flow rate up to 2 $m^3/s$, an increase of habitat quantity given the increase of the wetted area followed by a rather constant trend up to 5 $m^3/s$.

The habitat results obtained with the 3D bottom velocity field are used as a reference to determine the difference to the habitat results obtained with the velocity fields from 2D-modelling.

Figure 48B illustrates the simulated HSI-values using depth-averaged flow velocities as input for habitat modelling. A small loss of suitable habitats is observed for this investigation. The habitat suitability map shows less suitable habitat along the right shoreline and no suitable habitats in the main channel. The habitat loss is also clearly demonstrated for the areas of HSI-classes >0.6. While up to 2 $m^3/s$ no visible differences occur, the suitable areas assume lower value from 2 $m^3/s$ to 7 $m^3/s$. In comparison to the WUA of the bottom flow velocity simulated with a 3D model, the habitat loss is 16%. This loss of habitats becomes even more relevant considering the different habitat preferences applied for focal velocities (3D-modelling) and depth-averaged velocities (2D-modelling) because the habitat preferences for focal velocities are more restrictive compared to those for depth-averaged velocities. The reason for this habitat loss is a systematic overestimation of depth-averaged velocities, which neglect the strong bed heterogeneity and secondary currents induced by boulders and groynes leading to a reduction of the velocity magnitudes.

The last comparison includes the habitat results from bottom flow velocities obtained by 3D modelling and 2D modelling using the logarithmic-law. As both velocity fields represent the velocities close to the river bed the same habitat preferences (focal velocities) are used. Similarly, to the depth-averaged approach, small suitable habitats are simulated in the main channel. However, the habitats along the shoreline show a higher quantity and quality compared to the habitat results

obtained from depth-averaged velocities. The areas of HSI-classes for the entire range of flow rates during hydropeaking shows also a constant trend flow rates > 5 $m^3/s$. However, the reduction is not as large as for the scenario with depth-averaged velocities. The habitat loss at a discharge of 7 $m^3/s$ is 6% compared to the habitat availability obtained with the bottom velocities of 3D modelling.

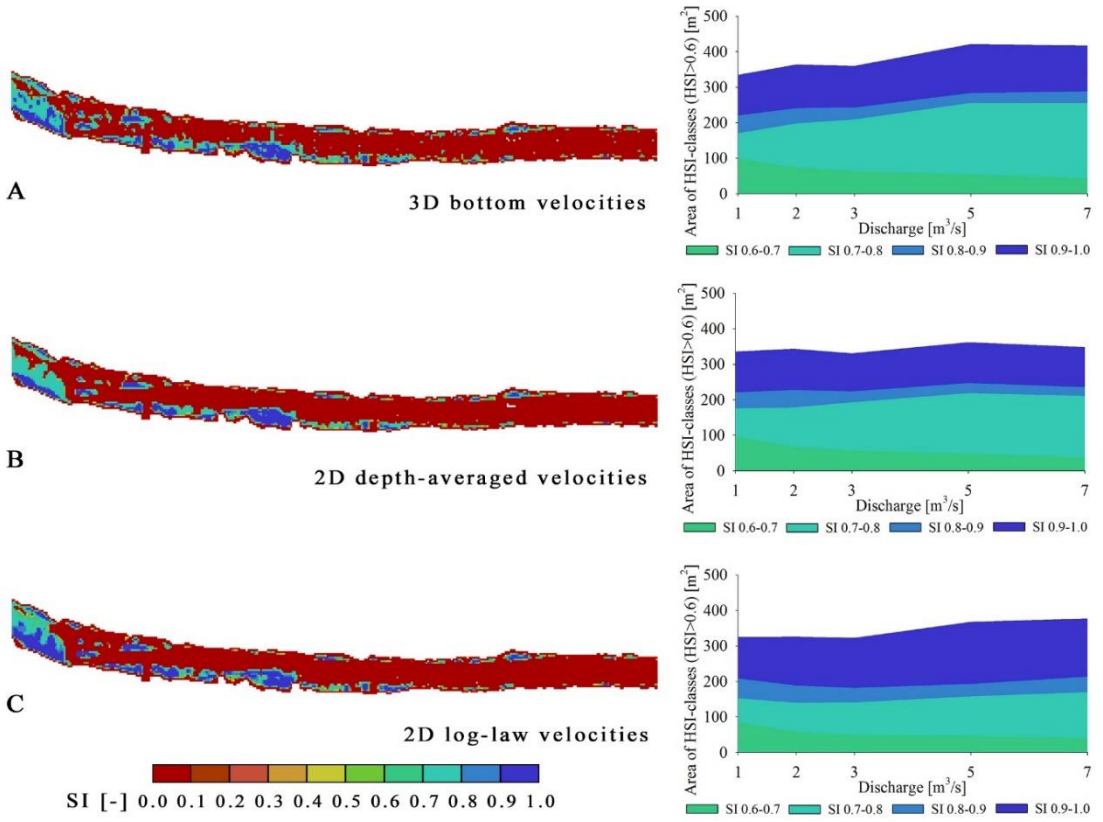


Figure 48. Habitat suitability maps of brown trout (adult stage) considering different velocity field as input for habitat suitability modelling. The maps represent high flow rates close to the peak flow (Q = 7 $m^3/s$). A: bottom velocities from 3D modelling, B: depth-averaged velocities from 2D modelling, C: bottom velocities from 2D modelling using the logarithmic-law. Groynes in the right riverbanks.

Comparing Figure 48 with Figure 38 is possible to observe an increase of suitable area for the adult life stage of brown trout, especially along the right riverbank. This aspect underlines that the groynes

proposed can be used from the fish as shelters areas to protect themselves during hydropeaking. The increase of HSI areas between the actual state and the proposed mitigation measure is about 100 $m^2$ that corresponds to a percentage value of about 33%. To observe that the area, which presents the higher increase, is characterized by the best Suitability Index value (0.9-1.0) therefore the increase of suitable areas is mainly related to an increase of areas that present very good habitat quality.

Figure 49 summarizes the results of habitat simulations with different velocity inputs in form of weighted usable areas (WUA) for HSI > 0.6.

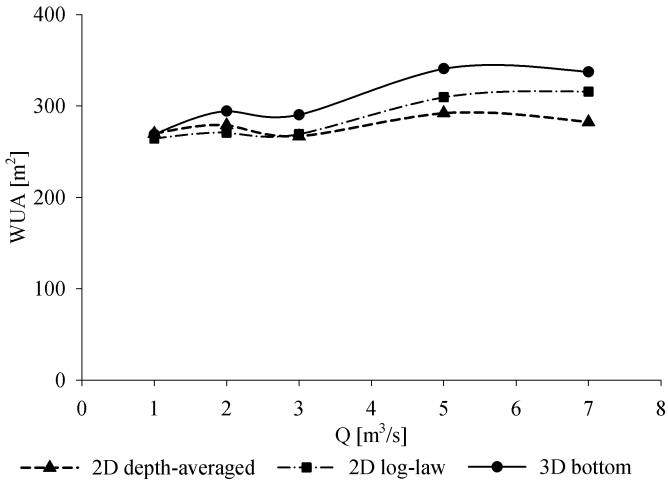


Figure 49. Weighted usable areas (WUA) for the three different velocity inputs in habitat modelling for the entire range of flow rates during hydropeaking events. Adult fish life stage. Groynes in the right riverbanks.

Figure 49 indicates a continuous increase of habitat availability for all considered flow velocity fields, because of the increase of the wetted area with velocities in the preferred range of adult brown trouts. For flow rates up to 7 $m^3/s$ a decrease of the WUA-values is observed only if 2D

approach with depth-averaged velocities is considered.

Figure 49 shows, moreover, an increasing difference between the WUA-values obtained from 3D modelling and 2D modelling with increasing flow rates.

Comparing WUA trend between actual state (Figure 39) and the proposed mitigation measure (Figure 49) is possible to note that, for the actual state increasing the flow rate, the WUA tends to a constant value. On the other hand, the WUA function for the mitigation project present an increasing trend with the flow rate. At Q = 7 $m^3/s$ the difference between actual state and mitigated is about 40%.

### 6.2.3 Alternating groynes, habitat 2D-3D, YOY

The present proposed mitigation measure consist in the installation of five alternating groynes from right to left riverbank. The purpose is to understand the influence of groyne arrangement on habitat suitability.

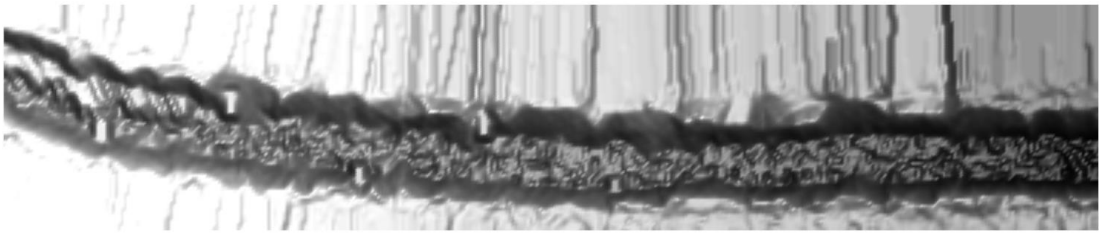

Figure 50. Groynes alternating configuration.

As for all the others habitat analysis, the focus is set on HSI-values > 0.6 to emphasize the relevance of highly suitable habitats (Figure 51, right).

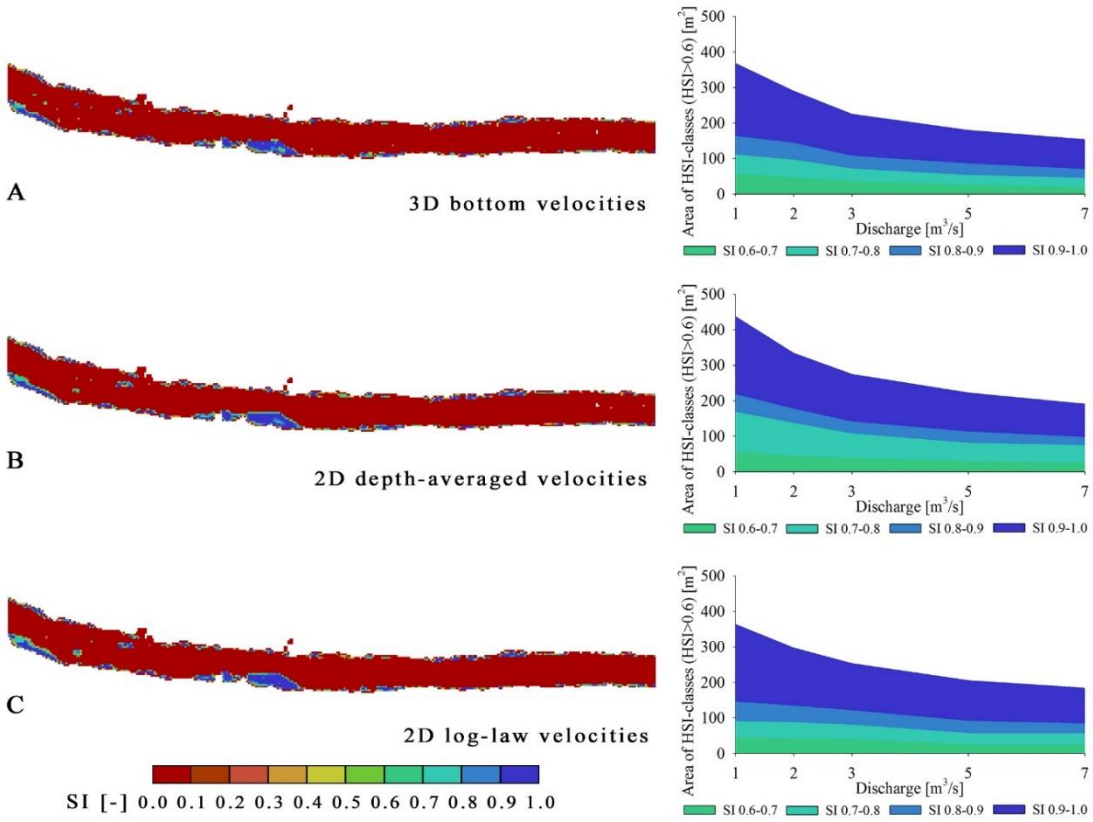


Figure 51. Habitat suitability maps of brown trout (YOY stage) considering different velocity field as input for habitat suitability modelling. The maps represent high flow rates close to the peak flow (Q = 7 $m^3/s$). A: bottom velocities from 3D modelling, B: depth-averaged velocities from 2D modelling, C: bottom velocities from 2D modelling using the logarithmic-law. Alternating groynes.

In Figure 51A the results of habitat modelling applying the bottom velocity field from 3D modelling are shown. The habitat suitability map indicates that suitable habitats for YOY life stage are mainly located close to shoreline without suitable habitats in the main channel.

Comparing Figure 51 with Figure 36 is possible to observe a small increase of suitable areas in along the right and left shoreline where are present the suggested groynes.

The area of HSI-classes for HSI > 0.6 shows a decrease of habitat

quantity given the increase of flow velocities.

Figure 51B illustrates the simulated HSI-values using depth-averaged flow velocities as input for habitat modelling. The habitat suitability map shows very similar results with Figure 51A. Similar results between bottom 3D and depth-averaged 2D approach are visible if integrated assessments, such as WUA functions, are used.

The last comparison includes the habitat results from bottom flow velocities obtained by 3D modelling and 2D modelling using the logarithmic-law. Similarly, to the others velocity field approaches no suitable habitats are simulated in the main channel.

Figure 52 summarizes the results of habitat simulations with different velocity inputs in form of weighted usable areas (WUA) for HSI > 0.6.

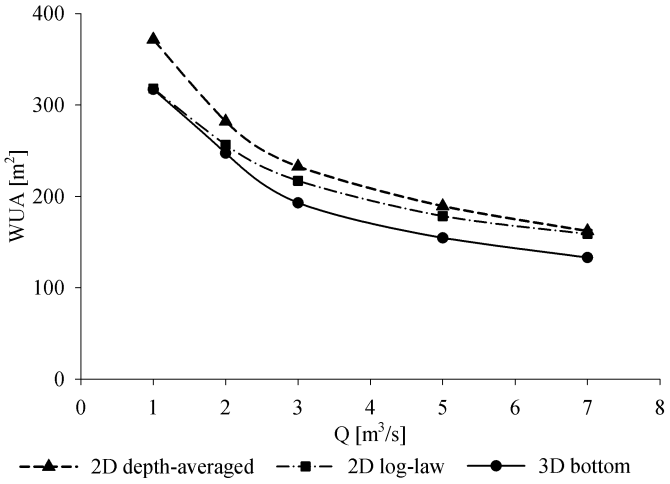


Figure 52. Weighted usable areas (WUA) for the three different velocity inputs in habitat modelling for the entire range of flow rates during hydropeaking events. YOY fish life stage. Alternating groynes.

Comparing the WUA curves from 2D and 3D bottom velocity approach, we can observe that the results are very similar. The differences are, for all investigated flow velocity fields, not as high as for the adult stage. This aspect is due to a very narrow preference curve

for the velocity quantity. Moreover, the YOY stage, presents a high preference for small to moderate water depth that implicate the presence of good habitat areas only near the banks.

Comparing the result from the actual state (Figure 37) and the mitigated one (Figure 52) is possible to observe that the increase of WUA values is related especially to low flow rates (1 $m^3/s < Q < 3$ $m^3/s$).

Adopting this type of mitigation measures, at Q = 2 $m^3/s$ the percentage WUA difference between actual state and mitigated is about 35%. However, at Q = 7 $m^3/s$, the percentage difference reduces to 8%. The efficiency of this mitigation measure tend to reduce increasing the flow rate.

### 6.2.4 Alternating groynes, habitat 2D-3D, Adult

The second comparison aims to compare simulated HSI-values for the adult life stages of brown trout. Similar to the analysis of HSI-values for the YOY stage, the results of habitat modelling (Figure 53) are evaluated based on their spatial distribution in form of habitat maps and on WUA functions.

In Figure 53A the results of habitat modelling applying the bottom velocity field from 3D modelling are shown. This habitat suitability map indicates that most suitable habitats are located close to the shoreline and behind boulders. The area of HSI-classes for HSI >0.6 shows up to 2 $m^3/s$ an increase of habitat quantity given the increase of the wetted area followed by a rather constant trend up to 3 $m^3/s$.

The habitat results obtained with the 3D velocity field close to the river bed are used as a reference to assess the difference to the habitat results obtained with the velocity fields from 2D-modelling.

Figure 53B illustrates the simulated HSI-values using depth-averaged flow velocities as input for habitat modelling. A small loss of suitable habitats is observed for this investigation. The habitat suitability map shows less suitable habitat along the right shoreline and no suitable

habitats in the main channel. The habitat loss is also clearly demonstrated for the areas of HSI-classes >0.6. While up to 2 $m^3/s$ no visible differences occur, the suitable areas assume lower value for flow rates between 2 $m^3/s$ and 7 $m^3/s$. In comparison to the WUA of the near bed flow velocity simulated with a 3D model, the habitat loss is about 20%.

The last comparison includes the habitat results from bottom flow velocities obtained by 3D modelling and 2D modelling using the logarithmic-law. As both velocity fields represent the velocities close to the river bed the identical habitat preferences (focal velocities) are used. Similarly, to the depth-averaged approach small suitable habitats are simulated in the main channel. However, the habitats along the shoreline show a higher quantity and quality compared to the habitat results obtained from depth-averaged velocities. The areas of HSI-classes for the entire range of flow rates during hydropeaking shows also a constant trend flow rates > 5 $m^3/s$. However, the reduction is not as large as for the scenario with depth-averaged velocities. The habitat loss at a discharge of 7 $m^3/s$ is 11% with respect to the habitat availability obtained with the bottom velocities of 3D modelling.

Comparing Figure 53 with Figure 38 is possible to observe an increase of suitable area for the adult life stage of brown trout especially along the right and the left riverbank. This aspect underlines that the groynes proposed can be used from the fish as shelters areas to protect themselves during hydropeaking. The increase of HSI areas between the actual state and the proposed mitigation measure is about 55 $m^2$ that corresponds to a percentage value of about 18%. To observe that the area, which presents the higher increase, is characterized by the best Suitability Index value (0.9-1.0) therefore the increase of suitable areas is mainly related to an increase of areas that present very good habitat quality.

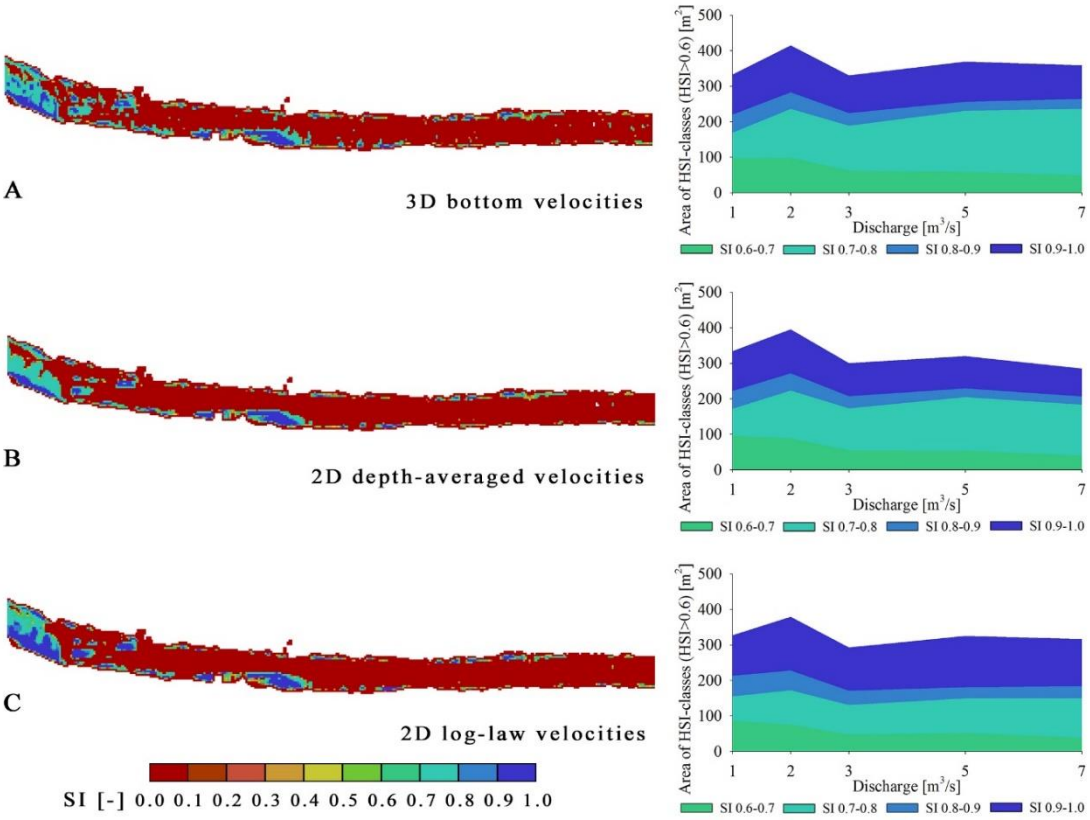


Figure 53. Habitat suitability maps of brown trout (adult stage) considering different velocity field as input for habitat suitability modelling. The maps represent high flow rates close to the peak flow (Q = 7 $m^3/s$). A: bottom velocities from 3D modelling, B: depth-averaged velocities from 2D modelling, C: bottom velocities from 2D modelling using the logarithmic-law. Alternating groynes.

Figure 54 summarizes the results of habitat simulations with different velocity inputs in form of weighted usable areas (WUA) for HSI > 0.6.

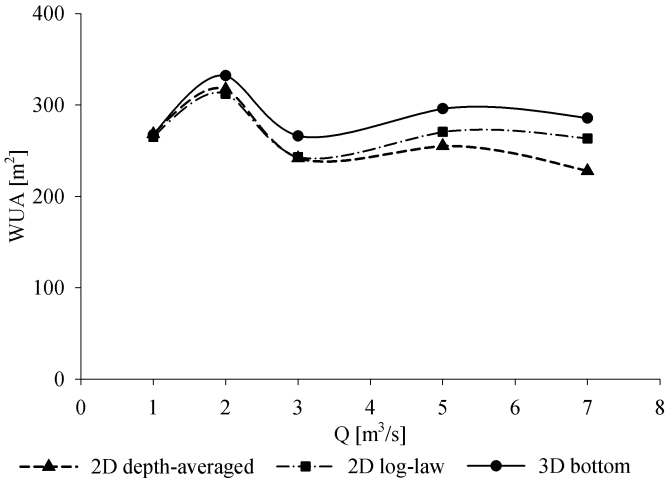


Figure 54. Weighted usable areas (WUA) for the three different velocity inputs in habitat modelling for the entire range of flow rates during hydropeaking events. Adult fish life stage. Alternating groynes.

Figure 54 indicates for all considered flow velocity fields an increase of habitat availability until 2 $m^3/s$, that is followed by a constant trend until 7 $m^3/s$. Figure 54 reveals, moreover, an increasing difference between the WUA-values obtained from 3D modelling and 2D modelling with increasing flow rates.

Comparing WUA trend between actual state (Figure 39) and the proposed mitigation measure (Figure 54), it is possible to note that for both the WUA trend is very similar and tends to a constant value for increasing flow rate. On the other hand, the WUA function for the mitigation project present higher values of usable areas for all the considered flow rates. Is interesting to note that for all the flow rates the difference between actual state and mitigated is about 20%.

### 6.2.5 Comparison and discussion

The mitigation measures proposed for the Rio Selva dei Molini are based on the introduction of morphological changes in the riverbed. The adopted solution is the use of small groynes made by boulders or gabions. The purpose is to create shelter zones for fish during hydropeaking peak

flow. We have to underline that a morphological change of the river could cause a different hydraulic response with possible flood problems for high discharges. Therefore, it is important to perform a hydraulic study of the reach to demonstrate that the mitigation measure does not influence so much the hydraulic safety of the reach.

In the present study, Rio Selva dei Molini presents a channelized morphology and, for the actual state, with hydropeaking peak flow rate of 7 $m^3/s$ the average simulated water depth in the studied reach is about 0.35m.

Adopting the mitigation measures is possible to observe a small increase of the average water depth. For the first groynes configuration (groynes on the right riverbank) the water depth rises to about 0.39 m with an increment of 4 cm. With the second configuration (alternating groynes) the water depth is about 0.38 m with an increment of 3 cm. The hydraulic safety is therefore, guaranteed.

To underline that the main purpose of this investigation is to maximize the habitat suitability. To understand the effect of the mitigation measures, a comparison between WUA curves for different flow rates is investigated. Figure 55 reports the comparison of WUA curves for YOY life stage and adult life stage for the actual state and the mitigated ones.

From Figure 55 (up) is possible to observe, for the YOY life stage, that both the groynes configuration increase the Usable Areas with a consequent increase of suitable habitat. To underline that, for low flow rates ($1\ m^3/s < Q < 2\ m^3/s$), the higher increment of habitat is obtained. The difference between actual state and mitigated one, decreases increasing the flow rate. Therefore, the efficiency for both the mitigation measures tends to decrease as far as the flow rate increases. However, the use of groynes only in the right riverbank, seems to be the best choice for the YOY life stage. In fact, the WUA curve for this configuration present always higher values compared with the actual state and the

second configuration, and an asymptotic trend for high flow rate without present a continuous decreasing trend. This aspect can be ascribed to a different effect on hydraulics for the right riverbank configuration. As described above, this configuration involves an in average higher water depth, that reflects on more stable good habitat areas downstream proposed groynes.

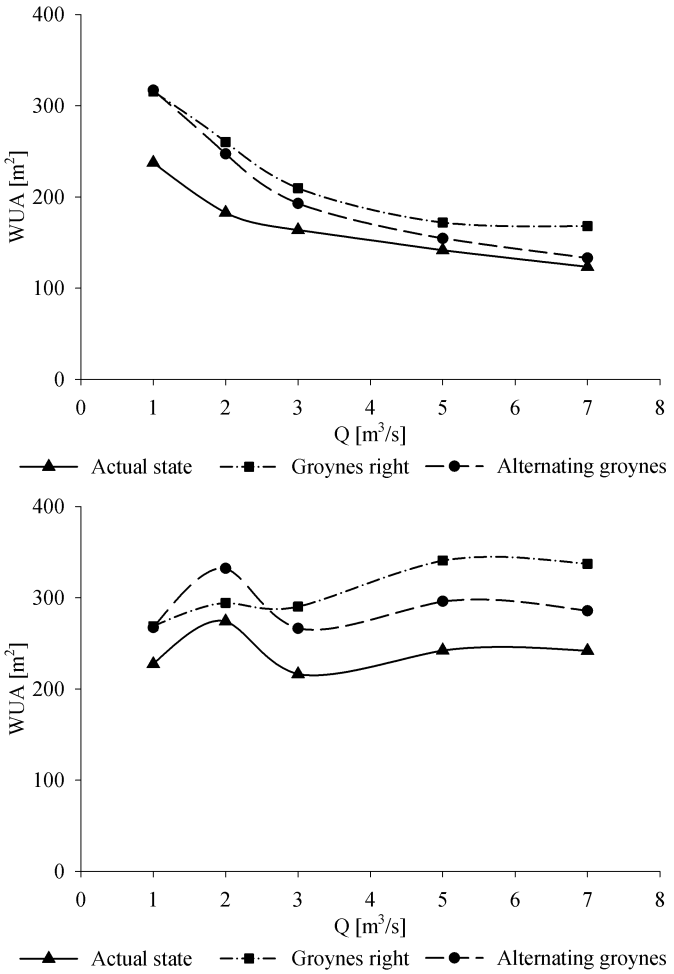


Figure 55. Comparison of WUA curves between actual state and the two proposed morphological mitigation measures. WUA curves for YOY life stage (up) and adult life stage (down).

Also for the adult life stage (Figure 55 down), both the groynes

configuration increase, for all the studied flow rates, the habitat suitability in comparison with the actual state. The use of alternating groynes involves a constant increase of WUA values for all the flow rates. The WUA trend for this configuration present a maximum at 2 $m^3/s$, as for the actual state, and a consecutive decrease of habitat for higher discharges (3 $m^3/s$) followed by a stable WUA value to 7 $m^3/s$.

The groyne configuration at the right riverbank, instead, shows a different WUA trend with a continuous increasing of suitable areas for increasing flow rate. In this configuration the maximum of WUA value is at 5 $m^3/s$. To underline that the difference between the actual state increase with the flow rate. Therefore, for low flow rates the alternating configuration seems, for adult life stage, the best mitigation measure. Instead, for high flow rates, the right riverbank configuration is the better one with more stable areas with god habitat quality downstream the groynes.

As described, the proposed morphological measures were studied without changing the operation of Molini HPP. As evident from Figure 55, to maximize the habitat suitability both for YOY and adult life stage, the flow rate should be regulated to a value between 1 $m^3/s$ and 2 $m^3/s$. Unfortunately, it is not possible to regulate the flow rate between these values without strongly reducing the gains of HPP operator. In fact, the operator should increase the minimum flow rate in hours that are not economical favourable and reduce the peak flow.

A possible alternative should be the construction of a by pass tunnel that connects the outlet of Molini HPP to the Aurino River that is already the final receiver of hydropeaking wave. The by pass should work only when the discharge in the hydropeaked reach of Rio Selva dei Molini is higher than 2 $m^3/s$. So the maximum flow rate in the by pass can be estimated about 6 $m^3/s$ for the mouth of June (Table 6).

# 7. CONCLUSION

The present thesis is focused on mitigation measures against hydropeaking effects and on methods to quantify the habitat suitability.

Habitat suitability modelling requires as input hydraulic variables such as water depth and velocity field. The flow field can be estimated using different approaches in order to obtain the depth-averaged velocity, which is usually used for habitat modelling, or the bottom velocity.

The thesis highlights that to estimate the habitat suitability is necessary to take into account a twofold problem. The first one is that different numerical schemes (2D and 3D), applied on complex river topographies, can give different results in terms of large scale circulations. Moreover, the methods analysed in the present work to calculate the velocity field (depth-averaged velocity, reconstruction near bed velocity with logarithmic-law profile from a 2D model, direct use of the 3D CFD model for near bed velocity) determine different results in habitat suitability simulations. The results highlight that, as reported by (Martínez-Capel et al., 2004; Milhous, 1999), the use of the bottom velocities is the key to a better habitat estimation. In particular, it is possible to reconstruct the vertical velocity profile through a theoretical approach from 1D and 2D simulations (for example by using a logarithmic-law profile) (Milhous, 1999) but this approach is not precise enough for the very complex bathymetric conditions that are present in alpine streams. A more realistic hydraulic simulation of separation zones and low velocity areas downstream of roughness elements can be performed best by applying a 3D approach.

This is important if focal velocities are used as an input in habitat modelling tools, especially because focal velocities are more selective from a biological point of view (Ayllón et al., 2010). Moreover, in the context of peak flows during hydropeaking events, the bottom flow velocities are important to adequately represent the availability of

shelter habitats.

Simultaneously, field studies show that fish prefer areas close to the bottom (Heggenes, 1996; Martínez-Capel et al., 2004). Therefore, is necessary to modify the preference curves for the velocity considering the velocity field near the bottom.

The present work has compared the availability of suitable habitat areas for brown trout in a reach of the Valsura River and Rio Selva dei Molini (Bolzano, Italy) using three different approaches to reconstruct the velocity field. In particular, although a comparison between theoretical approaches to simulate bottom velocities and different suitable habitat is present in the scientific literature (Martínez-Capel et al., 2004; Milhous, 1999), the use of a fully 3D CFD model has never been thoroughly analysed.

The results highlighted the effect of 2D versus 3D hydrodynamic modelling on simulated habitat suitability. Laboratory experiments, comparing measured and simulated flow velocities, showed the improved velocity field reproduction for the 3D model compared to the 2D depth averaged and the log-law 2D model.

From an ecological point of view, for the YOY life stage the differences in habitat quality, considering different velocity field reconstructions, were not that evident. The YOY life stage, in fact, presents narrow preference curves for flow velocity, with no suitable habitats for flow velocities higher than 0.5 m/s, and prefers shallow water areas that are present only near the banks.

Habitat suitability results, for adult brown trout, showed a remarkable difference between 3D and 2D modelled velocity fields, especially for higher flow rates. The results using 3D hydraulic modelling highlighted the formation of suitable habitat areas in the recirculation and separation regions downstream of large boulders and groynes, which were not detected by habitat results using depth-averaged velocity information or bottom flow velocities of 2D models

using the logarithmic law.

In conclusion, the results of 3D hydrodynamic modelling allows one for an improved description of niche habitats over a wide range of flow rates. This is an essential aspect for investigations on the ecological implications induced by hydropeaking and need to be considered in the planning process of mitigation scenarios. For example, the habitat simulation results of the case study in the Valsura River confirm the capability of boulders and groynes (morphological mitigation measures) to increase the habitat availability and to provide continuously usable habitats for adult brown trout during hydropeaking events. This aspect is also highlighted by habitat simulation for Rio Selva dei Molini if morphological mitigation measures are adopted. In this case, the use of two type of groynes configurations are analysed. Both configurations involve an increase of suitable areas for brown trout downstream groynes, where the velocity field complexity is better reproduced by a 3D approach.

Moreover, two possible mitigation measures for Valsura River and Rio Selva dei Molini are proposed.

For Valsura River, in order to choose the best solution, a detailed hydraulic, ecological and power production analysis of the Valsura reach actual state was performed. From the results of the ecological measurements on the hydropeaked stretch and on the unaffected Passirio River and from the results of hydraulic and habitat modelling, target discharges for a sustainable ecological status were developed.

The consequences of the implementation of the ecological targets through operational measures, on the hydropower plants operation, the water balance and the peak energy production, were described.

Even if the operational solution allows the maintenance of the ecological discharge targets, it presents negative effects on energy production, given that the power plant in its peak energy production is restricted. An optimized constructive multipurpose solution consisting

on the combination of a demodulation gallery of 95,000 $m^3$ and a bypass hydropower plant, which transports the water directly to Adige River, can merge ecological purposes with energy production purposes and even produce operational benefits.

For Rio Selva dei Molini a morphological mitigation measure is proposed with the use of two types of groynes configuration. In this case, both configuration increase the habitat suitability for all the flow rates analysed.

Many rivers and HPPs in the Alps face similar problems and the approach presented in the current work can be adopted on other projects. Nonetheless, the theme remains highly complex and hydropeaking mitigation projects will always have to address the relevant topics in a specific way for each single hydropeaked river.

The outcomes of this study are highly valuable for further investigations on mitigating the ecological implications of hydropeaking and represents a major advancements compared to common approaches, which use predominantly depth-averaged flow velocities as input parameter for habitat modelling.

## 7.1 RECOMMENDATIONS FOR FUTURE WORK

To better understand the hydropeaking effects on biota further investigations are required. Hydropeaking is an unsteady event and a better and more detailed analysis of the effects of the unsteady process should be deeper investigated (Shen and Diplas, 2010; Song and Graf, 1996). The possibility to analyse the unsteady effects could entail a better representation of the habitat variation along the time. For example the suitable areas for the young fishes can experience more frequent variations than habitat for adult life stages (Boavida et al., 2013). Moreover, in the presented approach univariate preference functions were applied, that do not allow for a consideration of interacting habitat parameters. Multivariate approaches, such as fuzzy-logic, might also

account for shelter habitats by taking into account large boulders that lead to a reduction of bottom flow velocities.

Furthermore, should be investigated the possibility to connect the micro-scale habitat simulations with meso-scale approach to have a better prediction for bigger case study but with a good habitat analysis where the complex heterogeneity of the riverbed is better simulated by a 3D approach.

Finally, the hydropeaking mitigation projects effects on human safety, along the hydropeaked river stretches, should be studied.

# 8. APPENDIX

## 8.1 APPENDIX 1

## 8.2 APPENDIX 2

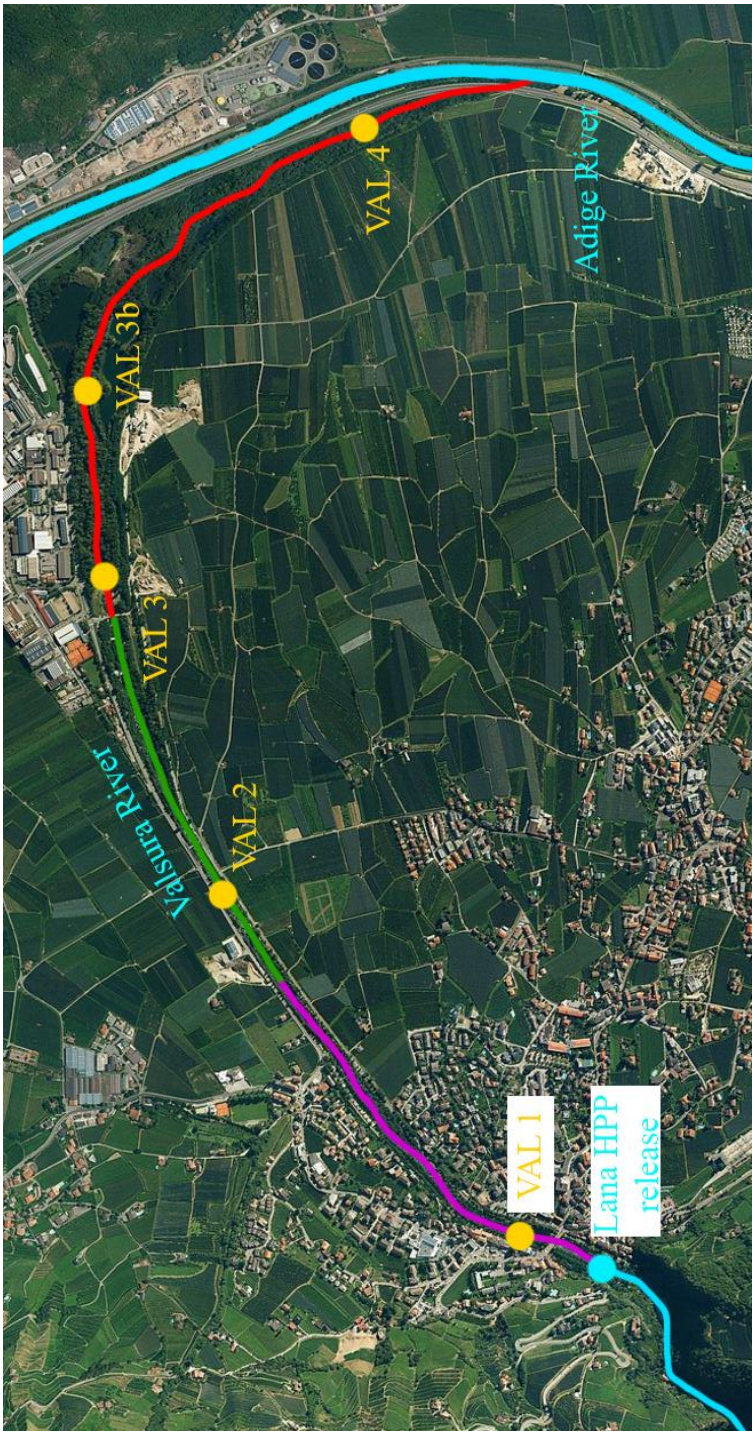

# 9. REFERENCES

Ahmadi-Nedushan, B., St-Hilaire, A., Bérubé, M., Robichaud, É., Thiémonge, N., Bobée, B., 2006. A review of statistical methods for the evaluation of aquatic habitat suitability for instream flow assessment. River Res. Appl. 22, 503–523. doi:10.1002/rra.918

Anselmetti, F.S., Bühler, R., Finger, D., Girardclos, S., Lancini, A., Rellstab, C., Sturm, M., 2007. Effects of Alpine hydropower dams on particle transport and lacustrine sedimentation. Aquat. Sci. 69, 179–198. doi:10.1007/s00027-007-0875-4

Armanini, A., Righetti, M., Sartori, F., 2010a. Experimental analysis of fluvial groynes. Sbe.Hw.Ac.Uk.

Armanini, A., Sartori, F., Tomio, G., 2010b. Analysis of a fluvial groynes system on hydraulic scale model. River FLow 2010.

Armstrong, J.., Kemp, P.., Kennedy, G.J.., Ladle, M., Milner, N.., 2003. Habitat requirements of Atlantic salmon and brown trout in rivers and streams. Fish. Res. 62, 143–170. doi:10.1016/S0165-7836(02)00160-1

Auer, S., Zeiringer, B., Führer, S., Tonolla, D., Schmutz, S., 2017. Effects of river bank heterogeneity and time of day on drift and stranding of juvenile European grayling (Thymallus thymallus L.) caused by hydropeaking. Sci. Total Environ. 575, 1515–1521. doi:10.1016/j.scitotenv.2016.10.029

Ayllón, D., Almodóvar, a., Nicola, G.G., Elvira, B., 2010. Ontogenetic and spatial variations in brown trout habitat selection. Ecol. Freshw. Fish 19, 420–432. doi:10.1111/j.1600-0633.2010.00426.x

Baumann, P., Klaus, I., 2003. Gewässerökologische Auswirkungen des Schwallbetriebes. Mitteilungen zur Fischerei MFI Bundesamt für Umwelt.

Bezzola, G.R., 2002. Fliesswiderstand und Sohlenstabilität natürlicher Gerinne. doi:10.3929/ethz-a-004288999

Boavida, I., Santos, J.M., Ferreira, M.T., Pinheiro, A., 2013. Fish Habitat-Response to Hydropeaking. Proc. 2013 IAHR Congr. 1–8.

Bovee, K.D., 1986. Development and evaluation of habitat suitability criteria

for use in the instream flow incremental methodology.

Bruno, M.C., Maiolini, B., Carolli, M., Silveri, L., 2009. Short time-scale impacts of hydropeaking on benthic invertebrates in an Alpine stream (Trentino, Italy). Limnologica 40, 281–290. doi:10.1016/j.limno.2009.11.012

Carolli, M., Bruno, M.C., Siviglia, A., Maiolini, B., 2012. Responses of benthic invertebrates to abrupt changes of temperature in flume simulations. River Res. Appl. 28, 678–691. doi:10.1002/rra.1520

Casulli, V., 1999. A semi-implicit finite difference method for non-hydrostatic, free-surface flows. Int. J. Numer. Methods Fluids 30, 425–440. doi:10.1002/(SICI)1097-0363(19990630)30:4<425::AID-FLD847>3.0.CO;2-D

Casulli, V., Cheng, R.T., 1992. Semi-implicit finite difference methods for three-dimensional shallow water flow. Int. J. Numer. Methods Fluids 15, 629–648. doi:10.1002/fld.1650150602

Casulli, V., Walters, R., 2000. An unstructured grid, three-dimensional model based on the shallow water equations. Int. J. Numer. Methods Fluids 32, 331–348. doi:10.1002/(SICI)1097-0363(20000215)32:3<331::AID-FLD941>3.0.CO;2-C

Casulli, V., Zanolli, P., 2002. Semi-implicit numerical modeling of nonhydrostatic free-surface flows for environmental problems. Math. Comput. Model. 36, 1131–1149. doi:10.1016/S0895-7177(02)00264-9

Charmasson, J., Zinke, P., 2011. Mitigation Measures Against Hydropeaking, in: Sintef Energy Research Norway (Ed.), EnviPEAK Publications. p. 51.

Costa, R.M.S., Martínez-Capel, F., Muñoz-Mas, R., Alcaraz-Hernández, J.D., Garófano-Gómez, V., 2012. Habitat suitability modelling at mesohabitat scale and effects of dam operation on the endangered Júcar Nase, Parachondrostoma Arrigonis (river Cabriel, Spain). River Res. Appl. 28, 740–752. doi:10.1002/rra.1598

Eurelectric, 2015. Hydropower supporting a power system in transistion. Brussels.

Fambri, F., Dumbser, M., Casulli, V., 2014. An efficient semi-implicit method for three-dimensional non-hydrostatic flows in compliant arterial vessels. Int. j. numer. method. biomed. eng. 30, 1170–1198. doi:10.1002/cnm.2651

Fang, H.-W., Rodi, W., 2003. Three-dimensional calculations of flow and suspended sediment transport in the neighborhood of the dam for the Three Gorges Project (TGP) reservoir in the Yangtze River. J. Hydraul. Res. 41, 379–394. doi:10.1080/00221680309499983

Gostner, W., Lucarelli, C., Theiner, D., Krager, A., Premstaller, G., Schleiss, A.J., 2011. A holistic approach to reduce negative impacts of hydropeaking. Dams Reserv. under Chang. Challenges 857–865.

Greenberg, L., Svendsen, P., Harby, A., 1996. Availability of microhabitats and their use by brown trout (Salmo trutta) and grayling (Thymallus thymallus) in the River Vojman, Sweden. Regul. Rivers Res. Manag. 12, 287–303. doi:10.1002/(Sici)1099-1646(199603)12:2/3<287::Aid-Rrr396>3.3.Co;2-V

GSEP, G.S.E.P., 2015. Powering Innovation for a sustainable future.

Hauer, C., Holzapfel, P., Leitner, P., Graf, W., 2016a. Longitudinal assessment of hydropeaking impacts on various scales for an improved process understanding and the design of mitigation measures. Sci. Total Environ. doi:10.1016/j.scitotenv.2016.10.031

Hauer, C., Schober, B., Habersack, H., 2013. Impact analysis of river morphology and roughness variability on hydropeaking based on numerical modelling. Hydrol. Process. 27, 2209–2224. doi:10.1002/hyp.9519

Hauer, C., Siviglia, A., Zolezzi, G., 2016b. Hydropeaking in regulated rivers – From process understanding to design of mitigation measures. Sci. Total Environ. doi:10.1016/j.scitotenv.2016.11.028

Heggenes, J., 2002. Flexible Summer Habitat Selection by Wild, Allopatric Brown Trout in Lotic Environments. Trans. Am. Fish. Soc. 131, 287–298. doi:10.1577/1548-8659(2002)131<0287:FSHSBW>2.0.CO;2

Heggenes, J., 1996. Habitat selection by brown trout (Salmo trutta) and young Atlantic salmon (S-salar) in streams: Static and dynamic hydraulic modelling. Regul. Rivers-Research Manag. 12, 155–169. doi:10.1002/(sici)1099-1646(199603)12:2/3<155::aid-rrr387>3.3.co;2-4

Heggenes, J., Bagliniere, J.L., Cunjak, R. a, 1999. Spatial niche variability for young Atlantic salmon (Salmo salar) and brown trout (S-trutta) in heterogeneous streams. Ecol. Freshw. Fish 8, 1–21 ST–Spatial niche variability for young Atl. doi:10.1111/j.1600-0633.1999.tb00048.x

Heggenes, J., Brabrand, Å., Saltveit, S.J., 1991. Microhabitat use by brown trout, Salmo trutta L. and Atlantic salmon, S. salar L., in a stream: a comparative study of underwater and river bank observations. J. Fish Biol. 38, 259–266. doi:10.1111/j.1095-8649.1991.tb03112.x

Heggenes, J., Wollebæk, J., 2013. Habitat use and selection by brown trout in streams, in: Maddock, I., Harby, A., Kemp, P., Wood, P. (Eds.), Ecohydraulics: An Integrated Approach. John Wiley & Sons, Ltd, Chichester, UK, pp. 159–176.

Hill, J., Grossman, G.D., 1993. An Energetic Model of Microhabitat Use for Rainbow Trout and Rosyside Dace. Ecology 74, 685. doi:10.2307/1940796

ISPRA, 2015. Fattori di emissione atmosferica di CO2 e sviluppo delle fonti rinnovabili nel settore elettrico. doi:978-88-448-0695-8

Jackson, H.M., Gibbins, C.N., Soulsby, C., 2007. Role of discharge and temperature variation in determining invertebrate community structure in a regulated river. River Res. Appl. 23, 651–669. doi:10.1002/rra.1006

Jungwirth, M., Moog, O., Schmutz, S., 1990. Auswirkungen der Veränderungen des Abflußregimes auf die Fisch- und Benthosfauna anhand von Fallbeispielen 10, 193–234.

Kopecki, I., 2008. Calculational Approach to FST- Hemispheres for Multiparametrical Benthos Habitat Modelling.

Korman, J., Campana, S.E., 2009. Effects of Hydropeaking on Nearshore Habitat Use and Growth of Age-0 Rainbow Trout in a Large Regulated

River. Trans. Am. Fish. Soc. 138, 76–87. doi:10.1577/T08-026.1

KWO, 2013. Das Beruhigungsbecken in Innertkirchen verbessert die Gewässerökologie in der Aare.

Maddock, I., 1999. The importance of physical habitat assessment for evaluating river health. Freshw. Biol. 41, 373–391. doi:10.1046/j.1365-2427.1999.00437.x

Martínez-Capel, F., García de Jalón, D., Rodilla-Alamá, 2004. On the estimation of nose velocities and their influence on the physical habitat simulation for Barbus Bocagei. Hydroécologie Appliquée 14, 139–159. doi:10.1051/hydro:2004009

Meile, T., Boillat, J.-L., Schleiss, a. J., 2011. Hydropeaking indicators for characterization of the Upper-Rhone River in Switzerland. Aquat. Sci. 73, 171–182. doi:10.1007/s00027-010-0154-7

Meile, T., Fette, M., Baumann, P., 2005. Synthesebericht Schwall/Sunk Publikation des Rhone-Thur Projektes. Proj. Rep. 48.

Milhous, R.T., 1999. Nose velocities in physical habitat simulation. XXVIII IAHR Congr.

Milhous, R.T., Waddle, T.J., 2012. Physical Habitat Simulation (PHABSIM) Software for Windows (v.1.5.1).

Noack, M., Schneider, M., Wieprecht, S., 2013. The Habitat Modelling System CASiMiR: A multivariate Fuzzy-Approach and its Applications, in: Maddock, I., Harby, A., Kemp, P., Wood, P. (Eds.), Ecohydraulics: An Integrated Approach. John Wiley & Sons, Ltd, Chichester, UK, pp. 75–91.

Parasiewicz, P., 2007. The MesoHABSIM model revisited. River Res. Appl. 23, 893–903. doi:10.1002/rra.1045

Pellaud, M., 2007. Ecological response of a multi-purpose river project macro-invertebrates richness and fish habitat value 3807, 197.

Person, É., 2013. Impact of hydropeaking on fish and their habitat. Commun. du Lab. Constr. Hydraul. - 55 5812, 139. doi:http://dx.doi.org/10.5075/epfl-thesis-5812

Pisaturo, G.R., Righetti, M., Dumbser, M., Noack, M., Schneider, M., Cavedon,

V., 2017. The role of 3D-hydraulics in habitat modelling of hydropeaking events. Sci. Total Environ. 575. doi:10.1016/j.scitotenv.2016.10.046

Poff, N.L., Allan, J.D., Bain, M.B., Karr, J.R., Prestegaard, K.L., Richter, B.D., Sparks, R.E., Stromberg, J.C., 1997. The Natural Flow Regime. Bioscience 47, 769–784. doi:10.2307/1313099

Premstaller, G., Cavedon, V., Pisaturo, G.R., Schweizer, S., Adami, V., Righetti, M., 2017. Hydropeaking mitigation project on a multi-purpose hydro-scheme on Valsura River in South Tyrol/Italy. Sci. Total Environ. 574, 642–653. doi:10.1016/j.scitotenv.2016.09.088

Pretty, J.L., Harrison, S.S.C., Shepherd, D.J., Smith, C., Hildrew, A.G., Hey, R.D., 2003. River rehabilitation and fish populations: assessing the benefit of instream structures. J. Appl. Ecol. 40, 251–265. doi:10.1046/j.1365-2664.2003.00808.x

Riedl, C., Peter, A., 2013. Timing of brown trout spawning in Alpine rivers with special consideration of egg burial depth. Ecol. Freshw. Fish 22, 384–397. doi:10.1111/eff.12033

Rosenfeld, J., Whiteway, S.L., Biron, P.M., Zimmermann, A., Venter, O., Grant, J.W.A., 2010. Do in-stream restoration structures enhance salmonid abundance? A meta-analysis. Can. J. Fish. Aquat. Sci. 67, 831–841. doi:10.1139/F10-021

Sabaton, C., Souchon, Y., Capra, H., Gouraud, V., Lascaux, J.-M., Tissot, L., 2008. Long-term brown trout populations responses to flow manipulation. River Res. Appl. 24, 476–505. doi:10.1002/rra.1130

Schälchli, U., Eberstaller, J. Moritz, C., Schmutz, S., 2003. Notwendige und wünschbare Schwallreduktion im Alpenrhein.

Schleiss, A., 2007. L'hydraulique suisse: Un grand potentiel de croissance par l'augmentation de la puissance. Bull. SEV/AES 24–29.

Schneider, M., 2001. Habitat- und Abflussmodellierung fuer Fliessgewaesser mit unscharfen Berechnungsansaetzen. University of Stuttgart, Germany.

Schneider, M., Noack, M., 2009. Untersuchung der Gefährdung von Jungfischen durch Sunkereignisse mit Hilfe eines

Habitatsimulationsmodells 101, 107–112.

Schneider, M., Noack, M., Gebler, T., Kopechi, L., 2010. CASIMIR - Handbook for the module habitat simulation.

Schweizer, S., Schmidlin, S., Tonolla, D., Büsser, P., Monney, J., Schläppi, S., Wacher, K., 2013. Schwall/Sunk-Sanierung in der Hasliaare – Phase 1a: Gewässeröokologische Bestandaufnahme (No. 3).

Schweizer, S., Tonolla, D., Bruder, A., Vollenweider, S., 2015. Schwall und Sunk – ein kurzer Überblick 15–20.

Shen, Y., Diplas, P., 2010. Modeling Unsteady Flow Characteristics of Hydropeaking Operations and Their Implications on Fish Habitat. J. Hydraul. Eng. 136, 1053–1066. doi:10.1061/(ASCE)HY.1943-7900.0000112

Shirvell, C.S., Dungey, R.G., 1983. Microhabitats Chosen by Brown Trout for Feeding and Spawning in Rivers. Trans. Am. Fish. Soc. 112, 355–367. doi:10.1577/1548-8659(1983)112<355:MCBBTF>2.0.CO;2

Song, T., Graf, W.H., 1996. Velocity and Turbulence Distribution in Unsteady Open-Channel Flows. J. Hydraul. Eng. 122, 141–154. doi:10.1061/(ASCE)0733-9429(1996)122:3(141)

Stansby, P.K., Zhou, J.G., 1998. Shallow-water flow solver with non-hydrostatic pressure: 2D vertical plane problems. Int. J. Numer. Methods Fluids 28, 541–563. doi:10.1002/(SICI)1097-0363(19980915)28:3<541::AID-FLD738>3.0.CO;2-0

Tanno, D., 2012. Physical habitat modeling for the assessment of macroinvertebrate response to hydropeaking.

Taylor, M.K., Cooke, S.J., 2012. Meta-analyses of the effects of river flow on fish movement and activity. Environ. Rev. 20, 211–219. doi:10.1139/a2012-009

Terna, R.I., 2015. Rapporto mensile sul sistema elettrico - consuntivo Settembre 2015.

Toffolon, M., Siviglia, A., Zolezzi, G., 2010. Thermal wave dynamics in rivers affected by hydropeaking. Water Resour. Res. 46, n/a-n/a.

doi:10.1029/2009WR008234

Tonolla, D., Bruder, A., Schweizer, S., 2017. Evaluation of mitigation measures to reduce hydropeaking impacts on river ecosystems ??? a case study from the Swiss Alps. Sci. Total Environ. 574, 594–604. doi:10.1016/j.scitotenv.2016.09.101

Tuhtan, J. a., Noack, M., Wieprecht, S., 2012. Estimating stranding risk due to hydropeaking for juvenile European grayling considering river morphology. KSCE J. Civ. Eng. 16, 197–206. doi:10.1007/s12205-012-0002-5

Wilcox, D.C., 2006. Turbulence Modeling for CFD, Third. ed. DCW Industries, Inc.

Wu, W., Rodi, W., Wenka, T., 2000. 3D Numerical Modeling of Flow and Sediment Transport in Open Channels. J. Hydraul. Eng. 4–15.

Yin, X.A., Yang, Z.F., Petts, G.E., 2012. Optimizing enviromental flows below dams. River Res. Appl. 28, 703–716. doi:10.1002/rra.1477

Zolezzi, G., Siviglia, A., Toffolon, M., Maiolini, B., 2011. Thermopeaking in Alpine streams: event characterization and time scales. Ecohydrology 4, 564–576. doi:10.1002/eco.132

# ACKNOWLEDGEMENTS

Ci sono molte persone che vorrei ringraziare per avermi aiutato e supportato in questi anni del dottorato.

Prima di tutto, grazie ai miei genitori senza i quali non avrei raggiunto certi obiettivi e mi hanno aiutato mentalmente a non mollare mai.

Grazie di cuore ai miei supervisor, Prof. Righetti e Prof. Dumbser per essere stati una guida sempre presente durante tutto il ciclo del dottorato. È stato un onore aver potuto lavorare con voi cercando di assimilare il più possibile dalle vostre competenze. In particolare grazie Maurizio per la pazienza, la tua conoscenza e per il legame professionale che si è creato nel tempo.

Un ringraziamento sincero va anche al Dr. –Ing. Noack dell'Università di Stoccarda. Grazie per avermi fatto da guida nel periodo "fuori sede" e fatto partecipe di molte attività. Grazie anche a Matthias, Ianina e Giulia. Senza di voi la mia ricerca non sarebbe potuta andare avanti.

Un sincero ringraziamento a tutti i tecnici del laboratorio di idraulica di Trento. Fabio, grazie per avermi sopportato in ufficio, il tuo regno. Grazie Paolo per i sopralluoghi e i disegni. Lorenzo ed Andrea, siete i migliori tecnici che un laboratorio possa avere. La vostra simpatia e disponibilità è sempre stata di grande aiuto.

Grazie a Valentina e Georg (Alperia) per avermi inserito nei vostri progetti, per essere stati dei maestri e degli ottimi compagni.

Un ringraziamento speciale a tutti i nuovi amici che ho avuto la fortuna di incontrare in questi anni. In particolare vorrei ringraziare gli amici con i quali si è formato un legame importante.

Grazie Sabrina per essere stata la prima collega d'ufficio a dovermi sopportare. Per avermi fatto partecipe delle tue attività di ricerca (che sono fantastiche) e per essere stata sempre disponibile quando avevo dubbi.

Giulia, ti metto per seconda solo perché hai preso il posto della Sabrina da poco tempo. Grazie perché porti sempre allegria in laboratorio facendomi dimenticare i momenti di difficoltà. Grazie per essere così sportiva ed essere la miglior spalla nelle nostre partite a tennis. Mi stai facendo sudare come un dannato!

Grazie Elisa per essere bionda in un laboratorio di more. No, seriamente grazie per essere stata sin da subito un'ottima amica. Per le nostre serate passate a ragionamenti senza senso al Satellite fino al dover chiudere la saracinesca.

Andrea, grazie per essere un Amico. E la A maiuscola non è un caso. Grazie perché sproni sempre a fare meglio, a cercare di dare il massimo in tutto quello che bisogna portare a termine.

Anna, davvero non saprei come ringraziarti. Sei l'amica più sincera che potessi mai avere avuto; grazie per la tua capacità di farmi sempre ridere per qualsiasi cosa, per essere stata un punto di riferimento mentale e professionale. Grazie per i tempi, spesi benissimo, con le nostre elucubrazioni mentali e con i video dementi. Davvero grazie! Ti devo ancora una statua 1:1, lo so!

Grazie ancora di cuore a tutti!

Giuseppe